# THE SEISMO-DEFORMATION OF KAROO AQUIFERS INDUCED BY THE PUMPING OF A BOREHOLE

*by*

**Panganai Dzanga**

*Thesis*
*submitted in fulfilment of the requirement of the degree of*

**Doctor of Philosophy**

*in the Faculty of Natural and Agricultural Sciences,*

*Department of Geohydrology,*

*University of the Free State*

*Bloemfontein,*

**Republic of South Africa**

*September 2003*

**Promoter:** **Professor J.F. Botha, PH.D.**

**Co-Promoter:** **Professor A.H.J. Cloot, D.Ing.**

# ACKNOWLEDGEMENTS

The research emanated from a Water Research Commission project entitled: *Karoo Aquifers: Deformations, Hydraulic and Mechanical Properties* conducted by Prof J.F Botha and Prof. A.H. Cloot.

The financing of the research was done partly by South African Nuclear Energy Corporation (NECSA) for which I am grateful.

I would like to take this opportunity to thank the following people who made this research a success:

**Prof AH Cloot**, the co-promoter, for guiding the research and for critiquing the mathematics and numerical models; and

**Prof JF Botha**, the promoter, for laying the basis of the research and reviewing the work.

I would like to thank also the Council for Geoscience, in particular Dr G Graham and the entire seismological unit for allowing me to use their facilities and equipment.

Above all I thank the Almighty for giving me strength and wisdom.

*In memory of my mum, Gladys and my sister Chengetai*

## TABLE OF CONTENTS

## LIST OF FIGURES

## LIST OF TABLES

## PHYSICAL SYMBOLS

### Latin symbols

| | | |
|---|---|---|
| $c_p$ | = Speed of compressional body waves | $[LT^{-1}]$ |
| $c_R$ | = Phase velocity of Rayleigh waves | $[LT^{-1}]$ |
| $c_T$ | = Speed of low frequency tube waves | $[LT^{-1}]$ |
| $E$ | = Longitudinal or Young modulus of elasticity | $[MT^{-1}]$ |
| $\mathbf{e}$ | = Strain tensor | [1] |
| $\mathbf{e}^0$ | = Residual strains induced by stresses | [1] |
| $\mathbf{e}^1$ | = Strain depended on the stresses and pressure | [1] |
| $e$ | = Dilatational strain or volumetric dilatation | [1] |
| $e_{ij}, e_{ij}$ | = The $ij-th$ elements of the strain tensor | [1] |
| $e_{xx}$ | = Extensional strain in the $x$-direction | [1] |
| $e_{yy}$ | = Extensional strain in the $y$-direction | [1] |
| $e_{zz}$ | = Extensional strain in the $z$-direction | [1] |
| $F_k$ | = Strength of sources and sinks of the species k | $[T^{-1}]$ |
| $G$ | = Shear transverse modulus of elasticity | $[MT^{-1}]$ |
| $g$ | = Acceleration of gravity | $[LT^{-2}]$ |
| $\mathbf{i}, \mathbf{j}, \mathbf{k}$ | = The unit Cartesian vectors | [1] |
| $\mathbf{k}$ | = Permeability tensor | $[L^2]$ |
| $\mathbf{K}$ | = Hydraulic conductivity tensor | $[LT^{-1}]$ |
| $\mathbf{r}$ | = Radius of displacement vector | $[L]$ |
| $\mathbf{S}$ | = Surface forces per unit area of a body | $[MT^{-1}]$ |
| $S_o$ | = Specific storativity | [1] |
| $Q$ | = Magnitude of discharge rate | $[L^3T^{-1}]$ |
| $\mathbf{u}$ | = Displacement vector | [L] |
| $u, v, w$ | = Cartesian components of the displacement vector | [L] |
| $\mathbf{v}$ | = Velocity of the centre of mass | $[LT^{-1}]$ |

| | | |
|---|---|---|
| $\mathbf{v}^k$ | = Velocity of material specie k | [$LT^{-1}$] |
| $\mathbf{x}$ | = Cartesian coordinates $(x, y, z)$ | [L] |
| $x, y, z$ | = Cartesian coordinates | [L] |
| $X, Y, Z$ | = Cartesian coordinates | [L] |

**Greek symbols**

| | | |
|---|---|---|
| $a$ | = Characteristic constant of a given soil | [$M^{-1}T$] |
| $a$ | = Volumetric compressibility of the rock matrix | [$M^{-1}T$] |
| $b_w$ | = Volumetric compressibility of the water | [$M^{-1}T$] |
| $a$ | = Speed of compressional waves | [$LT^{-1}$] |
| $b$ | = Speed of shear waves | [$LT^{-1}$] |
| $\Delta$ | = Dilatation; a small increment | [1] |
| $d(t)$ | = Dirac delta function of time | [T] |
| $\Delta t$ | = Time increment from $t_n$ to $t_{n+1}$ | [T] |
| $\Delta V$ | = Elementary volume element | [$L^3$] |
| $\Delta V_m$ | = Elementary volume of rock matrix | [$L^3$] |
| $\Delta V_a$ | = Elementary volume of air | [$L^3$] |
| $\Delta V_w$ | = Elementary volume of water | [$L^3$] |
| $e$ | = Porosity of a porous medium | [1] |
| $e_0$ | = Residual porosity of the medium | [1] |
| $v$ | = Poisson's ratio | [1] |
| $q$ | = An arbitrary angle | [1] |
| $q_w$ | = Residual water content of soil | [1] |
| $r$ | = Density of a body at a given point in space | [$ML^{-3}$] |
| $r_w$ | = Density of water | [$ML^{-3}$] |
| $r_k$ | = Density of material specie k | [$ML^{-3}$] |
| $\mathbf{s}$ | = Stress tensor | [$MT^{-1}$] |
| $\mathbf{s}_0$ | = Residual stress associated with $\mathbf{e}_0$ | [$MT^{-1}$] |
| $\mathbf{s}^1$ | = Non-linear stress tensor corresponding to $\mathbf{e}^1$ | [$MT^{-1}$] |
| $s^C$ | = Limiting compressive stress of rock grains | [$MT^{-1}$] |

| | | |
|---|---|---|
| $s^T$ | = Maximum tensile stress of rock matrix | $[MT^{-1}]$ |
| $w$ | = Frequency | $[T^{-1}]$ |

## MATHEMATICAL SYMBOLS

### Latin symbols

| | |
|---|---|
| $\hat{\mathbf{H}}_p^{n+1}$ | = Finite element approximation vector of $H_p(\mathbf{x},t)$ |
| $\nabla$ | = Gradient or nabla operator |
| $\mathbf{d}^e, \mathbf{s}^0, \mathbf{s}^b, \mathbf{b}^m$ | = Finite element approximation vectors |
| $D_z$ | = Partial derivative with respect to the variable $z$ |
| $\mathbf{f}, \mathbf{b}$ | = Finite element approximation vectors |
| $\mathbf{I}$ | = Unit Cartesian tensor |
| $K$ | = Constant, gain factor |
| $\mathbf{L}$ | = Arbitrary differential operator |
| $l_k(t)$ | = Lagrange interpolation polynomials |
| **M, H, V, W** | = Finite element approximation matrices |
| **n** | = Outwardly directed unit normal vector to a surface |
| **P, Q, R** | = Finite element approximation matrices |
| $s$ | = A line segment |
| $u(\mathbf{x})$ | = Arbitrary function in the variables $\mathbf{x}$ |
| $\hat{\mathbf{u}}(\mathbf{x},t)$ | = Finite element approximations of $u(\mathbf{x},t)$ |
| $\hat{\mathbf{u}}^n$ | = Finite element approximations vector of $\hat{\mathbf{u}}(\mathbf{x},t)$ |
| $w, a, m$ | = Subscripts denoting water, air and rock species (k) |
| $\mathbf{x}$ | = Set of independent variables |

### Greek symbols

| | |
|---|---|
| $d\Omega$ | = Boundary of $\Omega$ |
| $\Phi(x, y, z)$ | = Potential function |
| $f_i(\mathbf{x})$ | = Set of known, piecewise continuous polynomials |
| $g$ | = Finite element approximation vector |
| $l$ | = General eigenvalue parameter |
| $\Omega$ | = Domain of a specie or medium |

**Note**: The amplitudes of seismic traces presented in this thesis are expressed in counts, which is the way the Event Acquisition Recording System (EARS) used in the investigations displays results. These counts are related to the actual ground displacement through the equation:

$$M(f) = D/X(f) \qquad (i)$$

where $M(f)$ is magnification at frequency (counts/meter), $D$ is peak-to-peak amplitude (in counts), $X(f)$ is displacement of seismometer mass (meter) and $f$ is frequency (Hz). The actual ground motion in metres is given as

$$X(f) = iC/m(2pf)^2 \qquad (ii)$$

where $m$ is seismometer mass (kg), $C$ is calibration constant ($N/A$ or m kg $s^{-2}$ $A^{-1}$) and $i$ is input current (A).

# CHAPTER 1

# INTRODUCTION

## 1.1 GENERAL

Groundwater is the largest source of potable water in South Africa given that the country is semi-arid to arid with approximately 50 per cent of the geology constituting the Karoo Supergroup (Botha *et al*., 1998). The Supergroup is characterised by multi-stratification of sediments (Truswell, 1970), which were intruded and veneered in places by the Jurassic dolerite dykes and sills during a period of extensive magmatic cataclysm that took place over almost the entire Southern African subcontinent during one of the phases in the Gondwanaland break-up (Chevallier *et al*., 2001). They represent the roots and the feeders of the extrusive Drakensberg basalt that are dated around 180 My making it one of the largest outpouring of flood basalt in the world (Chevallier et a*l*., 2001). What is significant for hydrogeology are horizontal fractures, which are the major groundwater conduits that developed as a result of these post-Karoo tectonic events. The horizontal fractures are not only common at the parting planes of the sediments but can also be intercepted within a single lithological unit. Several morpho-tectonic models were proposed to explain the magma emplacement and the fracturing of the sediments and the most recent model is that of Chevallier *et al*., (2001). They proposed an integrated and complementary mechanism of emplacement where the dykes play a dominant role. The details and the justifications of the theory are covered extensively in Chevallier *et al*., (2001).

The complexity of the Karoo geology has made the groundwater flow and the surrounding mechanics difficult to understand. Several techniques (Bangoy *et al*., 1992; Bangoy *et al*., 1994; Barker, 1988, Helweg, 1994) have been applied to simulate groundwater flow in these aquifers but with little success and most of the investigations conducted have revealed that these aquifers are very complex, both in geometry and hydraulics. A typical example is the work of Botha and co-workers (1998), which was focused on understanding the geology, geometry and physical properties of Karoo aquifers in South Africa, which that revealed, among other things, the deformability of these aquifers. The development of secondary features in UO5, a borehole at the Campus Test Site of University of the Free State, over a period of three years as depicted by the televiewer results, Figure1.1 (Botha *et al*., 1998) is a clear testimony of matrix dynamics.

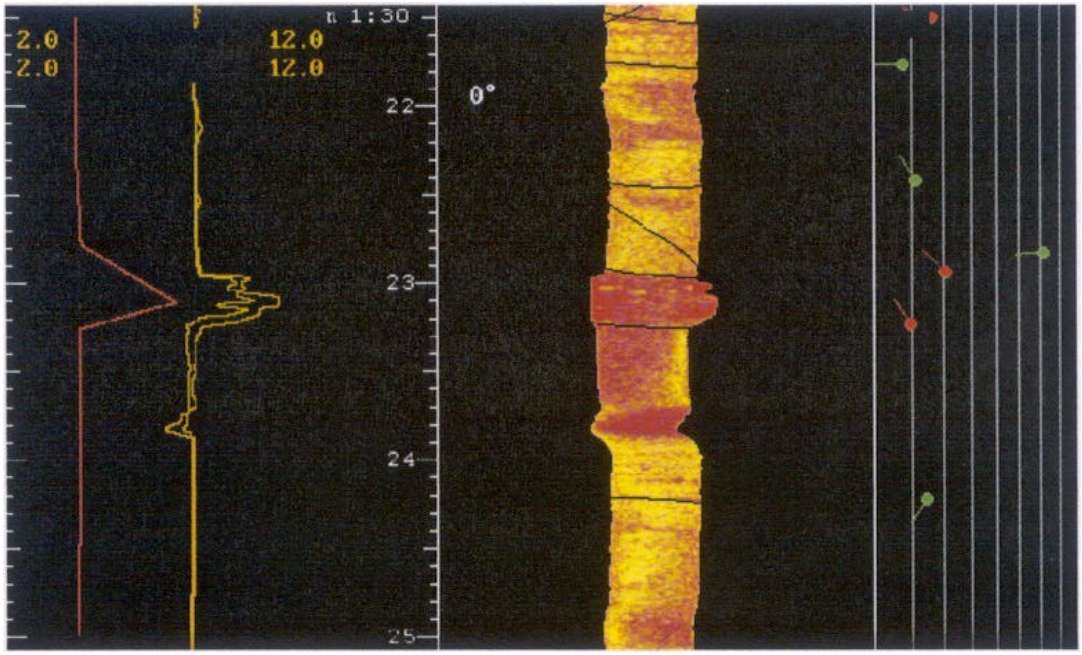


**Figure 1.1:** Calliper and acoustic scanner images of Borehole UO5 on the Campus Test Site. The position of the main water-yielding fracture is shown by the calliper curve on the left and its orientation by the tadpoles on the right [Botha and Cloot, 2002].

The borehole was excessively pumped during the 1993–1996 period for academic and research purposes since it was the highest yielding borehole at that time. Ever since this observation the deformation of Karoo aquifers became a topical issue that saw Botha and Cloot (2002) pursuing the subject. In their work they focused on aquifer deformation caused by the interaction of groundwater and the solid matrix. The seismo-effect of the pump was not part of the study, however. It is the latter that forms the basis of this work.

## 1.2 BACKGROUND

The most effective and cheapest procedure for understanding the geometry and physical properties of an aquifer is by analysing pumping test data. As pointed out above, the physical and mechanical properties of the Karoo aquifers are quite complex and differ from the homogeneous and isotropic geological formations as evidenced by the deviations in the drawdown curves as seen in literature data (Krusemann & Ridder, 1994; De Marsily, 1986; Theis, 1935).

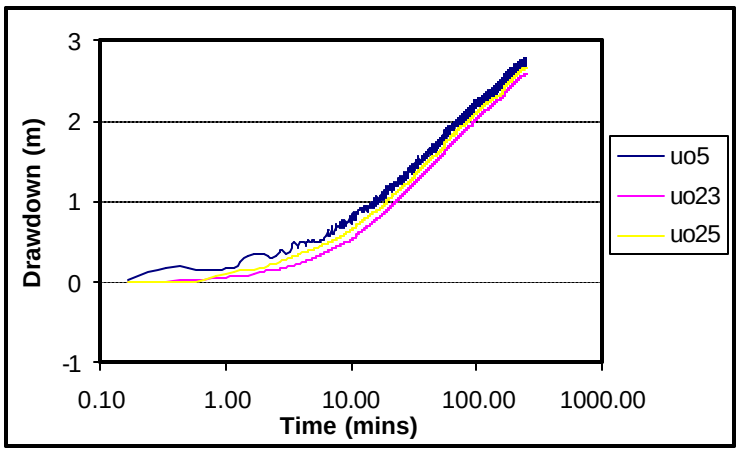


**Figure 1.2:** Small oscillations in pumping test data captured in borehole UO5 at 10-second intervals using a pressure transducer. The borehole was pumped at 1.26 l/s. UO23 and UO25 were used as observation boreholes during the test. The test was conducted at Campus Test Site, University of the Free State.

The most outstanding observation of interest to this work is the presence of oscillations in some of the drawdown curves (Figure 1.2). In order to elaborate the magnitude of the oscillations, the pumping test data of borehole UO5 were further processed. A Theis model was fitted to the data (Figure 1.3) and the effect of water loss was filtered from the field data (Figure 1.4). This exercise was applied to the oscillatory part of the data, which is the first 1960 seconds. A Fourier transform of the data (Figure 1.5) showed that a range of frequencies is involved in the generation of oscillations displayed in Figure 1.4.

It is clear from this analysis that oscillations exist in pumping test data. In most cases they are often dismissed as noise. However, the inconspicuousness of oscillations in some drawdown curves is due to the poor and rudimentary sampling techniques employed during pump testing. In essence, the use of equipment with poor resolution and the preconceived idea of the data expected have led to one fundamental phenomenon in Karoo hydrogeology, if not in hydrogeology in general, being overlooked.

It is evident in Figure 1.2 that this phenomenon is more prominent in pumping boreholes than in observation boreholes, indicating distance and pumps dominancy. There are several theories postulated about the phenomenon and the most relevant is that of Biot (1956) on system deformation.

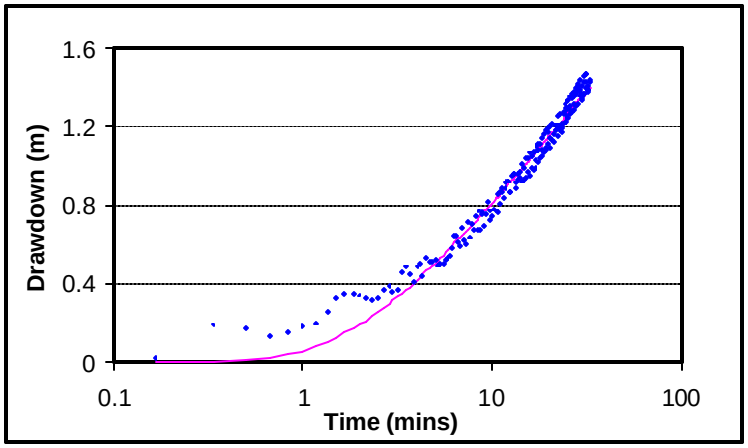


**Figure 1.3:** The Theis fit (pink) to the pumping test data of borehole UO5. The objective is to remove the drawdown effect in the signal

The essence of Biot's theory is that *a system (an aquifer in this case) oscillates when disturbed by an external force as it restores its equilibrium state*. The removal of groundwater offsets the system from its equilibrium state setting it into oscillations as it reverts to its initial state. Botha and Cloot (2002) investigated the applicability of the theory to the impact of discharge rate on the deformation of aquifer matrix.

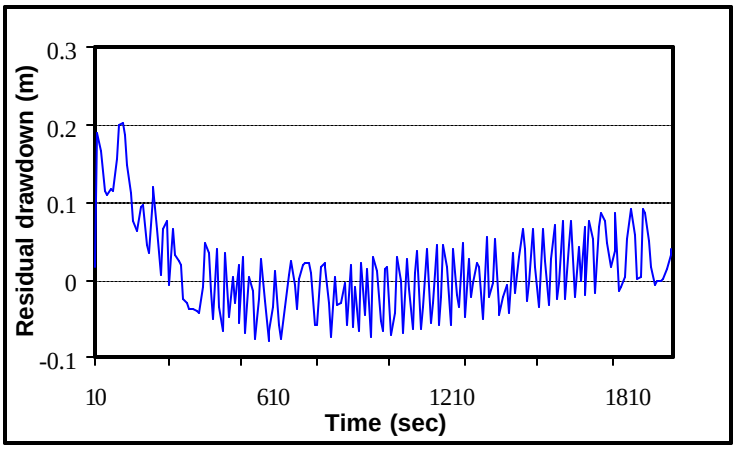


**Figure 1.4:** The residual drawdown after removing the effect of water loss from pumping test data of borehole UO5. It clearly demonstrates the oscillatory behaviour of the data.

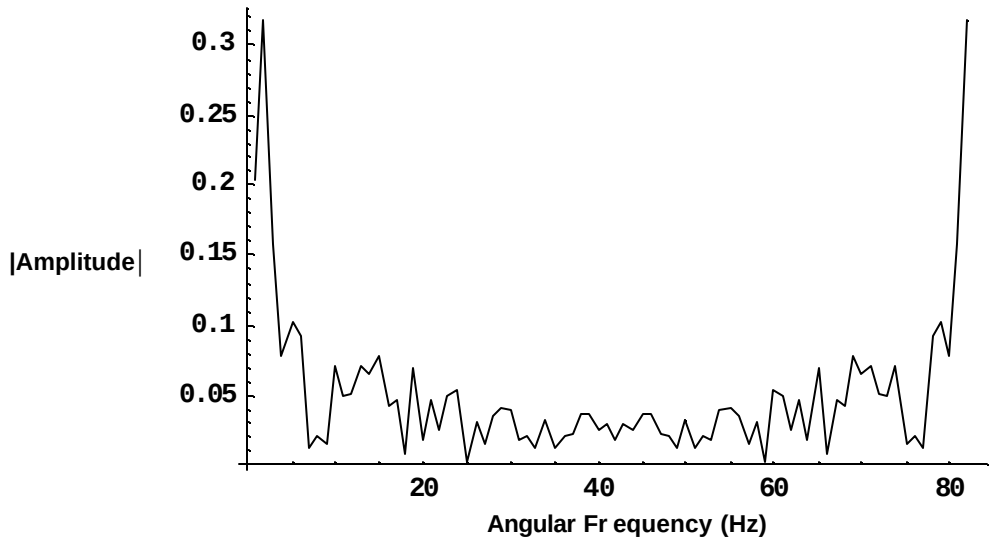


**Figure 1.5:** The Fourier transform of the oscillatory data in Figure 1.4 showing the range frequencies involved**.**

## 1.3 OBJECTIVE OF THE STUDY

The purpose of the work is to investigate the pump as the causative factor of oscillations observed in drawdown curves captured from boreholes intersecting bedding fractures in Karoo aquifers.

## 1.4 SCOPE OF THE RESEARCH

The framework of the research revolves around the mechanical effects of the pump on groundwater dynamics. The aspects of the pump of interest to the research are the vibrations and the sound generated during pumping. The responses of borehole water to aquifer deformation and to sound pressure form the focal point of the research. This is grafted on the premise that for the oscillations to develop, the aquifer should deform oscillatory and hence the proposed diaphragmatic deformation hypothesis. The second line of reasoning is based on the direct impact of pump sound on borehole water. The pressure variations caused by pump sound on borehole water might be the causative factor for the development of the oscillations in drawdown curves. It is for this reason that sound forms part of the arguments in justifying the dominant effect of pumps on groundwater behaviour. Whatever way the problem is diagnosed; the elastic

and the seismic theories will play fundamental roles. These theories are an integral part of the problem domain of the research.

The quantification of energy transmitted, reflected or attenuated as the seismic waves propagate through aquifer lithologies will not form part the research. However, qualitative arguments based on these processes will be raised in highlighting the impact of the mechano-effects of the pump on groundwater flow.

It is important to state explicitly upfront that the work covered in this research may have the same fundamentals as the research of Botha and Cloot (2002) but the focuses are different. The work of the latter gravitates towards forging a relationship between the hydraulic and mechanical properties of aquifers by investigating the influence of abstraction (water removal from an aquifer) and not the mechano-effects of the pump.

## 1.5 THE APPROACH

The hypothesis forming the basis of the research postulates that the mechanical effects of electrical and diesel pumps induce mechano- and geo-acoustic deformations in an aquifer leading to the oscillatory response of borehole water.

The conceptualisation of the sequence of events is shown in Figure1.6. According to the model, the pump seismicity instigates the driving force **F** with components acting perpendicularly to the fracture. Opposing the force **F** is the hydrodynamic force **H** (an assumption) of water in the fracture**.** In a case where the aquifer is losing water the opposing forces **B** and **D** develop (Hughes and Brighton, 1967; Raudkivi and Callander, 1975). These forces result from the flowing of water. The force **B** is positive in the sense that it is acting in the direction of pumping and, likewise, the opposing force **D** is negative.

As the system loses water with time, the impact of the force **F** increases, offsetting the dynamic equilibrium with **H**, although strictly speaking **F** will remain constant. This is due to the fact that less and less water will be available to counteract **F,** gradually subjecting the fracture to strain and stress which could contribute to the eventual collapse of the fracture if allowed to continue without monitoring. The borehole yield will ultimately drop or even *dry up* altogether.

A typical example is the groundwater supply of Nourpoort, a Karoo town in Northern Cape, which has an aquifer with four boreholes within a distance of 5 m on the same horizontal fracture, which were drilled consecutively after the previous borehole dried up. The boreholes are equipped with electric pumps, which are operated at full capacity during peak demands, especially holidays when the water demand increases.

In order to justify the hypothesis, both theoretical and field investigations are conducted. One- and two-dimensional mathematical models are developed taking into account the intrinsic characteristics of an aquifer and the behaviour of a pump. The hydraulic and mechanical characteristics of an aquifer are considered. The models simulate the phenomenon at different levels.

The one-dimensional model is strictly based on the mechanical properties of an aquifer. The presumption is that the oscillations observed are caused by the direct response of the water level of the borehole to aquifer deformation when subjected to a harmonic external force.

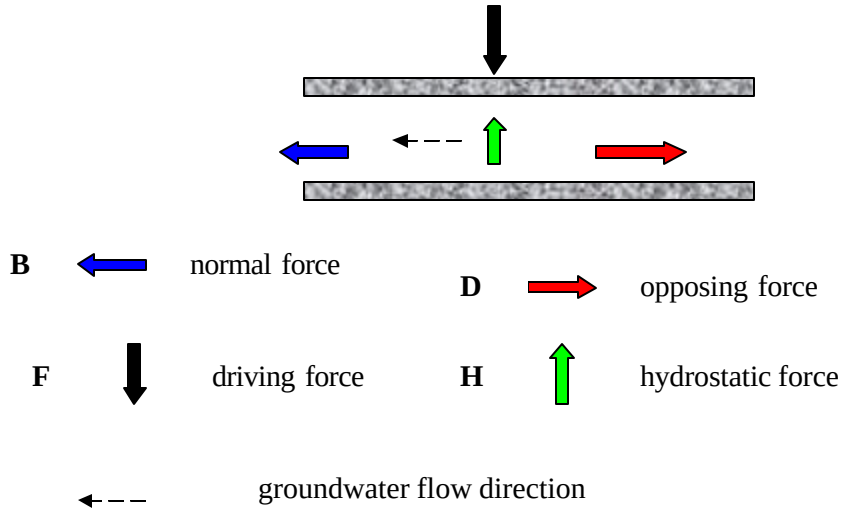


**Figure 1.6:** Force orientation in fracture flow

The two-dimensional mathematical model of Botha and Cloot (2002) is modified to assimilate the pump seismicity. The model takes into account both the hydraulic and elastic properties of an aquifer. It is an advanced form of the one-dimensional model.

Several field investigations were conducted aimed at verifying the mathematical models and reproducing the oscillations shown in Figure 1.2. Seismic instruments, pressure transducers and submersible pumps were used in the investigations. It should be highlighted here that the pressure transducers used in capturing data in Figure 1.2 had higher resolutions than the transducers used in the investigations covered in this thesis. The Campus Test Site at the University of the Free State was the selected test ground mainly because the oscillations were detected in one of the boreholes at the site. The other reason was that the geometry and the geology of the aquifer are well understood and documented.

## 1.6 THE STRUCTURE OF THE THESIS

The diaphragmatic phenomenon of the fracture system forms the basis of the research covered in the thesis. Because the phenomenon is pump driven, the evolution and distribution of forces in the system become crucial to the study. In the aquifer system, the forces are manifest as seismic waves that instigate the proposed diaphragmatic deformation. Hence, an outline of elastic and seismic theories is done in Chapter 2. The translation of proposed physical processes into mathematical models giving rise to both one- and two-dimensional models is conducted in Chapter 3. In Chapter 4, the models are solved numerically and compared with field observations. The conclusions and recommendations are outlined in Chapter 5.

# CHAPTER 2

## SEISMIC THEORY AND BOREHOLES WAVES

### 2.1 INTRODUCTION

Like any other material, rocks deform when subjected to an external force. Depending on the magnitude and the physical properties of these rocks the deformation can be elastic or plastic. During elastic deformation the rock returns to its initial state when the external force is removed. In plastic deformation the rock will not regain its original state on removal of the external force. Nearly all rocks undergo plastic deformation once the applied force exceeds a certain elasticity threshold. The deformation of rocks is investigated by analysing the strain and stress distribution. These investigations constitute the field of elasticity in material sciences.

The theory of elasticity essentially entails the study of internal forces in a solid body. These forces arise from the interaction between the molecules in the body; which ensures the existence of a solid body as such and hence its strength. They also act when no external forces are applied to the body. The theory of elasticity focuses on the effects of forces on a body.

In this research the body of interest is an aquifer and the source of external force is an operating pump. The pump vibrations generate a force that will propagate through an aquifer as a seismic wave, which, according to the proposed hypothesis, instigates a diaphragmatic deformation on coming into contact with a bedding fracture. Therefore, apart from the theory of elasticity, seismic theory also plays a crucial role in this work. Since seismic theory is grafted on the theory of elasticity, the latter is discussed as a subsection of the former in Section 2.2.

It is the reaction of groundwater to the diaphragmatic deformation of the bedding fracture that is suspected of being the main cause of oscillations present in the drawdown curves. This may be one way in which the pump can be held responsible for the generation of oscillations. Another way is through the sound it generates during operation. The variation in sound pressure causes borehole water level to fluctuate accordingly. As a result, the water waves generated propagate throughout the fracture. This may be the reason for poorly defined oscillations in observation boreholes (Figure 1.2). Borehole waves are an integral part of the system and for that reason are described in Section 2.3. The general discussions are given in Section 2.4.

## 2.2 SEISMIC THEORY

### 2.2.1 Theory of elasticity

In general the size and shape of a solid body can be changed by applying forces to the external surface of the body. These forces are opposed by internal forces that resist the change in size and shape. As a result, the body tends to return to its original condition when the external forces are removed. This property of resisting changes in size or shape and of returning to the undeformed condition when the external forces are removed is elasticity. This is a common phenomenon in materials, and aquifers should be no exception.

The bedding fractures of the Karoo Supergroup, like any other rocks, can be considered perfectly elastic provided the deformations are small. The threshold of fracture elasticity depends on the physical properties of the rocks forming an aquifer.

The theory of elasticity relates the applied forces to the changes in size and shape that result. The relations between the applied forces and the deformations are expressed in terms of the concepts of stress and strain.

*2.2.1.2 Stress*

Stress is a force per unit area. When a force is applied to a body, the stress is the ratio of the force to the area on which the force is applied. For a force perpendicular to the area, the stress is said to be a normal stress (the pressure) for example. When the force applied is tangential to the element of area, the stress is called shearing stress. For a body surface in the *z*-direction, the normal and the shearing stresses acting on this surface are expressed as $s_{zz}$, $s_{zx}$ and $s_{zy}$ respectively. Similar components for the *x* and *y* surfaces are given by ($s_{xx}$, $s_{xy}$, $s_{xy}$) and ($s_{yy}$, $s_{yx}$, $s_{yz}$) respectively. These components are illustrated in Figure 2.1.

The harmonic force generated by the pump should be dominant in the horizontal plane since the rotations are in that plane. In the field, a geophone (sensor) sensitive to three components (Z, N, E) of ground motion was used and the response indicated that the force from the pump also has a vertical component (Z). It is the component orthogonal to the hydrostratigraphic unit that causes the proposed diaphragmatic deformation.

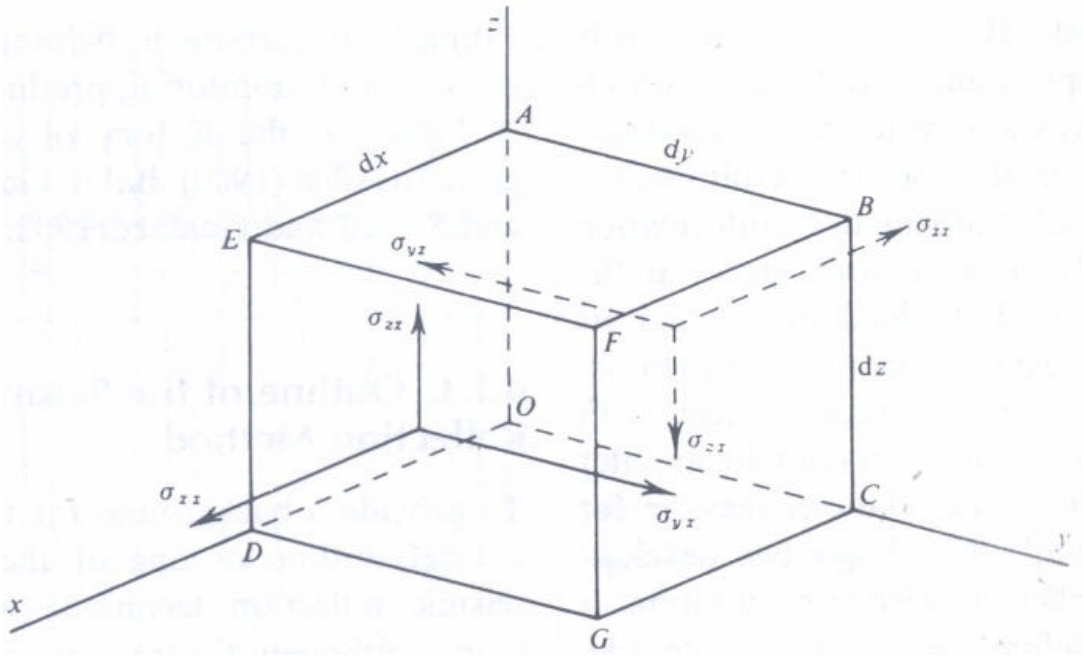


**Figure 2.1:** The components of stress [Telford *et al*., 1990]

*2.2.1.2 Strain*

When an elastic body is subjected to stresses, changes in shape and dimension occur. These changes are strains and can be resolved into certain fundamental types. It is the evolution of strains that manifests in the diaphragmatic deformation proposed. The derivation of expressions of strain is done in most textbooks on material sciences and seismology (Telford *et al.*, 1990) and repeating it here is not necessary. However, of relevance to the research is the knowledge of normal strains and shearing strains. If $(u, v, w)$ are the components of displacement of a point $P(x, y, z)$, these strains may be expressed as (Telford *et al.*, 1990):

Normal strains:

$$e_{xx} = \frac{\partial u}{\partial x}$$

$$e_{yy} = \frac{\partial v}{\partial y}$$

$$e_{zz} = \frac{\partial w}{\partial z}$$

Shearing strains:

$$\left.\begin{aligned} e_{xy} &= e_{yx} + \frac{1}{2}\left[\frac{\partial v}{\partial x} + \frac{\partial u}{dy}\right] \\ e_{yz} &= e_{zy} + \frac{1}{2}\left[\frac{\partial w}{\partial y} + \frac{\partial v}{dz}\right] \\ e_{zx} &= e_{xz} + \frac{1}{2}\left[\frac{\partial u}{\partial z} + \frac{\partial w}{dx}\right] \end{aligned}\right\}$$

The normal strains are of particular interest to this work. The changes in dimensions given by the normal strains result in fracture volume change; the change in volume per unit volume is dilatation and is represented by $\Delta$. This is expressed as

$$D = e_{xx} + e_{yy} + e_{zz} = \frac{\partial u}{\partial x} + \frac{\partial v}{\partial y} + \frac{\partial w}{\partial z}$$

In the case of a fracture, the aperture opening is at maximum when uncompressed and least at minimum when subjected to normal stresses from a pump.

*2.2.1.3 Hooke's law*

Hooke's law relates strain to the stress subjected to a body when the strains are small. The law states that a *given strain is directly proportional to the stress producing it.* In general, Hooke's law for an isotropic medium is expressed in the simple form (Telford *et al.*, 1990):

$$s_{ii} = l'D + 2Ge_{ii}; \qquad i = x, y, z \tag{2.1}$$

$$s_{ij} = Ge_{ij}; \qquad i, j = x, y, z \; i \neq j \tag{2.2}$$

where $l'$ and $G$ are the Lamé constants. The parameter $G$ is a measure of the resistance to shearing strain and is referred to as the modulus of rigidity or shear modulus.

Equation (2.1) states that a normal stress may produce strains in directions other than the direction of the stress; Equation (2.2) states that shearing stresses are associated with only shearing strain.

If the stress is increased beyond the elastic limit, Hooke's law no longer holds and strains increase more rapidly. Strains resulting from stresses that exceed this limit do not disappear entirely when the stresses are removed. The premise at this stage is that during its evolution, a water-supplying fracture to a pumping borehole will build a history on its deformation each time the elastic limit is exceeded. It will eventually collapse as a result of fatigue. It is this phenomenon that may be responsible for the failure of boreholes in the Karoo aquifers, which would have been pumped over a long period of time. The duration to the point of failure is coupled to discharge rate (Botha and Cloot, 2002) which is proportional to the intensity of the vibrations. The latter relation is demonstrated later in the thesis.

*2.2.1.4 Elastic constants*

In addition to the Lamé constants, the Young Modulus (E) and the Poisson's ratio $v$ can also be used to formulate relations of physical quantities in the theory of elasticity. The use of constants is usually a matter of choice.

The Young Modulus and the Poisson's ratio $v$ are expressed as:

$$E = \frac{s_{xx}}{e_{xx}} = \frac{G(3l' + 2G)}{l' + G} \tag{2.3}$$

$$\begin{aligned} v &= \frac{-e_{yy}}{e_{xx}} \\ &= \frac{-e_{zz}}{e_{xx}} = \frac{l'}{2(l' + G)} \end{aligned} \tag{2.4}$$

The Young Modulus in particular gives a direct relation of physical quantities of immediate relevance to the research, that is, a relationship between the normal stress caused by pump vibrations and the resultant fracture deformation.

According to Figure 1.6, in response to the normal stresses, the water generates a hydrodynamic pressure $H_p$ on fracture planes, which in the vertical plane can be expressed as

$$s_{zz} = -H_p,$$

The shearing stress is zero and hence

$$s_{xy} = s_{yz} = s_{xz} = 0$$

Then, $k$ is the ratio of the pressure to the dilatation (Telford *et al.*, 1990) given as

$$\text{bulk modulus} = k = \frac{-H_p}{\Delta} = \frac{3l' + 2G}{3} \qquad (2.5)$$

The minus sign is inserted to make $k$ positive.

Equation (2.5) illustrates the weakening effect of the hydrodynamic pressure as the system loses water. Ideally, the physical fracture volume does not increase but the volume occupied by water decreases, reducing the effective hydrostatic pressure necessary to counteract the normal stress due to pump vibrations.

### 2.2.2 Wave equation

By applying the continuity and mass conservation principles, fracture deformation can be expressed as a function of time and distance from a driving external force.

Newton's second law of motion states that an unbalanced force equals the mass times the acceleration. Force acting on an aquifer in the $z$ direction will cause motion in that particular direction. The unbalanced force per unit volume in the $z$ direction is given as

$$r\frac{\partial^2 w}{\partial t^2}$$

The displacement of the formation in the $z$ direction is given as $w$, time as $t$ and the density of the formation is represented by $r$. The force is, however, counter-balanced by the inter-granular stresses acting in all three directions, resulting in Equation (2.6):

$$r\frac{\partial^2 w}{\partial t^2} = \frac{\partial s_{zx}}{\partial x} + \frac{\partial s_{zy}}{\partial y} + \frac{\partial s_{zz}}{\partial z} \qquad (2.6)$$

Similar equations can be written for motion along the $x$ and $y$ axes. Thus,

$$r\frac{\partial^2 u}{\partial t^2} = \frac{\partial s_{xx}}{\partial x} + \frac{\partial s_{xy}}{\partial y} + \frac{\partial s_{xz}}{\partial z}$$

$$r\frac{\partial^2 v}{\partial t^2}=\frac{\partial s_{yx}}{\partial x}+\frac{\partial s_{yy}}{\partial y}+\frac{\partial s_{yz}}{\partial z}$$

Using the Hooke's law the stresses can be replaced by the strains as follows:

$$r\frac{\partial^2 w}{\partial t^2}=\frac{\partial s_{zx}}{\partial x}+\frac{\partial s_{zy}}{\partial y}+\frac{\partial s_{zz}}{\partial z}$$

$$=l'\frac{\partial \Delta}{\partial z}+2G\frac{\partial e_{zx}}{\partial x}+G\frac{\partial e_{zy}}{\partial y}+G\frac{\partial e_{zz}}{\partial z}$$

$$=l'\frac{\partial \Delta}{\partial z}+G\left\{2\frac{\partial^2 w}{\partial z^2}+\left(\frac{\partial^2 v}{\partial z\partial y}+\frac{\partial^2 w}{\partial y^2}\right)+\left(\frac{\partial^2 w}{\partial x^2}+\frac{\partial^2 u}{\partial z\partial x}\right)\right\}$$

$$=l'\frac{\partial D}{\partial z}+G\nabla^2 w+G\frac{\partial}{\partial z}\left(\frac{\partial u}{\partial x}+\frac{\partial v}{\partial y}+\frac{\partial w}{\partial z}\right)$$

$$=(l'+G)\frac{\partial \Delta}{\partial z}+G\nabla^2 w \qquad (2.7)$$

By analogy the equations for $u$ and $v$ are written as

$$r\frac{\partial^2 u}{\partial t^2}=(l'+G)\frac{\partial \Delta}{\partial x}+G\nabla^2 u \qquad (2.8)$$

$$r\frac{\partial^2 v}{\partial t^2}=(l'+G)\frac{\partial \Delta}{\partial y}+G\nabla^2 v \qquad (2.9)$$

The wave equation is obtained by differentiating the three equations with respect to $x$, $y$ and $z$ and adding these results. This gives

$$r\frac{\partial^2}{\partial t^2}\left(\frac{\partial u}{\partial x}+\frac{\partial v}{\partial y}+\frac{\partial w}{\partial z}\right)=(l'+G)\left(\frac{\partial^2 \Delta}{\partial x^2}+\frac{\partial^2 \Delta}{\partial y^2}+\frac{\partial^2 \Delta}{\partial z^2}\right)+G\nabla^2\left(\frac{\partial u}{\partial x}+\frac{\partial v}{\partial y}+\frac{\partial w}{\partial z}\right)$$

that is,

$$r\frac{\partial^2 \Delta}{\partial t^2}=(l'+2G)\nabla^2\Delta$$

or

$$\frac{1}{a^2}\frac{\partial^2 D}{\partial t^2}=\nabla^2 D \qquad a^2=\frac{l'+2G}{r} \qquad (2.10)$$

The generalised wave equation is therefore expressed in the form

$$\frac{1}{J^2}\frac{\partial^2 y}{\partial t^2} = \nabla^2 y \qquad (2.11)$$

The wave equation (Equation 2.11) relates a time derivative of a displacement (the left side) to spatial derivatives (the right side); and the constant of proportionality is $J^2$. The constant is a composition of aquifer properties that includes the shear modulus and density. The rotational aspects of the system that are not of interest to the research are thus ignored.

It should be noted that Equation (2.11) describes the wave motion in general through a body. It demonstrates the relation between the mechanical properties of a body and the external force applied. It therefore implies that the pump vibrations in the aquifer are propagated in the form of a wave. For Equation (2.11) to be problem specific, the intrinsic properties of the body should be incorporated as well as the characteristics of the external force. For the purpose of the research, aquifer properties and pump vibrations are considered. This is an exercise that is conducted in the next chapter.

## 2.3 BOREHOLE WAVES

The generalised wave equation (Equation 2.11) can assume different forms depending on the physics of a system. By introducing system-specific quantities the model transforms to problem specific. This principle is revisited in Chapter 3 where the problem-specific model will be derived.

In general, when pumping a borehole two major aspects of relevance to the research manifest, namely, the tube waves and the seismic waves. Tube waves are waves travelling in the direction of the axis of the fluid-filled borehole and the seismic waves in this instance are the waves that propagate in the rock. The theory of tube waves in boreholes has been covered extensively in literature (White, 1965; Biot, 1952). The work is specific to the petroleum industry, however.

In an empty cylindrical hole, a kind of surface wave can propagate along the axis of the hole with energy confined to the vicinity of the hole. These waves exhibit dispersion with phase velocity increasing with the wavelength. At wavelengths much shorter than the radius of the hole they approach Rayleigh waves (Aki and Richards, 1980). The phase velocity reaches the shear velocity at wavelengths of about three times the radius. Beyond this cut-off wavelength, they attenuate quickly by radiating S-waves. In a fluid-filled cylindrical hole, in addition to a series of multi-reflected conical waves propagating in the fluid, tube waves exist without a cut-off for the

entire period range. At short wavelengths, they approach Stoneley waves for the plane liquid-solid interface. For wavelengths longer than about 10 times the hole radius, the velocity of tube waves becomes constant, given by the bulk modulus $k$ of the fluid and the rigidity $m$ of the solid, as $v = c(1+k/m)^{-1/2}$, where $c$ is the acoustic velocity (Aki and Richards, 1980).

The main source of tube waves investigated is sound pressure (White, 1965). Coupled with this phenomenon is the direct effect of Rayleigh waves on the fluid in a borehole. The analogy in this case is that the pump generates seismic waves that propagate into the aquifer according to the seismic theory covered in Section 2.2. The vibrations and the sound waves can also propagate along the borehole to the water level. White (1965) investigated the impact of the pressure waveform created by the passage of a Rayleigh wave.

The work of White (1965) not only strengthens the basis of this research but also demonstrates the complexity of the dynamics. A brief description of his work is outlined below.

### 2.3.1 Tube waves in permeable formation

Most geological formations penetrated by boreholes are porous and permeable to varying degrees. As mentioned in Chapter 1, a bedding fracture is the highest attainable permeability in the Karoo Supergroup.

When pumping, the pressure transients in the borehole will cause water to flow in and out of the wall of the hole, provided it is not cased. This forced flow consumes some energy, which affects the phase velocity of waves travelling along the fluid column (White, 1965). This phenomenon is illustrated in Figure 2.2.

The phenomenon shows that there are two ways in which the proposed diaphragmatic deformation manifests. The water flushed out of the borehole by a harmonic force can also force the fracture to open and close diaphragmatically. The pressure build-up in this case concentrates in the fracture by virtue of its high porosity.

Since it is not within the scope of this research to decouple the effect of sound from the vibrations, and since the latter can somehow be quantified in the field, it is necessary to illustrate some of the solutions obtained by White (1965) on the effect of Rayleigh waves. The Rayleigh wave at this stage is assumed to be the waveform manifesting from pump vibrations.

In his theoretical approach to investigating the impact of Rayleigh waves on the generation of tube waves, White (1965) considered a pressure waveform created by

the passage of a Rayleigh wave. The two potentials describing the Rayleigh wave are the compressional wave potential $f$ and the shear wave potential $y_y$ given as

$$f(x,z,t) = \frac{1}{2p}\int_{-\infty}^{\infty} A(w)e^{-\bar{m}x}e^{-ilz}e^{iwt}dw$$

$$y_y(x,z,t) = -\frac{1}{2p}\int_{-\infty}^{\infty} \frac{2i\,\mathrm{sgn}\,w(1-c_R^{\,2}/a^2)^{1/2}}{2-c_R^2/b^2}A(w)e^{-\bar{k}x}e^{-ilz}e^{iwt}dw$$

satisfying

$$\frac{\partial^2 f}{\partial x^2}+\frac{\partial^2 f}{\partial z^2}=\frac{1}{a^2}\frac{\partial^2 f}{\partial t^2} \qquad (2.12)$$

and

$$\frac{\partial^2 y_y}{\partial x^2}+\frac{\partial^2 y_y}{\partial z^2}=\frac{1}{b^2}\frac{\partial^2 y_y}{\partial t^2} \qquad (2.13)$$

respectively.

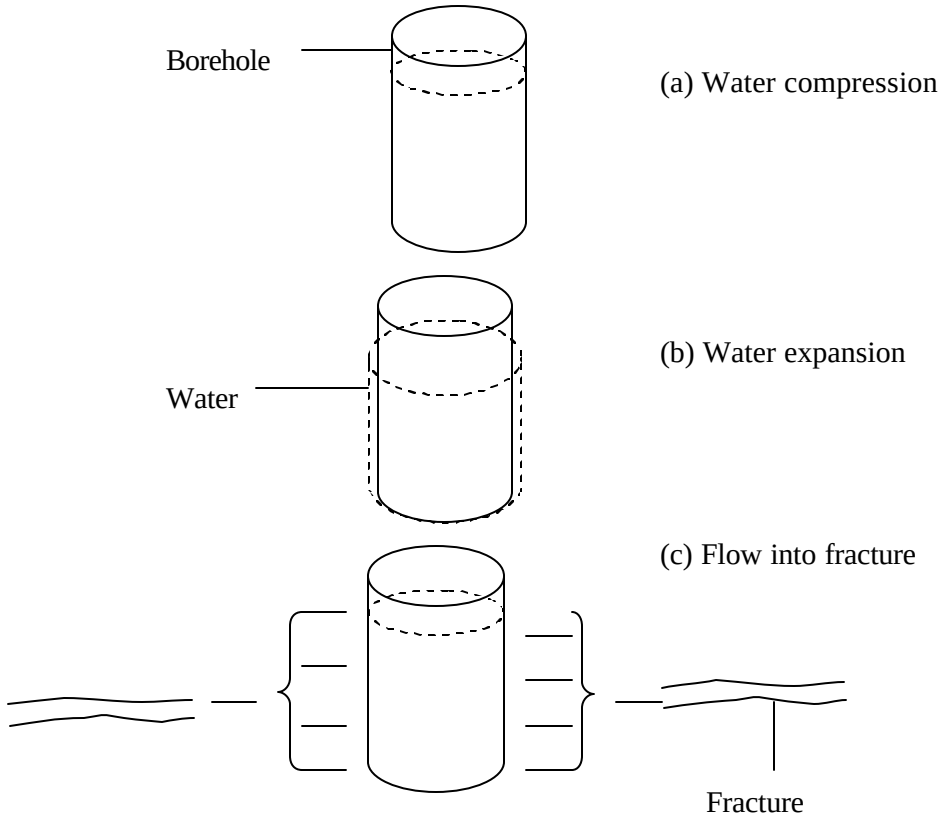


**Figure 2.2:** The three contributions to volume flow for tube waves into a fracture [adapted and modified from White, 1965]

It should be noted that *y*-direction is treated as a boundary, thus $y_y$ and the system of wave equations is based on the coordinate system in Figure 2.3. This is a component of $y$ in the *y*-direction and not a partial derivative.

The parameters used are defined as

$$\overline{m} = (1/c_R^2 - 1/a^2)^{1/2}|w|,$$

$$\overline{k} = (1/c_R^2 - 1/b^2)^{1/2}|w|,$$

$$l = w/c \qquad \text{(wave number)}$$

where $a$ is the speed of compressional waves (Equation 2.10) in the solid, $b$ is the speed of shear waves $b = \sqrt{G/r}$, $A(w)$ is the wave amplitude as a function of frequency, $c_R$ is the phase velocity of the Rayleigh wave, $c_T$ is the speed of low frequency tube waves and $w$ is the angular frequency. By definition

$$\text{sgn}(x) = \begin{cases} -1 & x < 0 \\ 0 & x = 0 \\ 1 & x > 0 \end{cases}$$

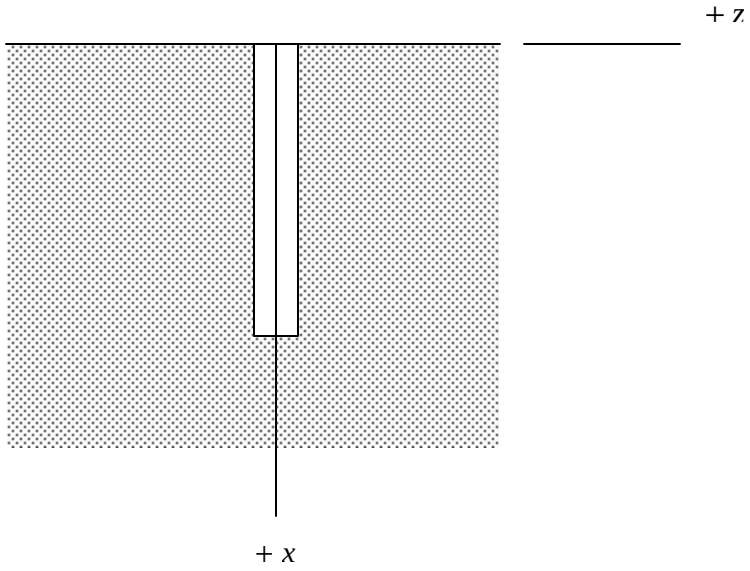


**Figure 2.3:** Coordinates for discussion of a Rayleigh wave coupled to a fluid-filled borehole

Equation (2.11) is similar to Equation (2.12), which is a compressional wave. By considering the shear stresses, Equation (2.13) is generated. The latter is not of much use to this work and is therefore ignored since the focus is on the effect of normal stresses on the hydrostratigraphic unit.

The final waveform was seen to consist of a convolution of the assumed waveform $f(T)$ with a relatively simple function consisting of two terms. For terms in the total expression varying as $e^{-\bar{m}x}$, $K = K_p = (1/c_R^2 - 1/a^2)^{1/2}$. For terms varying as $e^{-\bar{k}x}$, $K = K_s = (1/c_R^2 - 1/b^2)^{1/2}$. These steps were applied to the total expression, and the elastic constants were all expressed as velocity ratios. By using these expressions, White (1965) found that the pressure in a borehole caused by the passage of a Rayleigh wave was characterised by horizontal particle velocity $f(T)$ to be

$$P(X,T) = f(T) * \left[ (R_p + R_s) d\left(T - \frac{X}{c_T}\right) - \frac{R_p K_p X}{p(K_p{}^2 X^2 + T^2)} - \frac{R_s K_s X}{p(K_s{}^2 X^2 + T^2)} \right] \quad (2.14)$$

where $R_p$ and $R_s$ are defined as

$$R_p = \frac{\begin{array}{c} r_T c_T{}^2 [4(c_R{}^2/b^2 - 2c_R{}^2/a^2 + 1)(1 - b^2/a^2) \\ + (2 - c_R{}^2/b^2)(1 - 2b^2/a^2)](2 - c_R{}^2/b^2) \end{array}}{c_R(3 - 4b^2/a^2)(1 + c_T{}^2/c_R{}^2 - c_T{}^2/a^2)[(2 - c_R{}^2/b^2) - 2(1 - c_R{}^2/b^2)^{1/2}(1 - c_R{}^2/a^2)^{1/2}]}$$

$$R_s = \frac{4 r_T c_T{}^2 (1 - c_R{}^2/b^2)^{1/2}(1 - c_R{}^2/a^2)^{1/2}}{c_R(1 + c_T{}^2/c_R{}^2 - c_T{}^2/b^2)[2(1 - c_R{}^2/b^2) - 2(1 - c_R{}^2/b^2)^{1/2}(1 - c_R{}^2/a^2)^{1/2}]}$$

The second term $R_p$ of Equation (2.14) is plotted in Figure 2.4 for several depths in the borehole. This is the pressure response when the horizontal particle velocity in the Rayleigh wave is an impulse.

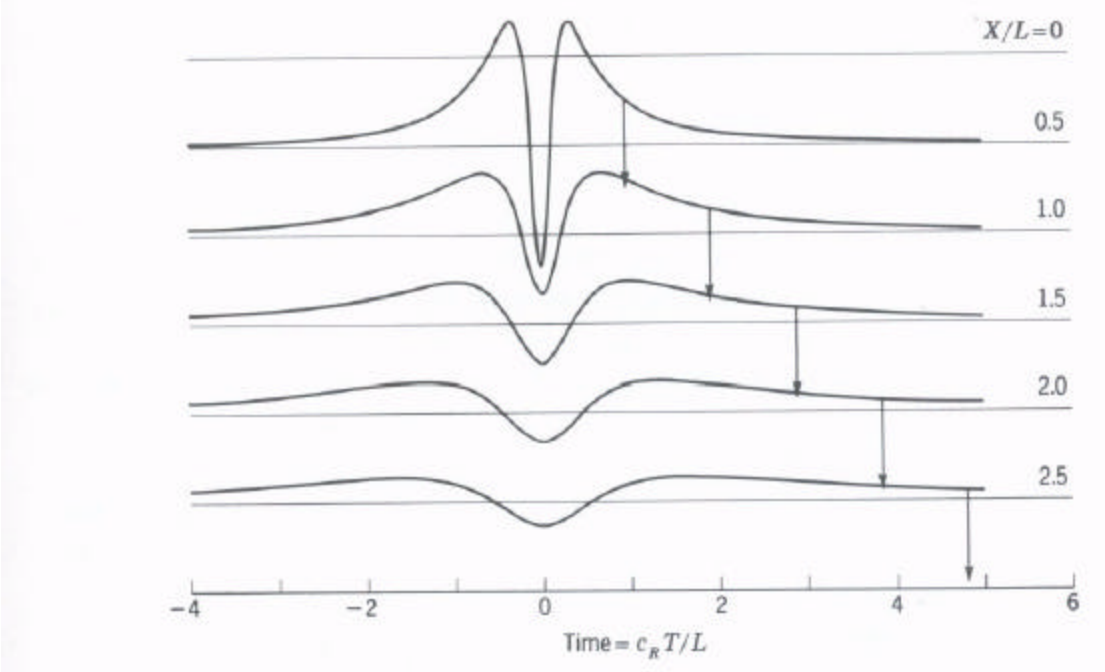


**Figure 2.4:** Pressure in a borehole caused by the passage of Rayleigh wave. Horizontal particle velocity in the Rayleigh wave is taken to vary as δ(t) at the origin [White, 1965].

It is interesting to note that a differently predefined Rayleigh wave the resultant pressure wave can have a different impact altogether. A prominent feature is the *d*

function, of opposite polarity to the assumed horizontal particle velocity, representing a tube wave travelling down the hole.

A Rayleigh wave from an oscillating source will presumably have a harmonic effect on borehole water. The periodicity of water level response will be of the same order of magnitude as the driving force although the phase may differ from the field observations mainly due to the development of secondary waves (Hugen's principle) that may distort the effect of the original wave.

In the case of the work of White (1965), it is important to note that the mathematical solution of the pressure depends on the conceptualisation of the effect of the Rayleigh wave.

### 2.3.2 Rayleigh waves

The manifestation of Rayleigh waves from pump vibrations and probably their dominance in aquifer deformation cannot be underestimated. It is for this reason that a discussion on these waves is covered in this section.

The characteristics of the Rayleigh waves are described in detail by Telford *et al.* (1990), Kearey and Brooks (1985). Foti (2000) compiled the characteristics of these waves for different media including the multilayered media such as the Karoo aquifers. For the multilayered systems, the following points regarding Rayleigh waves are worth highlighting (Foti, 2000):

i. The phase velocity is frequency dependent, also for an elastic medium (geometric dispersion).

ii. In general, for a given frequency several free vibration modes exist, each one characterised by a given wavenumber and hence a given phase velocity. The different modes involve different stress and displacement distributions with depth.

iii. It is necessary to distinguish group velocity from phase velocity.

iv. Particle motion on the ground surface is not necessarily retrograde.

In the presence of an external source acting on the ground surface it is necessary to account for mode superposition, that which has some major consequences:

a. The geometrical attenuation is a complicated function of the mechanical properties of the whole system.

b. The effective phase velocity is a combination of modal values and is spatially dependent.

v. Because of the difference between phase velocity and group velocity, mode separation takes place moving away from the source and hence the pulse changes shape.

It is also important to note the characteristics of these waves in homogeneous media in order to obtain an explanation for the dominance of some phenomena in Karoo aquifers and not in others. The characteristics concerning Rayleigh waves in a homogeneous half space are (Foti, 2000)

- Their velocity of propagation is quite similar to that of shear waves. The ratio between the two is a function of the Poisson ratio, but it is comprised in a very narrow range (0.87 to 0.96).
- The associated particle motion is elliptical retrograde on the surface, with the major axis being vertical.
- The propagation involves only a limited superficial portion of the solid, having a thickness nearly equal to one wavelength.
- Geometrical attenuation as the wave departs from a point source is related to the square root of distance and hence it is less sensible than for body waves.
- Considering a circular footing vibrating at low frequency, about 2/3 of the input energy goes in surface waves and only the remaining portion in body waves.
- Their material attenuation is much more influenced by shear wave attenuation than by longitudinal waves one.

As discussed above, White (1965) demonstrated theoretically the impact of Rayleigh waves on borehole waves leading to the generation of tube water waves; however, the system is more complicated when viewed holistically. There are two half-spaces of interest for a pumping borehole, namely, the ground surface and the atmosphere; and the intact geology and the inside of the borehole as the wave propagates vertically down the borehole. The propagation of the latter constitutes a point source for the subsequent waves that propagate into the geosphere (Hugen's principle). Owing to (*ii*), different wave trains are regenerated giving rise to phase velocities. Depending on the phase angle, the superposition of these different waves can lead to high displacements (Foti, 2000) which are capable of inducing significant deformations. In relatively homogeneous isotropic linear elastic halfspace Rayleigh waves are not

dispersive (Foti, 2000), that is, their velocity of propagation is a function of the mechanical properties of the medium, but it is not a function of frequency. It therefore follows that the manifestation of deformation in stratified media is not only dependent on frequency but also on the mechanical properties of the media. Again it can be postulated that the deformations are more pronounced when pumping the borehole at a certain frequency, hence explaining the inconspicuousness in some pumping test data.

## 2.4 DISCUSSIONS

The deformation of an aquifer and the propagation of vibrations depend on its mechanical properties.

The harmonic force imparted on an aquifer due to pump vibrations propagates as a seismic wave. Of significance is that the displacement measured on the ground surface is an indication of the strain and stress experienced by the aquifer (Equation 2.7). Depending on the elastic threshold of the geological formations involved, the intense pump vibrations can add to the fatigue and the failure of a fracture as observed by Botha and Cloot (2002). Considering only one aspect and ignoring the other in projecting the longevity of a system may give longer timeframes than the actual. The inclusion of pump seismicity in the model of Botha and Cloot (2002) may significantly alter the timeframes.

The development of borehole waves caused by sound pressure can also cause borehole water to oscillate (Newton's third law of motion). The important aspect is that water will also be flushed into the aquifer, specifically into the fracture. If the driving force is harmonic, the flushed water will also respond harmonically according to Newton's third law of motion. This excitation is imparted on to the fracture planes. In essence, the diaphragmatic response of an aquifer can also be driven from within by water and not just by the vibrations. This aspect is investigated in the field.

The work of White (1965), though theoretical, has an important bearing on the aquifer dynamics discussed in the following chapters. It highlights the action-reaction phenomenon that forms the core of the work covered in this thesis.

The work covered in this chapter is generic since the aim was to outline deformation and waves theories, which form the basis of the work that follows. Problem-specific models are therefore developed in Chapter 3.

# CHAPTER 3

# MODEL DEVELOPMENT

## 3.1 INTRODUCTION

In Chapter 2 it was shown that the external force applied to a body may be transmitted in the form a wave (Equation 2.11). Depending on the characteristics of the external force applied and on the mechanical properties of the body, Equation (2.11) becomes problem specific.

The aim of the chapter is to formulate problem-specific mathematical models taking into account the characteristics of the external force and of the body. The models should be descriptive of the diaphragmatic deformation principle proposed.

The pump vibrations are the source of the external force and the body of interest is an aquifer. A harmonic force will be generated by the vibrations. The amplitudes and wavelengths of the vibrations are to a larger extent determined by the specifications of the pump and the characteristics of the electricity supply (or generator for a diesel-driven pump). The mechanical properties peculiar to an aquifer should be incorporated into the model.

The impact of the pump on an aquifer is not decoupled into sound or seismic waves. The central argument is that the oscillations detected in drawdown curves are due to aquifer deformation induced by pump behaviour. Therefore, irrespective of whether the driving force is through the matrix or direct pressure on borehole water level, oscillations should develop.

Both one- and two-dimensional models are developed. The intention is to investigate the sensitivity and the detail involved in the manifestation of oscillations. The one-dimensional model is limited to the direct impact of pump vibrations on the water table. The model assumes a direct relationship between the force imparted on the aquifer and the response of the borehole water. The two-dimensional model is more comprehensive, however, allowing the use of all possible scenarios that may cause the oscillations shown in the drawdown curve (see Figure 1.2). It takes into account the geometry of the aquifer, that is, the properties of the matrix and fracture. It is essential to note that the oscillations in Figure 1.2 were observed when pumping and therefore by coupling the seismic effect of the pump to the groundwater flow and the

mechanical deformation models investigated by Botha and Cloot (2002), the field conditions are simulated.

Central to the analysis of both models is the assigning of boundary conditions. The formulation of boundary conditions is based on the physics of the system. For instance, the normal stress from a pumping borehole is treated and imposed at the borehole position as a harmonic function and a zero Dirichlet boundary condition is assigned far from the source term. In analysing the two-dimensional model, the Galerkin technique grafted on the finite element method is applied. The essence of the technique is discussed further on in this chapter.

The force generated by a pump is dominant in the horizontal plane by virtue of its rotation. However, it has a vertical component as well; confirmed in the field by the response of a geophone sensitive only to vertical ground motion. The characteristics of the geophone are elaborated on in the instrumentation section in Chapter 4. According to the hypothesis, it is the vertical component that engineers the proposed diaphragmatic deformation of a hydrostratigraphic unit and therefore only oscillations relative to the vertical component of the displacement are considered.

The one-dimensional model is formulated and solved analytically in Section 3.3. Similarly, the two-dimensional model is formulated in Section 3.4. In order to solve the two-dimensional model, the boundary conditions are explicitly imposed and are described in Section 3.5. The Galerkin technique, which is instrumental in solving these models, is outlined briefly in Section 3.6 and its application is illustrated in Section 3.7. The overall discussions are conducted in Section 3.8.

The numerical results are presented in Chapter 4 where a comparison with field data is made.

## 3.2 HYPOTHESES

In general, oscillations in drawdown curves are prevalent in boreholes equipped with electric and diesel pumps. At high discharge rates these pumps tend to vibrate intensely, generating mechano-, geo-acoustic and to some extent thermal deformations. These *pump effects* are intense close to the pump and could add significantly to the failure of horizontal fractures.

The proposed diaphragmatic principle argues that horizontal fractures deform during pumping. Fracture planes constrict and dilate forcing the water in between to respond accordingly as illustrated in Figure 3.1. The change in fracture aperture determines the amplitudes of oscillations that can be observed in sampled drawdown curves.

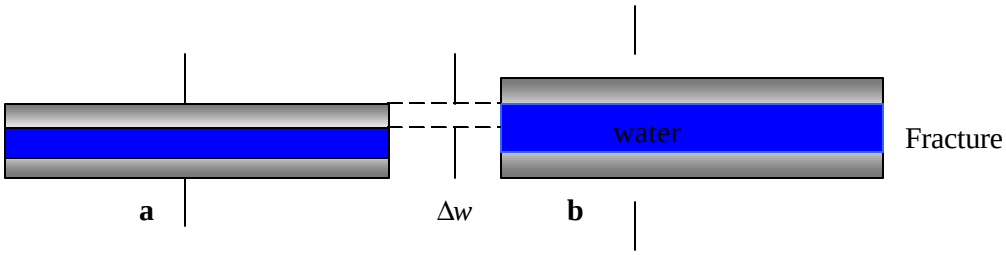


**Figure 3.1:** The diaphragm behaviour of a fracture with impermeable planes. Stage (a) is constriction and (b) dilation. The difference in aperture size between the two phases, $\Delta w$, forms the wave amplitude.

Fracture deformation can be induced during pumping activity in three ways namely:

- uneven pump frequency;
- discharge rate; and
- pump seismicity.

### 3.2.1 Deformations generated by uneven pump frequency

The flow of water from the fracture into the borehole and to the surface is not *constant*. This is something that is common at the borehole-fracture interface. Water flowing from the fracture to a borehole is not immediately discharged to the surface on reaching the pump owing to changes (jerks) in frequency caused by fluctuations in voltage (Driscoll, 1989). Rarefaction and compressional waves are generated as water flows back temporarily into the fracture. The resultant pressure waves exert force on the fracture planes causing the dilatation and constriction of the fracture when subsiding. It is this phenomenon of rarefaction and compressional waves that result in the diaphragmatic behaviour of the fracture. This *voltage jerk phenomenon* is commonly associated with diesel-driven pumps and rarely associated with electric pumps. Since the oscillations were observed in a borehole equipped with an electric pump, this hypothesis cannot be the main cause of oscillations in our specific case and therefore will be disregarded in this work.

### 3.2.2 Deformation due to fracture water loss

According to Biot's theory (1956), water abstraction from an aquifer should be the most obvious cause of fracture deformation. The loss of water through pumping will significantly reduce the hydrodynamic force **H,** according to the force distribution in

Figure1.6, leading to the dominance of the normal force from the mechanical vibrations of the pump. According to Biot's theory, the system (an aquifer in this case) will oscillate when disturbed. Biot (1956) developed a system of equations to justify this principle. Botha and Cloot (2001) adopted the theory and apply applied it to Karoo aquifers. The computed results did not show oscillations in the drawdown curves observed in the field, although they did indeed show that aquifers deform when pumped. However, their model did not take the seismicity caused by the pump into account. The inclusion of the pump seismicity in the numerical model in this work could make a difference.

### 3.2.3 Deformation due to pump seismicity

The mechanical vibrations of the pump generate a normal stress, which induces the constriction and dilatation of the fracture. Owing to the presence of water, a hydrostatic force opposing the normal force develops. Since the normal stress is harmonic, so is the hydrostatic force that results. The entire behaviour results in a diaphragmatic deformation and hence the oscillations that are observed in the pumping test data (Figure 1.2). Fracture constriction displaces water causing the water level of the borehole to rise. Dilation restores the fracture state by inducing an influx of water that leads to a drop in the water level of the borehole. It is the repetition of these two antagonistic processes that gives rise to the oscillations observed in the drawdown curves. The constriction and the dilatation processes are so rapid that it is difficult to observe the oscillations in manually sampled pumping test data. This could be the main reason why oscillations are not a feature familiar to most groundwater practitioners. The presence of oscillations in pump test data depends on the resolution and sensitivity of the equipment used (Botha *et al*., 1998).

Coupled with the direct effect of pump seismicity is the sound pressure variation. Pressure variation on the water level can also induce oscillations. It is, however, not within the scope of this research to decouple these two aspects of the pump. In view of the complexity of the dynamics, the focus will be on the pump vibrations.

For the purposes of this study, the last two hypotheses are regarded as the prime causative factors for the diaphragmatic deformation of fractures and for that reason they are investigated further.

## 3.3 ONE-DIMENSIONAL MODEL

The combination of theories discussed in subsections 3.2.2 and 2.2 is considered to be the major cause of fracture deformation in practical operations.

For practical purposes, the impact of pump seismicity can be investigated by switching on the pump without allowing the discharge of water. This explicitly forms the basis of the derivation of the one-dimensional model shown later in this chapter.

The derivation of the mathematical model is focused on the impact of seismic wave $y$ in Equation (2.11) on reaching a hydrostratigraphic unit. The unit of interest to the research is a deeply situated bedding fracture. The conceptual model shown in Figure1.6 is used for this purpose.

Considering the system in dynamic equilibrium, the force distribution can be expressed as:

$$\mathbf{F} + \mathbf{B} - \mathbf{H} - \mathbf{D} = \mathbf{0} \tag{3.1}$$

Since the behaviour of interest in the system is in the vertical plane, forces acting on the fluid in the horizontal plane can be ignored. This reduces the model to

$$\mathbf{F} - \mathbf{H} = \mathbf{0} \tag{3.2}$$

By virtue of the geometry of the system (borehole and groundwater flow behaviour) setup, which resembles a cylinder (Figure 3.2), the cylindrical coordinate system is considered (Figure 3.2).

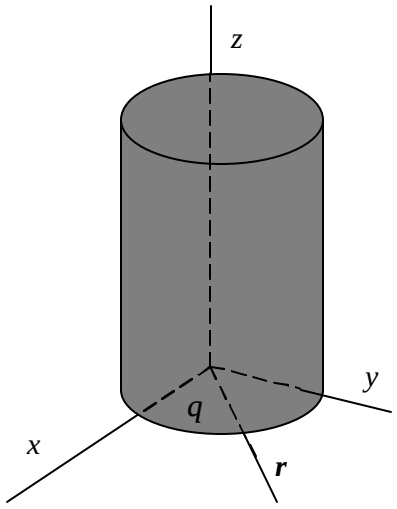


**Figure 3.2:** The cylindrical coordinate system applied with the centre of the borehole as the origin.

According to the coordinate system the groundwater flow velocity **V** would have three components given by

$$\mathbf{V} = \begin{bmatrix} v_r \\ v_q \\ v_z \end{bmatrix} \tag{3.3}$$

Since the research is focused on the vertical deformation caused by normal stress generated by the pump, the angular component $q$ of the dynamics can be ignored. The radial and vertical components of Equation 3.2 can be written as

$$F_r - H_r = 0$$

and

$$F_z - H_z = 0$$

respectively.

It should be reiterated that the driving force **F** consists of the normal stress from the pump and also the gravitational force. In this case the hydrodynamic force **H** is the force exerted by the fracture water when subjected to normal stress.

In formulating the mathematical model for the system, the approach adopted in subsection 2.2.2 is repeated. The normal force in this case is considered to be acting on the solid matrix of the aquifer. The fraction of the solid matrix in an aquifer is expressed as $(1-e)$ where $e$ is the porosity.

The approach will modify Equation (2.7) to

$$r_s(1-e)\frac{\partial^2 w}{\partial t^2} = \nabla^2 s_s \tag{3.4}$$

where $s_s$ is the actual stress acting on the solids, $r_s$ is the density of the solid matrix and $\nabla^2$ in this case in the cylindrical coordinates is reduced to:

$$\nabla^2 = \frac{\partial^2}{\partial r^2} + \frac{1}{r}\frac{\partial}{\partial r} \tag{3.5}$$

The Young modulus E is a constant and the displacement $w$ is a function of time $t$ and radial distance $r$, that is, $w = w(r,t)$. Using Equations (2.3), (2.4) and (3.5), Equation (3.4) is rewritten as

$$(1-e)\,r_s \partial^2_{t^2} w = G\frac{1}{r}\partial_r(r\partial_r w)\ ,\quad G=\frac{E}{2(1+v)} \qquad (3.6\ a)$$

where $v$ is the Poisson coefficient, $G$ is the shear modulus and $E$ is the Young modulus.

The mathematical model (Equation 3.6a) is descriptive of ground displacement with radial distance from the excited pump. If the deformities shown in Figure 1.1, including pump vibrations, are responsible for the collapse of bedding fractures in Karoo aquifers, then it clearly explains why successful boreholes are drilled within a few metres of the failed boreholes (Rasmussen, 1998).

The model is similar to Equation (2.7) except that it is specific to the aquifer scenario. Like Equation (2.7), the model describes the displacement of the ground as the pump vibrations propagate through the aquifer. The formulation of the model in terms of the radial component is due to the fact that the oscillations registered in a borehole are as a result of the summation effect of the normal force from the pump over the area of its influence.

The next step is to formulate a relation between the seismic wave propagating in an aquifer and the water-level response in a borehole. This is achieved by solving Equation (3.6).

In order to find the analytical solution of Equation (3.6) boundary conditions are applied. The following boundary conditions were selected in accordance with the assumed harmonic force generated by pump vibrations.

For undisturbed water level at time $t=0$, the boundary condition is given by

$$w(r,0)=\partial_t w(r,0)=0$$

This boundary condition simulates the condition when the pump is not operating, implying no ground displacement and velocity.

When pumping, ground motion at pump position is described by

$$w(R_o,t)=w_o \sin wt$$

The condition assumes the harmonic ground motion resulting from the pump vibrations. Far from the pumping borehole, that is a distance $L$, the ground motion is zero, thus

$$w(L,t) = 0$$

where $R_o$ is the radius of the borehole, $L$ is the length of the aquifer, and $w$ is the frequency of excitation.

The first step is to apply a transformation function, Equation (3.7), in order to generate homogeneous boundary conditions.

$$w = \mathrm{v} + w_o\left(\frac{r-L}{R_o-L}\right)\sin wt \qquad (3.7)$$

Inserting Equation (3.7) into Equation (3.6) yields an equation for v (Equation 3.6 b).

$$m^2\partial_{t^2}^2\mathrm{v} - \frac{1}{r}\partial_r(r\partial_r\mathrm{v}) = \frac{w_o}{(R_o-L)}\left[\frac{1}{r} + m^2(r-L)w^2\right]\sin wt \qquad (3.6\ \mathrm{b})$$

where $m^2 = \frac{(1-e)}{G}r_s$ from Equation (3.6). For Equation (3.7) to be consistent with the proposed boundary conditions, the following conditions are imposed:

$$\mathrm{v}(R_o,t) = 0;\ \mathrm{v}(L,t) = 0;\ \mathrm{v}(r,t) = 0;\ \partial_t\mathrm{v}\big|_{t=0} = \frac{-ww_o(r-L)}{(R_o-L)}$$

Applying the principle of superposition and expressing the solution $\mathrm{v}(r,t)$ as a sum of two solutions $v_1(r,t)$ and $v_2(r,t)$, that is as:

$$\mathrm{v}(r,t) = \mathrm{v}_1(r,t) + \mathrm{v}_2(r,t)$$

satisfying the respective equations defined as follows:

For $\mathrm{v}_1(r,t)$

$$m^2\partial_{t^2}^2\mathrm{v}_1 - \frac{1}{r}\partial_r(r\partial_r\mathrm{v}_1) = 0 \qquad (3.8\ \mathrm{a})$$

$$\mathrm{v}_1(R_o,t) = 0;\ \mathrm{v}_1(L,t) = 0$$

$$v_1(r,0) = 0\,;\ \partial_t v_1\big|_{t=0} = \frac{-ww_o(r-L)}{R_o - L}$$

and for $v_2(r,t)$

$$m^2\partial_{t^2}^2 v_2 - \frac{1}{r}\partial_r(r\partial_r v_2) = \frac{w_o}{R_o - L}\left[\frac{1}{r} + m^2(r-L)w^2\right]\sin wt \qquad (3.8\ b)$$

$$v_2(R_o,t) = 0\,;\ v_2(L,t) = 0$$

$$v_2(r,0) = 0\,;\ \partial_t v_2\big|_{t=0} = 0$$

### 3.3.1The solution of $v_1(r,t)$

The solution of $v_1(r,t)$ in Equation (3.8a) is determined in this section as follows:

Let $v_1(r,t)$ be a composite function of $R_1(r)$ and $T_1(t)$ expressed as:

$$v_1(r,t) = R_1(r)T_1(t) \qquad (3.9)$$

Substituting Equation (3.9) into Equation (3.8 a) we get Equations (3.10) and (3.11). The partition into two equations stems from the fact that both terms in Equation (3.8a) have to be zero for it to balance.

$$\Rightarrow \begin{cases} m^2\partial_{t^2}^2 T_1 + k^2 T_1 = 0 & (3.10) \\ \dfrac{1}{r}\partial_r(r\partial_r R_1) + k^2 R_1 = 0 & (3.11) \end{cases}$$

Equation (3.11) is satisfied by the Bessel functions of index 0;

$$R_1 = \mathrm{OJ}_o(kr) + ?\,\mathrm{Y}_o(kr)$$

applying b-c

$$\begin{cases} \mathrm{OJ_o}(kR_o) - ?\,\mathrm{Y_o}(kR_o) = 0 \\ \mathrm{OJ_o}(kL) - ?\,\mathrm{Y_o}(kL) = 0 \end{cases}$$

The non-trivial solution of Equation (3.11) is provided by:

$$\mathrm{J_o}(k_l R_o)\mathrm{Y_o}(k_l L) - \mathrm{J_o}(k_l \mathrm{L})\mathrm{Y_o}(k_l R_o)$$

that is, defining the eigenvalues $k_l$; $l = 1, 2, \cdots$

For such values we have

$$?_{\,l} = \frac{-\mathrm{O}_l \mathrm{J_o}(k_l R_o)}{\mathrm{Y_o}(k_l R_o)}$$

and $R_{1,l}$ reads

$$R_{1,l} = \mathrm{O}_l \left[ \mathrm{J_o}(k_l r) - \frac{\mathrm{J_o}(k_l R_o)\mathrm{Y_0}(k_l r)}{\mathrm{Y_o}(k_l R_o)} \right]$$

For $\mathrm{T}_1$ we have

$$T_{1,l} = E_l \sin\frac{k_l}{m}t + F_l \cos\frac{k_l}{m}t$$

$$\mathrm{v}_1 = \sum_l T_{1,l} R_{1,l}$$

$$\mathrm{v}_1 = \sum_l (a_{1,l} \sin\frac{k_l}{m}t + F_l \cos\frac{k_l}{m}t)(\mathrm{J_o}(k_l r) - \frac{\mathrm{J_o}(k_l R_o)\mathrm{Y_o}(k_l r)}{\mathrm{Y_o}(k_l R_o)}$$

but

$$\mathrm{v}_1(r,0) = 0$$

Implying $F_l = 0 \;\; \forall l$ hence,

$$\partial_t \mathrm{v}_1(r,0) = -\frac{ww_o(r-L)}{(R_o - L)} = \sum_l a_{1,l} \frac{k_l}{m}(\mathrm{J_o}(k_l r) - \frac{\mathrm{J_o}(k_l R_o)\mathrm{Y_o}(k_l, r)}{\mathrm{Y_o}(k_l R_o)})$$

Furthermore expanding $\frac{-ww_o(r-L)}{(R_o-L)}$ in Bessel series

$$= \sum_{m=1}^{\infty} C_{om} \mathrm{J}_o(k_m r)$$

This provides a set of equations for the remaining coefficients $a_{1,l}\ \forall l$ .

### 3.3.2 The solution for $\mathrm{v}_2(r,t)$

The solution of $\mathrm{v}_2(r,t)$ in Equation (3.8b) is determined in a similar way as $\mathrm{v}_1(r,t)$, but because of its heterogeneity the Duhamel method is applied.

In applying the Duhamel method to find $\mathrm{v}_2$, one replaces the inhomogeneous problem by a homogeneous equivalent assuming that the inhomogeneous term becomes the initial condition applied at time $t < t$ . In this case the homogeneous equivalent considered for Equation (3.8 b) is $V(r,t)$ and the homogeneous part becomes

$$m^2 \partial_{t'}^2 \mathrm{V} = \frac{1}{\mathrm{r}} \partial_r (r \partial_r \mathrm{V})$$

with the following boundary conditions:

$$V(R_o,t) = 0,\ V(L,t) = 0,\ V(r,t) = 0,$$

According to Duhamel method the initial boundary condition becomes

$$\partial_t V(r,t) = \frac{w_o}{(R_o - L)} \left[ \frac{1}{r} + m^2 (r-L) w^2 \right] \sin wt$$

Then it follows that $\mathrm{v}_2(r,t) = \int_0^t \mathrm{V}(r,t,t)dt$

We have

$$V = \sum_l (b_{1,l} \sin \frac{k_l t}{m} + b_{2,l} \cos \frac{k_l t}{m})(J_o(k_l r) - \frac{J_o(k_l R_o) Y_o(k_l r)}{Y_o(k_l, R_o)})$$

and therefore

$$V(r,t) = 0 \text{ and } b_{2,l} = b_{1,l} \tan \frac{(k_l t)}{m}$$

Implying

$$V = \sum_l b_{1,l} (\sin \frac{k_l t}{m} - \tan \frac{(k_l t)}{m} \cos \frac{k_l t}{m})(J_o(k_l r) - \frac{J_o(k_l R_o) Y_o(k_l r)}{Y_o(k_l, R_o)})$$

For $b_{1,l}$, again we make a Bessel expansion of

$$\frac{w_o}{(R_o - L)} \left[ \frac{1}{r} + m^2 (r - L) w^2 \right] \sin wt$$

and identifying the coefficient of this series with

$$\partial_t V\big|_t = (J_o(k_l r) - \frac{J_o(k_l R_o) Y_o(k_l r)}{Y_o(k_l R_o)}) \sum_l b_{1,l} \frac{k_l}{m} (\cos \frac{k_l t}{m} + (\tan \frac{k_l t}{m})(\sin \frac{k_l t}{m}))$$

Provide $b_{1,l} \quad \forall l \quad b_{1,l} = b_{1,l}(k_l, t)$

Further, one has $v_2(r,t) = \int_0^t V(r,t,t)dt$ that is

$$v_2(r,t) = (J_o(k_l r) - \frac{J_o(k_l R_o) Y_o(k_l r)}{Y_o(k_l R_o)}) \sum_l \left[ \int_0^t b_{1,l} (\sin \frac{k_l t}{m} - \tan \frac{k_l t}{m} \cos \frac{k_l t}{m}) dt \right]$$

Finally

$$w(r,t) = v_1 + v_2 + w_o \frac{(r - L)}{(R_o - L)} \sin wt$$

According to the proposed diaphragmatic deformation hypothesis, the changes in water level, $\Delta z$, are due to the constriction and dilation of the fracture resulting from the normal force from pump vibrations. In essence the integration of the displacements over the aquifer area at any given time expressed as:

$$\frac{4}{R_o} \int_{R_o}^{L} w(r,t) r dr$$

is equated to the changes in water level to give

$$\Delta z(t) = \frac{4}{R_o}\int_{R_o}^{L} w(r,t)rdr \qquad (3.12)$$

## 3.4 THE TWO-DIMENSIONAL MODEL

The model (Equation 3.12) formulated in the preceding section addressed the problem in one dimension. In this section a two-dimensional model is formulated which takes into account both the vertical and the horizontal components of the system. By introducing the vertical component the hydrostatic force becomes effective. It is this additional aspect that separates the two models. However, strictly speaking the system of equations outlined in this section is not two- but three-dimensional and the two-dimensional aspect will only surface when solving the equations. From this point onwards in this thesis the hydrodynamic pressure that has been represented by $H_p$ is replaced simply by a $p$ to be consistent with the notation in Botha and Cloot (2002).

As stated in Chapter 1, the two-dimensional model is grafted on the work of Botha and Cloot (2002) and the only difference is in the way the system of the equations is solved.

The generalised form of Equation (3.4) is given as

$$r_s(1-e)\partial^2\mathbf{?}/\partial t^2 = \nabla\cdot\mathbf{s} + \mathbf{F}^m \qquad (3.13)$$

where

$$\nabla = \hat{\mathbf{r}}\frac{\partial}{\partial r} + \hat{\mathbf{?}}\frac{\partial}{r\partial q} + \hat{\mathbf{z}}\frac{\partial}{\partial z}$$

with $\mathbf{F}^m$ accounting for external forces such as gravity and $\underline{\underline{s}}$ is the stress tensor. As before the angular variations are ignored.

### 3.4.1 Water response

According to the proposed hypothesis, the normal stress caused by pump vibrations will generate strain $e$ on a fracture, which can be expressed in terms of aperture change as

$$e = \nabla \cdot \mathbf{u} \qquad (3.14)$$

The volumetric dilatation $e$ is negative when the fracture is constricted by the normal stresses from the pump and positive when dilated. Coupled with the strain change s is the change in porosity. The change in fracture water content $q_w$ can be described with an equation of the form

$$q_w(s, p) = e = e_o + e(s, p) = e_o + e(x, y, z, t) \qquad (3.15)$$

where $e_o$ is the residual porosity of the fracture inherited from the matrix history.

The density of the water, $r_w$, will also be affected by the stresses experienced by the fracture and the pressure exerted by the fluid. The impact of these forces can be described through the constitutive relation for density of a fluid

$$D_p r_w = b r_w \text{ where } D_p = \partial / \partial p$$

where $b_w$ is the isothermal compressibility coefficient of the water, which can be expressed as (Kruseman and De Ridder, 1994):

$$b_w = \frac{-dV_w / V_w}{dp}$$

where $V_w$ is the volume of water and the change in hydrodynamic pressure is given by $dp$. The negative sign shows the inverse relation between the two variables. The density is therefore expressed with an equation of the form

$$r_w(\mathbf{z}, t) = r_w^o [b_w p(\mathbf{z}, t)]$$

Applying the assumption that the rate of fracture deformation, $\mathbf{v}^f$ is small, together with Equation (3.14), the classical groundwater equation (Botha, 1996; Bear, 1979):

$$D_t(r_w q_w) = \nabla \bullet [r_w(\mathbf{K} \nabla j - q_w \mathbf{v}^f)] + r_w F_w$$

can be rewritten in the form

$$\rho_w D_t e + \beta_w \rho_w e D_t p = \nabla \bullet [\rho_w (\mathbf{K} \nabla j)] + \rho_w F_w \qquad (3.16)$$

where $j$ is the piezometric head. In a saturated medium, assuming that $e_o$ is constant, the left hand side of Equation (3.16) can expressed as

$$\rho_w^2 g(D_p e + \beta_w e) D_t j = \rho_w^2 g(D_p e + \beta_w e) D_t j \qquad (3.17)$$

For a seismic wave to be transmitted effectively in an aquifer the assumptions made are that the grains of the rock matrix are compressible and the normal stress caused by pumping remains constant. The assumptions allow the volumetric compressibility of the rock matrix to be defined as (Botha, 1996; Bear, 1972; Bear 1979):

$$\alpha = -\frac{1}{V_b} D_s V_b = \frac{1}{1-e} D_p e \qquad (3.18)$$

Substituting Equation (3.17) into Equation (3.16) gives

$$\rho_w^2 g(D_p e + \beta_w e) D_t j = \rho_w^2 g[(1-e)\alpha + \beta_w e] D_t j = \rho_w S_o D_t j \qquad (3.19)$$

The equation differs from the conventional models used to describe the flow of groundwater by the replacement of the volumetric compressibility of the rocks in the specific storativity, $S_o$, with the dilatational strain. Burbey (2001) also expressed this parameter in terms of the mechanical properties of the rock (Equation 3.20).

$$S_o = \rho_w g \left[ \frac{3(1-2\nu)}{2G(1+\nu)} + e\beta_w \right] \qquad (3.20)$$

The dilatational strain is the real physical mechanism controlling the specific storativity, $S_o$, of an aquifer. The relation is very important for the management and control of boreholes because the dilatational strain is a function of the displacement

vector **u**, which may not just depend on the compressibility of the fracture, but also on other parameters such as the discharge rate of a borehole (Botha and Cloot, 2002). According to the research, the storativity determines the volume of water that may be available when a fracture deforms diaphragmatically.

### 3.4.2 The rock specie

The characteristics and behaviour of the rock specie are described in detail in the work of Botha and Cloot (2002), and in this section the essential aspects relevant to this work are highlighted.

If it is assumed that there are no sources and sinks of the rock matrix specie and that the solids in the matrix are in compressible ($r_m$ is a constant), the continuum equation for the rock matrix reduces to

$$D_t(1-e) = -\nabla \cdot [(1-e)\mathbf{v}^m] \tag{3.21}$$

and the equation of motion is expressed as

$$r_s(1-e)\frac{d}{dt}\mathbf{v}^m = \nabla \cdot \mathbf{s}^m + \mathbf{B}^m$$

where use was made of the relations $q_m = (1-e)$ and $r_m = r_m(1-e)$. It will again be assumed that $\mathbf{v}^m$, which is nothing other than the time derivative of the displacement experienced by the rock matrix, henceforth denoted by $\mathbf{u}$, is small. The convective terms in the equation of motion for the rock matrix may therefore be ignored and the total time derivative replaced by its equivalent partial derivative to obtain

$$r_s(1-e)D_t^2\mathbf{u} = \nabla \cdot \mathbf{s}^m + \mathbf{B}^m \tag{3.22}$$

This equation will obviously not be complete unless explicit expressions are provided for the stress tensor and the body forces. To achieve this, the stress tensor $\mathbf{s}^m$ will, according to Newton's third law of motion, consists of two components – the stresses experienced by the rock matrix, $\mathbf{s}$ and its interaction with the fluid pressure.

Therefore the stress tensor for a water-saturated rock matrix in the subsurface of the earth is of the form

$$\mathbf{s}^{m} = \mathbf{s} + ep\mathbf{I} \tag{3.23}$$

where I is the unit Cartesian tensor.

If it is assumed that the deformations experienced by the rock matrix are small, Hooke's law can be used to relate the stress tensor, $\mathbf{s}$, to the strain tensor, $\mathbf{e}$, and hence the displacements $\mathbf{u}$. Biot (1941) expresses these relations in the form

$$\begin{aligned}
s_{11} + ep &= 2G(e_{11} + \frac{n}{1-2n}e) \\
s_{22} + ep &= 2G(e_{22} + \frac{n}{1-2n}e) \\
s_{33} + ep &= 2G(e_{33} + \frac{n}{1-2n}e) \\
s_{12} &= 2G\bar{e}_{12},\ s_{13} = 2G\bar{e}_{13},\ s_{23} = 2G\bar{e}_{23}
\end{aligned} \tag{3.24}$$

and the strain as

$$\begin{aligned}
e_{11} &= \frac{1}{E}[s_{11}(1+n) - ns + (1-2n)p] \\
e_{22} &= \frac{1}{E}[s_{22}(1+n) - ns + (1-2n)p] \\
e_{33} &= \frac{1}{E}[s_{33}(1+n) - ns + (1-2n)p] \\
e_{12} &= \frac{s_{12}}{2G},\ e_{13} = \frac{s_{13}}{2G},\ e_{23} = \frac{s_{23}}{2G}
\end{aligned} \tag{3.25}$$

with

$$s = s_{11} + s_{22} + s_{33}$$

the trace of the stress tensor $\mathbf{s}$ .

The possibility exists that rocks may not obey the linear functions Equations (3.24) and (3.25), especially near boreholes that are pumped at high discharge rates. In such cases the rock may not regain its original form once the stress is removed, but retains *residual strain*. This suggests that it would be more appropriate to express the strains as

$$\mathbf{e} = \mathbf{e}^{o} + \mathbf{e}^{1}(\mathbf{s}, p)$$

where $\mathbf{e^o}$ denotes the residual strains induced by stresses and $\mathbf{e}^1$ the dependence of the strains on the stresses and pressure.

Although there are a large number of functions that could be used to represent the non-linear behaviour of the stresses and strains, the present discussion will be based on the following non-linear relation

$$e_{ij}^{1} = \frac{s_{ij}^{T} s_{ij}^{C}}{E(s_{ij}^{t} + s_{ij}^{C})} \ln \frac{s_{ij}^{T}(s_{ij}^{1} + |s_{ij}^{C}|)}{|s_{ij}^{C}|(s_{ij}^{T} - s_{ij}^{1})}, \quad (i, j = 1,2,3) \tag{3.26}$$

where $\mathbf{s}^1$ is the tensor with elements given by the numerators of the expansions of $e_{ij}$ in Equation (3.25)

$$s_{ii}^{1} = [s_{ii}(1+n) - sn + (1-2n)p]$$

$$s_{ij}^{1} = (1+n)s_{ij} \quad (i, j = 1, 2, 3) \tag{3.27}$$

The approximation of $\mathbf{e}^1$ in Equation (3.26) has two advantages. The first is that it reduces to the linear expressions for the strains in Equation (3.25) if

$\left|s_{ij}^{C}\right| = a\, s_{ij}^{T}$ and $s_{ij}^{1} / s_{ij}^{T} \to 0$ as shown by the Taylor series of the components of $\mathbf{e}^1$

$$e_{ij}^{1} = \frac{s_{ij}^{1}}{E}\left[1 - (1-a)\frac{s_{ij}^{1}}{2a\, s_{ij}^{T}} + (1 - a + a^{2})\frac{(s_{ij}^{1})^{2}}{3(a\, s_{ij}^{T})^{2}} + \cdots + o\left(\frac{s_{ij}^{1}}{a\, s_{ij}^{T}}\right)^{n}\right]$$

This approximation is very useful because it can be used to linearise Equation (3.26) and to represent the linear part of Hooke's law when the aquifer deforms. The second advantage is that it represents many of the properties of the stress-strain relations for rocks, as represented in Jaeger (1969). These include plastic behaviour whenever the stresses become very large and the strengthening of the material under compression. This behaviour is best seen when comparing the various curves of the rocks in Jaeger with the graph of the inverse of Equation (3.26).

$$s_{ij}^{1} = (s_{ij}^{T} \left| s_{ij}^{C} \right|) \frac{\exp[w(e_{ij}^{1})] - 1}{\left| s_{ij}^{C} \right| \exp[w(e_{ij}^{1})] + s_{ij}^{T}}, \quad w(e_{ij}^{1}) = \frac{e_{ij}^{1} E(\left| s_{ij}^{C} \right| + s_{ij}^{T}}{\left| s_{ij}^{C} \right| s_{ij}^{T}} \qquad (3.28)$$

Equations (3.28) and (3.30) apply only in the case where the magnitudes of these stresses and strains increase non-linearly. It is because of this characteristic that they are referred to as the non-linear law of Hooke.

### 3.4.3 System of equations

In the work of Botha and Cloot (2002), the system of equations summarised in this section was used primarily to investigate the impact of the discharge rate on aquifer deformation.

In the thesis, these equations form the basis on which the effect of pump vibrations is built. This approach is grafted on the fact that the oscillations in Figure 1.2 were observed when the borehole was pumping and vibrating.

The capability of the equations hinged on how well they represent both the mechanical properties of the aquifer and the dynamics therein. These equations are as follows:

$$r_w D_t e + b_w r_w e D_t p = \nabla \cdot [r_w (\mathbf{K} \nabla j)] + F_w$$

$$r_s (1 - e) D_t^2 \mathbf{u} = \nabla \cdot \mathbf{s}^s + \mathbf{F}^s$$

$$q_w(\mathbf{s}, H_p) = e = e_o + e(\mathbf{s}, p)$$

$\mathbf{e} = \mathbf{e}^o + \mathbf{e}^1(\mathbf{s}, p)$ where $e^o$ is the residual strain.

$$e_{ij}^{1} = \frac{s_{ij}^{T} s_{ij}^{C}}{E(s_{ij}^{t} + s_{ij}^{C})} \ln \frac{s_{ij}^{T}(s_{ij}^{1} + |s_{ij}^{C}|)}{|s_{ij}^{C}|(s_{ij}^{T} - s_{ij}^{1})}, \quad (i, j = 1,2,3) \qquad (3.29)$$

$$s_{ij}^{1} = [s_{ij}(1+s) - ss + (1-2s)p]$$

$$s_{ij}^{1} = (1+s)s_{ij} \qquad (i, j = 1,2,3)$$

$$e = \nabla \cdot \mathbf{u} = e_{11} + e_{22} + e_{33}$$

The solving of these equations is based on the Petrov-Galerkin finite element approximation of the equations. It is the solving of these equations that marks the point of departure of the current work from the work of Botha and Cloot (2002).

## 3.5 BOUNDARY CONDITIONS

### 3.5.1 General

The above system of equations is solved by making use of boundary conditions which simulate the dynamics of the system as observed in the field.

The physics of the system evolves around the mechanics of the pump and the reaction of the aquifer to the pump. Assessing the impact of abstraction in isolation is not a priority of the research. In fact this aspect of the dynamics was addressed in the work of Botha and Cloot (2002). Since the proposed hypothesis involves hydrodynamic pressure, $H_p$, – although not extensive – simulations are conducted for different discharge rates to quantify its contribution to the development of oscillations. However, the boundary conditions imposed in the Botha and Cloot (2002) model will not be changed. Botha and Cloot (2002) assigned a constant flux boundary (Neumann boundary condition) to a borehole as the discharge rate and a constant head boundary (Dirichlet boundary condition) far from the pump when solving the groundwater flow equations. In order to solve the ground motion models a similar set of boundary conditions was added.

### 3.5.2 Boundary conditions applied to ground motion models

The boundary condition commonly applied to the system at any point in time prior to pumping is

$$w(r,0) = \partial_t w(r,0) = 0 \tag{3.30}$$

The condition states that for a borehole that is not pumping, the ground displacement is zero. When the pump is switched on, the ground motion induced at the edge of a borehole of radius $R_o$ is assumed to be of the form

$$w(R_o, t) = w_o \sin wt \tag{3.31}$$

Far from pump vibrations, that is, at a distance $L$ away, the ground motion is expressed as

$$w(L, t) = 0 \tag{3.32}$$

These conditions are the same as those applied to the one-dimensional model in Section 3.3.

### 3.5.3 Applying boundary conditions to the model

In the field the ground vibrations were observed to obey an exponential-like decay with distance from a pumping borehole (Figure 3.3), so when assigning the boundary condition (Equation 3.31), a distance $L_o < L$ is considered (Figure 3.4) where the vibrations are effective. In this scenario the pump vibrations are applied at the aquifer and the water response is monitored. This is the best representation of the proposed diaphragmatic deformation.

Similar to this set-up is the introduction of a foreign source of seismic energy. A hammer and a plate were used as external sources of energy and the reaction of the borehole water was monitored. In numerical terms the boundary conditions are depicted in Figure (3.5). The simulated drawdown curves are compared to field data.

Alternatively, the oscillatory function can be added to the flow to determine the aquifer response on the ground surface. The approach is instrumental in identifying the contribution of the intermittent flashing in and out of water in a fracture. The fracture deformation induced, as proposed in subsection 3.2.1, is simulated. The set-up in Figure 3.4 can be repeated here except that the boundary condition is applied to the flow, which is in accordance with the cup effect of the pump.

It should be noted that when applying these conditions in solving the numerical model, the condition

$$w(r, z=0, t) = w_o \sin wt \ , \ \forall r \in [R_o, L], \ \forall t \geq 0$$

is observed.

## 3.6 THE GALERKIN FINITE ELEMENT METHOD

The application of finite element approximation in solving a differential equation is common (Botha and Pinder, 1983; Cakmak *et al.*, 1987).

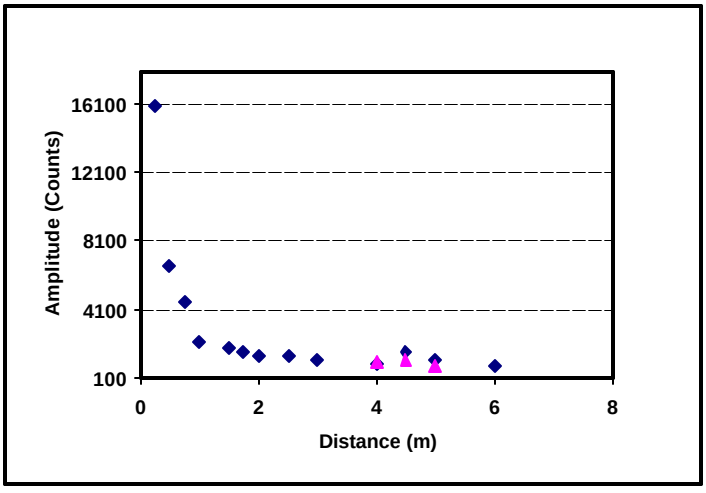


**Figure 3.3:** Ground motion with distance from an excited pump which is not discharging water. The pink triangles indicate the repetition of sampling at the stations. The amplitudes in counts are directly proportional to displacement in nanometres.

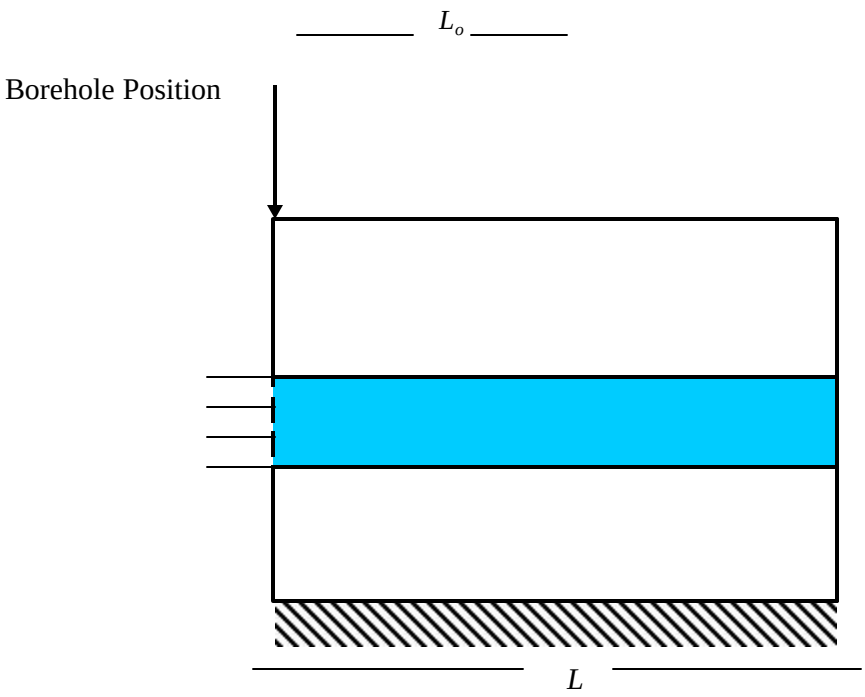


**Figure 3.4:** Boundary conditions assigned to the aquifer with particular reference to pump characteristics.

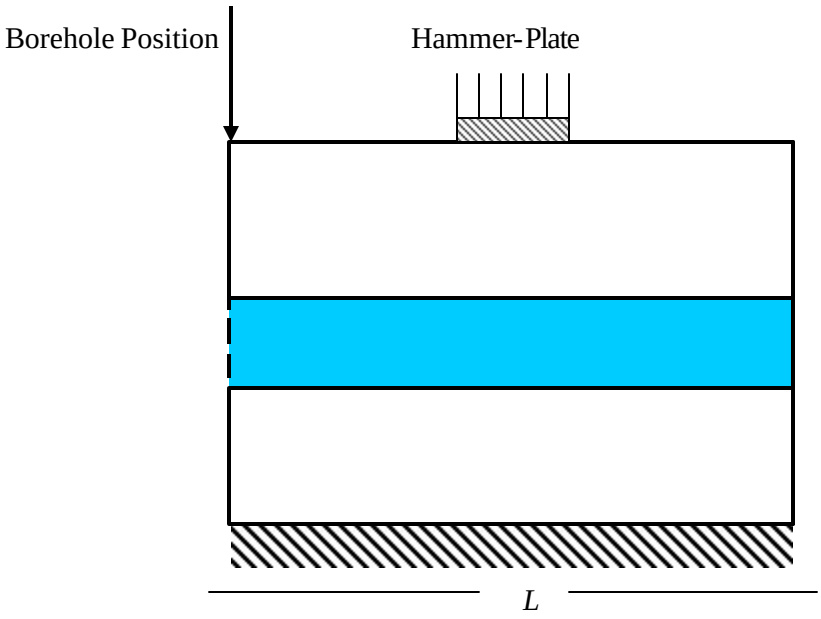


**Figure 3.5:** Boundary conditions assigned to the aquifer for the introduction of the hammer-plate as the source of seismic energy.

The basic principle behind the approximation is to approximate the dependent variable $u(\mathbf{x})$ in a differential equation such as

$$\mathbf{L}u(\mathbf{x}) = F \tag{3.33}$$

as the sum of set of known, piecewise continuous polynomials, $f_i(\mathbf{x})$ say, in the independent variables, $\mathbf{x}$,

$$u(\mathbf{x}) = \sum_{j=1}^{N} f_j(\mathbf{x}) u_j \tag{3.34}$$

The unknown coefficients, $u_j$, are then determined by substituting this sum into Equation (3.33) and forcing the set of weighted residuals

$$f_i(x)\sum_{j=1}^{n} f_j(\mathbf{x})u_j - F \qquad (i = 1, \cdots, m)$$

to be zero in some average sense. In the case of the Galerkin finite element method, this is achieved by integrating the residuals over the domain of the differential equation, $\Omega$, and equating each residual to zero. This operation generates, in general, a set of algebraic equations of the form

$$\int_{\Omega} f_i(\mathbf{x})[\mathbf{L}\sum_{j=1}^{n} f_j(\mathbf{x})u_j - F]d\Omega = 0\,, \qquad (i = 1, \cdots, n)$$

that can be solved for the unknown $u_j$, which on substitution into Equation (3.34) will yield an approximate solution of Equation (3.33).

## 3.7 DISCRETISATION OF THE MODEL

### 3.7.1 The conservation of fluid mass

The manifestation of the diaphragmatic deformation of a fracture is due to the compressibility of water $b_w$ (Equation 3.35) induced by seismic waves from a pump. The compressibility serves as a shock absorber preventing the collapsing of the

fracture. The water displaced in the process finds sanctuary in the borehole, which leads to water level fluctuations.

$$b_w = \frac{-dV_w / V_w}{dp} \tag{3.35}$$

To accommodate the compressibility of water, Eq uation (3.15) which is strictly valid for incompressible fluid flow is transformed so as to be applicable to compressible fluid flow. This is achieved by expressing the Darcy flux in terms of the permeability of the medium instead of the hydraulic conductivity as (Childs and Collis-George, 1950; Botha and Cloot, 2002)

$$\mathbf{K}\nabla j\ (x,t) = \frac{\mathbf{k}}{m}\nabla(p + r_w gz)$$

Although it is possible to relate the permeability tensor, $\mathbf{k}$, to the porosity of a porous medium, since there is no available information on the tensorial properties of the permeability for Karoo aquifers, it will be assumed that the permeability is a scalar, that the medium is isothermal and that the viscosity of the fluid $m$ is constant. Applying the assumptions and Equation (3.13) transforms the equation governing the conservation of fluid mass into a deformable porous medium and a compressible fluid which is found to be of the form

$$r_w D_t \nabla \cdot \mathbf{u} + b_w r_w e D_t p = \nabla \cdot [r_w (\frac{k}{m}\nabla(p + r_w gz)] + F_w \tag{3.36}$$

If the vectors

$$\hat{\mathbf{u}}(t) = \{\mathbf{u}_o(t), \mathbf{u}_1(t), \cdots \mathbf{u}_N(t)\}$$

$$\hat{\mathbf{p}}(t) = \{p_0(t), p_1(t), \cdots p_N(t)\} \tag{3.37}$$

are used to denote the time-dependent coefficients of the semi-discrete approximations for the displacement and pressure respectively, the system of

equations arising from the finite element discretisation of Equation (3.36) can be expressed symbolically as

$$\mathbf{p}\cdot D_t\hat{\mathbf{u}}(t)+QD_t\hat{\mathbf{p}}(t)+\frac{k}{m}[\hat{\mathbf{p}}(t)\mathbf{R}+\mathbf{b}]=\mathbf{?}+\mathbf{f} \tag{3.38}$$

Alternatively the time derivative approximations of, $D_t\hat{\mathbf{u}}(t)$ and $\hat{\mathbf{p}}(t)$, which are

$$D_t u_j(t)\cong\frac{u_j(t_{k+1})-u_j(t_k)}{\Delta t} \tag{3.39}$$

$$p_j\cong l_k(t)p_j(t_k)+l_{k+1}p_j(t_{k+1})$$

are used to transform (3.38) to

$$\mathbf{p}\cdot\hat{\mathbf{u}}+\hat{\mathbf{p}}^{n+1}(\mathbf{Q}+\frac{k}{m}\mathbf{R}\Delta t)=\mathbf{p}\cdot\hat{\mathbf{u}}^n+\mathbf{Q}\hat{\mathbf{p}}^n+(\mathbf{?}+\mathbf{f}-\frac{k}{m}\mathbf{b})\Delta t \tag{3.40}$$

The symbols **P**, **Q** and **R** in these equations are matrices with elements

$$p_{ij}=\int_\Omega r_w(\mathbf{x},t)f_i(\mathbf{x})\nabla f_j(\mathbf{x})d\Omega$$

$$q_{ij}=\int_\Omega b_w e(\mathbf{x},t)\,r_w(\mathbf{x},t)f_i(\mathbf{x})f_j(\mathbf{x})d\Omega$$

$$r_{ij}=\int_\Omega r_w(\mathbf{x},t)(1+b_w gz)\nabla f_i(\mathbf{x})\cdot\nabla f_j(\mathbf{x})d\Omega$$

while **f**, **?** and **b** are vectors with elements

$$f_i=\int_\Omega r_w(\mathbf{x},t)f_i(\mathbf{x},t)F(\mathbf{x},t)d\Omega$$

$$g_i=\int_s r_w(\mathbf{x},t)g(\mathbf{x},t)f_i(\mathbf{x},t)dS$$

$$b_i = \int_{\Omega} g r_w^2(\mathbf{x},t) D_z f_i(\mathbf{x},t) d\Omega$$

where

$$g(\mathbf{x},t) = \mathbf{n} \cdot (k/m) f_i(\mathbf{x}) \nabla j(\mathbf{x},t)$$

represents a Neumann boundary condition and therefore only exists if the prescribed boundary conditions entail either a non-homogeneous Neumann or a Cauchy boundary condition.

### 3.7.2 The equation of motion

The discretisation procedure is also applied to the equation of motion if provision is made for the non-linearities in the stresses associated with the matrix skeleton.

The equation of motion can be expressed as

$$r_s(1-e) D_t^2 \mathbf{u} = \nabla \cdot (\mathbf{s} + \mathbf{I}ep) + \mathbf{B}^m$$

where $p$ is the fluid pressure, $e$ the porosity of the medium, $\mathbf{s}$ are the stresses created by forces other than the water pressure and $\mathbf{I}$ the unit matrix. Multiplication of this equation by the basis function, $f_i(\mathbf{x})$, and the application of Green's theorem to the right-hand side of the equation yield

$$\int_{\Omega} r_s(1-e) f_i(\mathbf{x}) D_t^2 \mathbf{u} d\Omega = -\int_{\Omega} \nabla f_i(\mathbf{x}) \mathbf{s}\, d\Omega + \int_{\Omega} f_i(\mathbf{x}) \nabla \cdot \mathbf{I}ep d\Omega + \int_{\Omega} f_i(x) B^m d\Omega + \int_{d\Omega} f_i(\mathbf{x}) \mathbf{s} \cdot \mathbf{n} dS \qquad (3.41)$$

where $\mathbf{n}$ is the unit normal vector on the outside of the boundary, $d\Omega$ of $\Omega$. The first term on the right-hand side of Equation (3.41) can be simplified by replacing $\mathbf{s}$ with the linearised form of $\mathbf{s}^1$ in Equation (3.42) expressed in terms of the dilatational strain, $\mathbf{e}$, defined as

$$\mathbf{e} = \frac{1}{2}[\nabla \mathbf{u} + (\nabla \mathbf{u})^T]$$

and as

$$\mathbf{s} \cong \mathbf{s}_o + 2G[\mathbf{e} + \{\nu/(1-2\nu)\mathbf{I}\, e]$$

to obtain

$$\int_\Omega \nabla f_i(\mathbf{x})\mathbf{s}\, d\Omega = \int_\Omega G\nabla f_i(\mathbf{x}) \cdot [\nabla \mathbf{u} + (\nabla \mathbf{u})^T + \{\nu/(1-2\nu)\}\mathbf{I}e]d\Omega + \int_\Omega \nabla f_i(\mathbf{x})\mathbf{s}_o d\Omega$$

The spatial finite element approximation of Equation (3.41) is therefore given by

$$\mathbf{M}D_t^2\hat{\mathbf{u}}(t) + \mathbf{H}\hat{\mathbf{u}}(t) + \mathbf{V}\hat{\mathbf{u}}^T(t) - \mathbf{W}\hat{\mathbf{p}}(t) = \left(\frac{\nu}{1-2\nu}\right)\mathbf{d}^e + \mathbf{s}^o + \mathbf{b}^m + \mathbf{s}^b$$

or if Equation (3.39) is used to approximate the time derivative, $D_t^2\hat{\mathbf{u}}(t)$

$$\mathbf{M}\hat{\mathbf{u}}^{n+1} + (\Delta t)^2[\mathbf{H}\hat{\mathbf{u}}^{n+1} + \mathbf{V}\hat{\mathbf{u}}^{n+1} - \mathbf{W}\mathbf{p}^{n+1}] = \mathbf{M}[2\mathbf{u}^n - \mathbf{u}^{n-1}] + (\Delta t)^2\left[\left(\frac{\nu}{1-2\nu}\right)\mathbf{d}^e + \mathbf{s}^o + \mathbf{b}^m + \mathbf{s}^b\right] \quad (3.42)$$

The symbols $\hat{\mathbf{u}}(t)$ and $\hat{\mathbf{p}}(t)$ are defined as in Equation (3.37), while **M**, **H**, **V** and **W** are matrices with elements

$$m_{ij} = \int_\Omega f_i(\mathbf{x})\, r_s(1-e) f_j(\mathbf{x}) d\Omega$$

$$h_{ij} = \int_\Omega G\nabla f_i(\mathbf{x}) \cdot \nabla f_j(\mathbf{x}) d\Omega$$

$$v_{ij} = \int_\Omega G\nabla f_i(\mathbf{x}) \cdot [\nabla f_j(\mathbf{x})]^T d\Omega$$

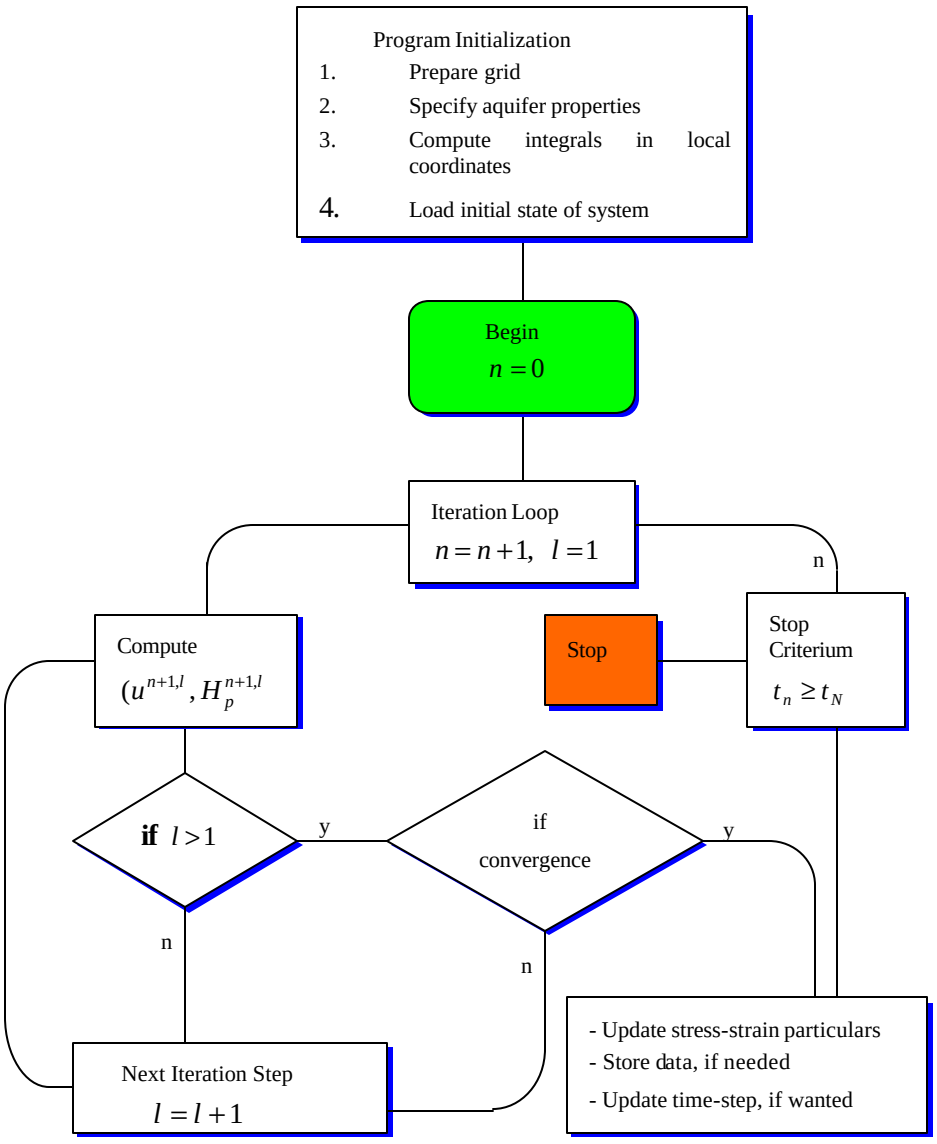


**Figure 4.3:** Flow chart of the general algorithm used to solve the system of Equations 3.40 and 3.42.

$$w_{ij} = \int_{\Omega} f_i(\mathbf{x}) e \nabla f_j(\mathbf{x}) d\Omega$$

and $\mathbf{d}^e$, $\mathbf{s}^o$ and $\mathbf{b}^m$ vectors with elements

$$d_i^e = \int_{\Omega} G f_i(\mathbf{x}) \mathbf{I} e d\Omega$$

$$s_i^o = \int_{\Omega} \nabla f_i(\mathbf{x}) \cdot s_o d\Omega$$

$$b_i^m = \int_{w} \nabla f_i(\mathbf{x}) \mathbf{B}^m d\Omega$$

$$s_i^b = \int_{d\Omega} f_i(\mathbf{x}) \mathbf{s} \cdot \mathbf{n} dS$$

Equations (3.40) and (3.42) represent a set of four equations, which can be used to solve for the four unknowns $\hat{\mathbf{u}}^{n+1}$ and $\hat{\mathbf{p}}^{m+1}$. It is important though to note this system of equations has to be solved iteratively if $\mathbf{s}$ is non-linear, as illustrated by the flow chart of the general algorithm in Figure 3.5.

## 3.8 DISCUSSIONS

Central to this chapter is the formulation of the mathematical models that will simulate the response of an aquifer when pumped. The one-dimensional model simulated the direct relation between the matrix deformation and water level response in an aquifer. The model does not take into account the hydrodynamic pressure the water may impose on the normal stresses generated by a pump. Apart from that it is independent of pumping.

The two-dimensional model is not directly developed in this chapter but a system of equations is adopted from Botha and Cloot (2002). In essence it is a three-dimensional model which is reduced to a two-dimensional model on solving. The idea of adopting the model is not to repeat the work of Botha and Cloot (2001) but to add the seismic effects caused by the pump to the model equations, which Botha and Cloot (2001) neglected to do. The pump seismicity is added as boundary conditions, which defined the framework of the mathematical solution of both the deformation models and the groundwater flow models. The Galerkin technique is then applied to solve the nonlinear models by generating approximating solutions using basis functions which

converge in the intended solution through iterations. This linearised the nonlinear models in a piecewise fashion, thus making the computations simpler and faster.

In the next chapter, the models are solved numerically.

# CHAPTER 4

# FIELD INVESTIGATIONS AND NUMERICAL RESULTS

## 4.1 GENERAL

Thus far the discussions have revolved mainly around the formulation of mathematical models and little has been mentioned about field investigations. Refocusing on practical investigations forms the central theme of this chapter with the purpose of investigating the scenarios generated in Chapter 3.

Several experiments aimed at investigating various causative factors suspected of directly or indirectly influencing the mechanics of oscillations were conducted. The experiments integrated the seismological and hydrogeological aspects of the system, taking into account the pump seismicity and borehole water responses. The geophone, Event Acquisition Recording System (EARS), equipped borehole and hammer constituted the seismological component with pressure transducers adding a hydrogeological dimension to the total package of the equipment used.

The chapter starts with a discussion of the Campus Test Site in Section 4.2, where the experiments were primarily performed, and this also forms the basis for the model developed by Botha and Cloot (2002). The section also outlines the geology and the hydrogeology of the aquifer highlighting its unique features. The field investigations are discussed in Section 4.3 and the comparison with the numerical results of both the one- and two-dimensional models is conducted in Section 4.4. The chapter concludes with a discussion summing up the field investigations and the numerical work in Section 4.5.

## 4.2 CAMPUS TEST SITE

### 4.2.1 Geology

The Campus Test Site at the University of the Free State covers an area of approximately 180 x 192 $m^2$, and was originally intended as a test site for postgraduate students. Several percussion boreholes and core-boreholes have been drilled into the aquifer over the years with the intention of understanding its intrinsic characteristics. The positions of the holes are shown in Figure 4.1. Five of the seven core-boreholes were drilled vertically and two at an inclination of $45^o$ to verify the

horizontal orientation of the fracture that forms the main conduit of water to boreholes on the site (Botha, *et al.*, 1998).

The geology of the site is characteristic of the Beaufort Group of the Karoo Supergroup (Kent and SACS, 1980). The site is situated partially on a basal outcrop of Spitskop Sandstone, but mainly on the underlying Campus Sandstone. Outcrops of the mudstones that overlie the Campus Sandstone are superficially covered by soil and clay.

### 4.2.2 Geometry

There are three aquifers present on the Campus Test Site, as shown in Figure (4.2). The first aquifer is a phreatic aquifer that occurs in a laminated alternation of mudstones and siltstones (6-9) m thick, and a fine-grained, cross-laminated rhythmite sequence (1-6) m thick. A black carbonaceous shale layer, (0.5-4) m thick separates the first aquifer from the second and main aquifer. This aquifer occurs in the 8-11 m thick Campus Sandstone layer, and is confined. Unique to the second aquifer is the presence of a bedding fracture approximately 21 m below the surface (Figure 4.3) that slices the sandstone hydrostratigraphic unit into two subunits. Tracer tests conducted at the Site showed that in borehole UO28, one of the boreholes used in the investigations covered in the thesis, the fracture is situated at a depth of 20.5 m (Chiang and Riemann, 2001).

The effective aperture width of the fracture is 10 mm (Botha *et al.*, 1998). The third aquifer, also a confined aquifer, occurs in a succession of interbedded mudstone.

## 4.3 FIELD INVESTIGATIONS

### 4.3.1 Instrumentation

In the investigations, STS 8730 pressure transducers (Figure 4.4 a) were installed in boreholes UP16 and UO28 to observe water levels. The transducers had the following specifications:

- Temperature range: –5°C to 50°C
- Max pressure: 3 bar

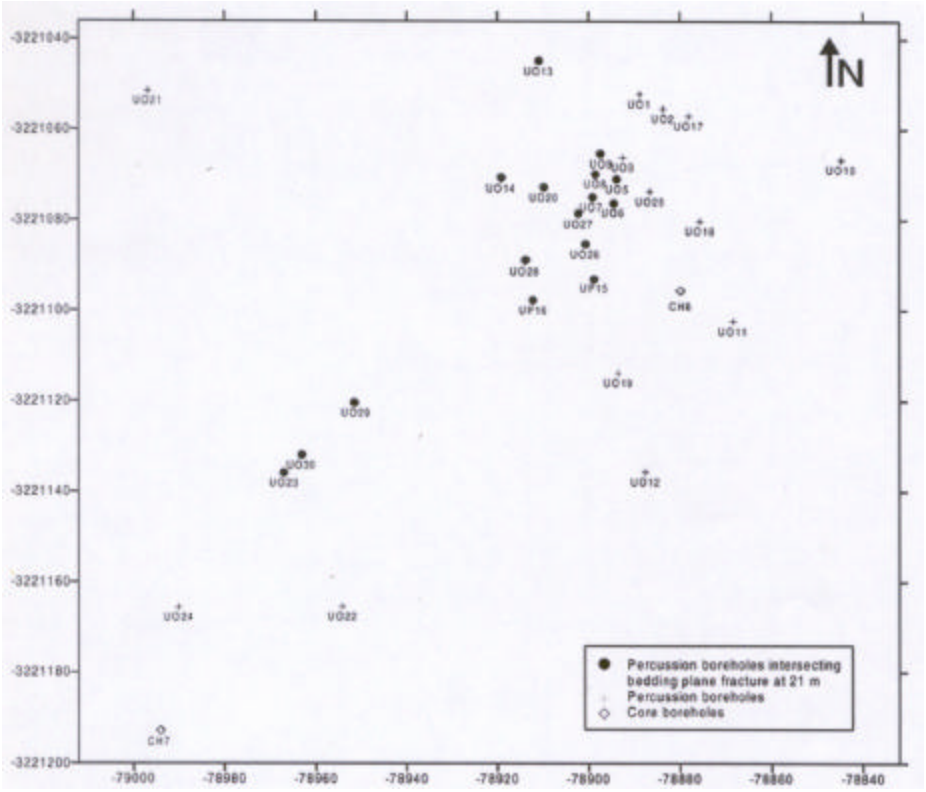


**Figure 4.1:** Borehole layout on the Campus Site. Coordinate origin (vertical axis) – 3221036m, (horizontal axis) –78832 (m)

The ground motion was recorded using Event Acquisition Recording System (EARS) (Figure 4.5 a) and the three-legged geophone (Figure 4.5 b) as the sensor. For the positioning and referencing of the data, a global positioning system (Figure 4.4 b) was connected to the EARS.

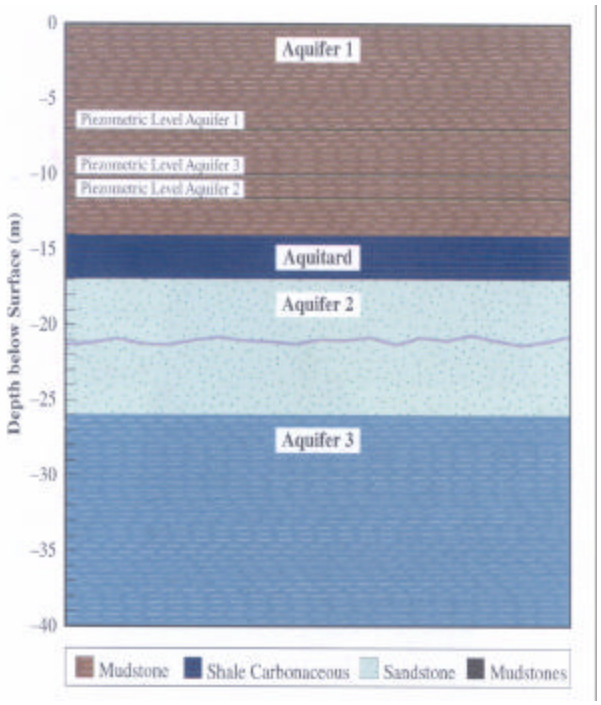


**Figure 4.2:** Schematic diagram of the different geological formations and aquifers present on the Campus Test Site [Botha *et al.*, 1998]


**Figure 4.3:** Captured borehole video images of the fracture in borehole UO23 at the test site. The fracture is at a depth of 21.1 – 21.2 m below ground level.

The specifications of the EARS as provided by the manufacturer are given in Table 4.1. In the experiment the buffer ring was set to 10 seconds. This is the period during which data will be recorded completely before it responds to any further excitations.

**Table 4.1:** Specifications of EARS

| SPECIFICATIONS |
|---|
| 3 Differential input channels |
| 18 bit Sigma-Delta Conversion |
| 108 dB Dynamic range |
| 4 Gain settings to interface with a variety of seismometers |
| Common mode rage of ± 2.5 volts @gain 1 |
| Sample rates: 25 up 200 samples per second |
| Automatic DC offset calibration |
| Integrated anti-alias filters<br>RS 232 interface to Data Acquisition unit |
| Power 10.8 KW |

A submersible pump installed in UP16 at a depth of 30 m was used in the investigations.

The SM-6 Geophone of the B-coil type was used in the investigations as a sensor. Three components of ground motion are recorded, namely the vertical (Z), the Northern (N) and the Eastern (E) (Figure 4.6). These components are helpful when characterising waves. The Rayleigh and the Love waves generated by a seismic source in the earth's surface are identified by the Z component, which the latter waves do not have (Telford *et al.*, 1990). The geophone specifications provided by the manufacturer are given in Table 4.2.

*a* *b*

**Figure 4.4:** The STS pressure transducers (a) used for water-level acquisition and the GPS (b) used for data referencing of ground motion in the EARS.


*a* *b*

**Figure 4.5:** The Event Acquisition Recording System (a) and the three-legged geophone (b) used in the acquisition of ground motion.

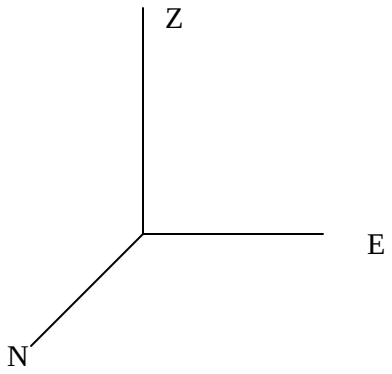


**Figure 4.6:** The configuration of the three components recorded by the geophone.

### 4.3.2 SEISAN

The SEISAN seismic analysis system is a complete suite of programs and a simple database for analysing earthquakes from analogue and digital data. The programs of relevance to this study are *dirf*, MAKEREA, MULPLT and EEV.

In the analysis conducted in this thesis, field data stored in the EARS are downloaded into a working directory (BLOEM) (C\SEISMO\WOR\BLOEM) created using MAKEREA. Two folders, REA and WAV, are also created automatically in the

process. The REA folder contains field readings and WAV stores the digital data files. For the program to recognise the data, the program *dirf* is run which assigns identification numbers to the traces. The MULPLT program is used for displaying traces. The picking of amplitudes, velocities, phase readings and plotting of traces is done using the EEV program.

The ground motion option was selected for the calculation of the ground motion. It offers the option of calculating displacement (nm), velocity (nm/sec) or acceleration (nm $s^{-2}$). The details of the SEISAN program are outlined in the SEISAN manual (Havskov and Ottemöller, 2001).

**Table 4.2:** The SM-6 geophone specifications

| SPECIFICATIONS | |
|---|---|
| **Frequency** | |
| Natural frequency | 4.5 Hz |
| Typical spurious frequency | 140 Hz |
| Tolerance | ±0.5 Hz |
| **Damping** | |
| Open circuit damping | 0.56 |
| Open circuit damping tolerance | +/- 5% |
| **Sensitivity** | |
| Open circuit sensitivity | 28.8 V/m/s (0.73 V/in/s |
| Tolerance | ±5% |
| Moving mass | 11.1g (0.39 oz) |
| **Resistance** | |
| Standard coil resistance | 375 Ω |
| Tolerance | ±0.5 % |
| **Physical** | |
| Diameter | 25.4 mm (1 in) |
| Height | 36 mm (1.42 in) |
| Weight | 81 g (2.85 oz) |
| Operating temperature range | - 40 $^{o}$C to 100$^{o}$C (-40$^{o}$F to +212 $^{o}$F) |

### 4.3.3 Experiments

#### 4.3.3.1 General

The investigations were conducted using boreholes UP16 and UO28, which are 8.95 m apart. Borehole UP16 is equipped with a submersible pump installed at 30 m below

ground level. In both boreholes pressure transducers were installed to keep track of groundwater fluctuations. Seismic stations were marked at 1 m intervals from UP16 to UO28 as shown by red dots in the schematic layout in Figure 4.7. The stations were used for seismic sounding. The hammer-plate and the sensor were configured on these stations and the water level was continuously recorded throughout the experiments. The downloading of the water-level readings from the pressure transducers was done at the end of the entire fieldwork.

To enhance the oscillatory behaviour in the water level signals, the first derivatives were conducted. The derivatives were plotted adjacent to the field readings. The forward derivative technique was used which is expressed as:

$$\frac{h_i - h_{i-1}}{\Delta t}$$

The piezometric heads $h_i$ and $h_{i-1}$ were captured at times $t_i$ and $t_{i-1}$ respectively (Wang and Anderson, 1982).

The traces captured in the field per experiment are incorporated in the text. The amplitudes of traces as recorded by the respective components of the geophone were determined and in cases where the components are not determined explicitly it should be assumed that the maximum amplitude of the composite signal is implied. The seismic traces are plotted on the vertical axis with amplitudes of traces recorded by the respective components of the geophone, and time in seconds is plotted on the horizontal axis. The numbers, which are illegible in some cases inside traces plots, are the minimum and maximum amplitudes of the signal that triggered the geophone.

In order to study the frequencies giving rise to the signals, Fourier transformation was conducted on a selected seismic signal. The main objective of the transformations was to determine the significance of mains frequency supplied to the pump in the overall ground motion caused by pump vibrations.

#### 4.3.3.2 Experiment 1

The purpose of the first experiment was to determine the characteristics of waves generated by the pump. The pump was switched on and not allowed to discharge water. Ground motion was recorded at stations at increasing distances from the pump.

The maximum amplitudes of ground motion at each station were plotted (Figure 4.8). The pink triangles in the figure are repeated readings intended to verify the first readings, which showed a deviation from the trend displayed by the preceding

readings. The amplitudes were read directly from the EARS monitor and no conversion to displacement was done since this needed post-processing software. However, it should be noted that the amplitudes displayed are directly proportional to the conventional displacement (Havskov and Ottemöller, 2001).

The seismic readings taken at stations 4, 4.5 and 5 metres showed amplitudes in nanometre range (Table 4.3). The corresponding seismic traces from stations 4, 4.5 and 5 are shown in Figures 4.9, 4.10 and 4.11. The responses of the water levels in both boreholes, UP16 and UO28, were captured and are shown in Figures 4.12 and 4.14 with the first derivatives in Figures 4.13 and 4.15 respectively.

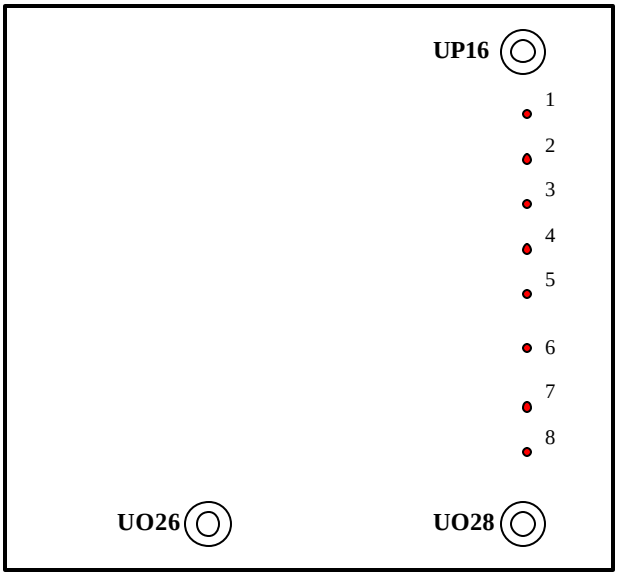


**Figure 4.7:** The schematic layout of the boreholes and stations on the Campus Test Site used in the field investigations

The graph (Figure 4.8) shows an exponential-like decay of the amplitude with distance from the pumping borehole. The characteristic is of a direct wave (surface wave) and not a body wave because of the closeness to the source (Kearey and Brooks, 1995; D'Arnaud Gerkins, 1989), which is typical of a Rayleigh wave (Telford *et al*., 1990), a member of the surface.

It travels along the surface of the earth and involves a combination of longitudinal and transverse motion. The characteristics of the Rayleigh waves are detailed in Chapter 2. The fact that the geophone recorded a vertical motion distinguished the wave from the Love wave – another member of the surface waves that propagates parallel to the ground surface. The amplitude of the Rayleigh wave decreases exponentially with depth (Telford *et al.*, 1990).

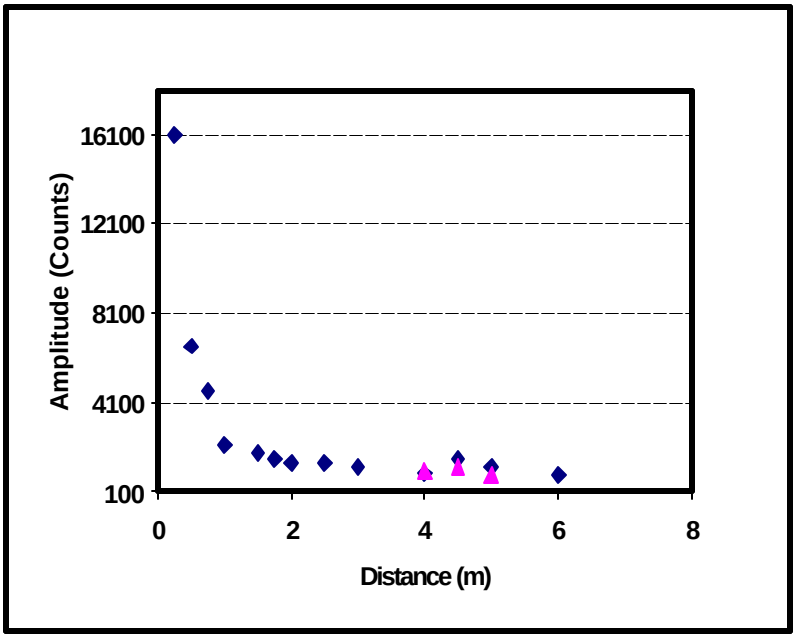


**Figure 4.8:** Ground motion with distance from an excited pump that is not discharging water. The pink triangles indicate the repetition of sampling at the stations. The amplitudes in counts are directly proportional to displacement in nanometres.

**Table 4.3:** Ground characteristics as the pump in UP 16 is excited without discharging

| Station | Ground Displacement (nm) | Ground Velocity (nm $s^{-1}$) | Ground Acceleration (nm $s^{-2}$) |
|---|---|---|---|
| 4 | 1529834.8 | 77811728.0 | 7103732224.0 |
| 4.5 | 1465853.1 | 75551728.0 | 7324891136.0 |
| 5 | 1253128.8 | 64297120.0 | 5460332032.0 |

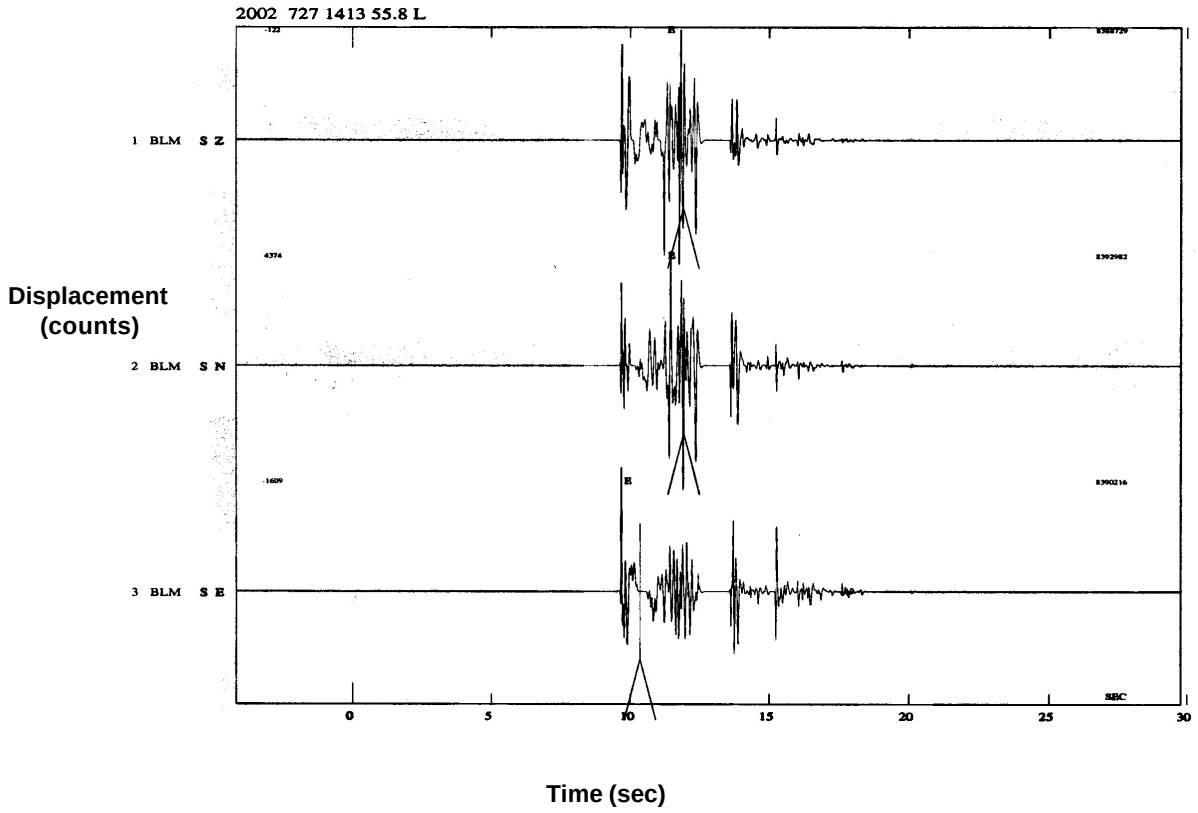


**Figure 4.9:** The seismic trace captured at 4 m from UP16 with the pump switched on but not discharging water. The components of the geophone are shown on the vertical axis and time on the horizontal axis. The minimum and maximum counts for each event recorded by the geophone components are also shown.

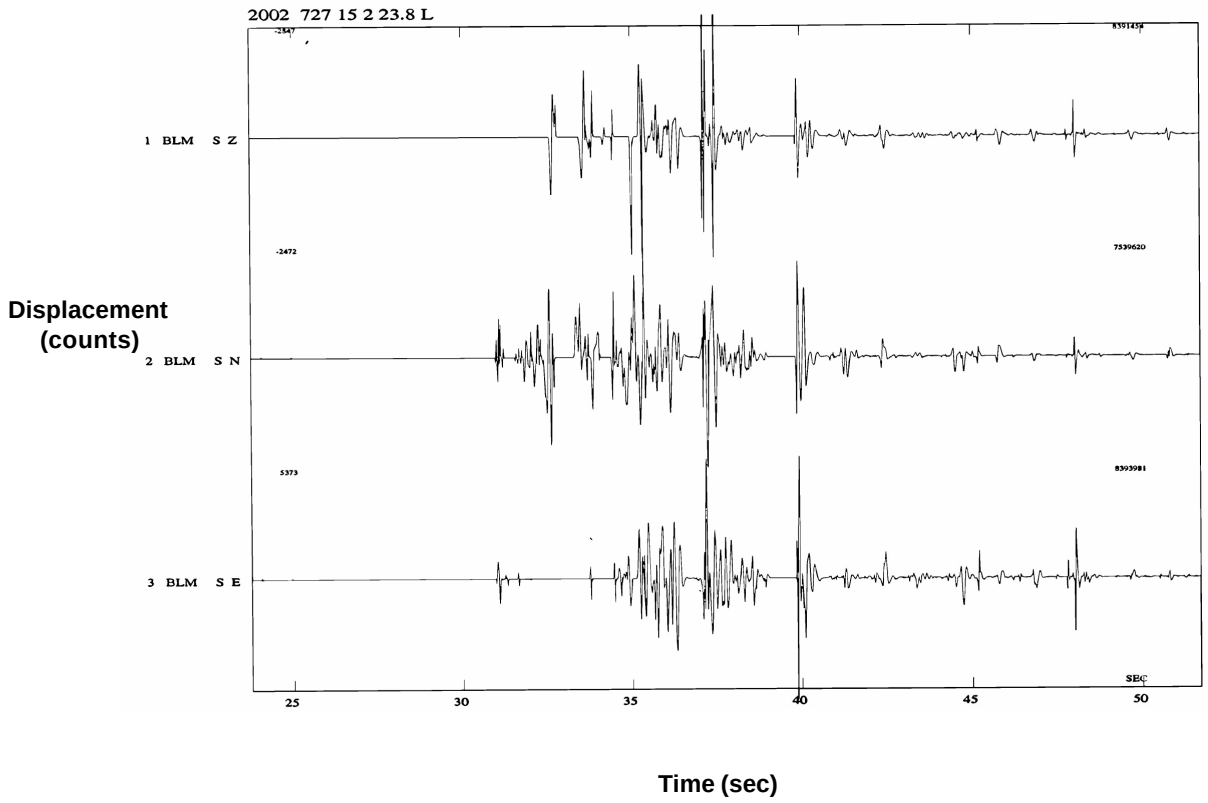


**Figure 4.10:** The seismic trace at 4.5 m from UP16 with the pump switched on but not discharging water. The components of the geophone are shown on the vertical axis and time on the horizontal axis. The minimum and maximum counts for each event recorded by the geophone components are also shown.

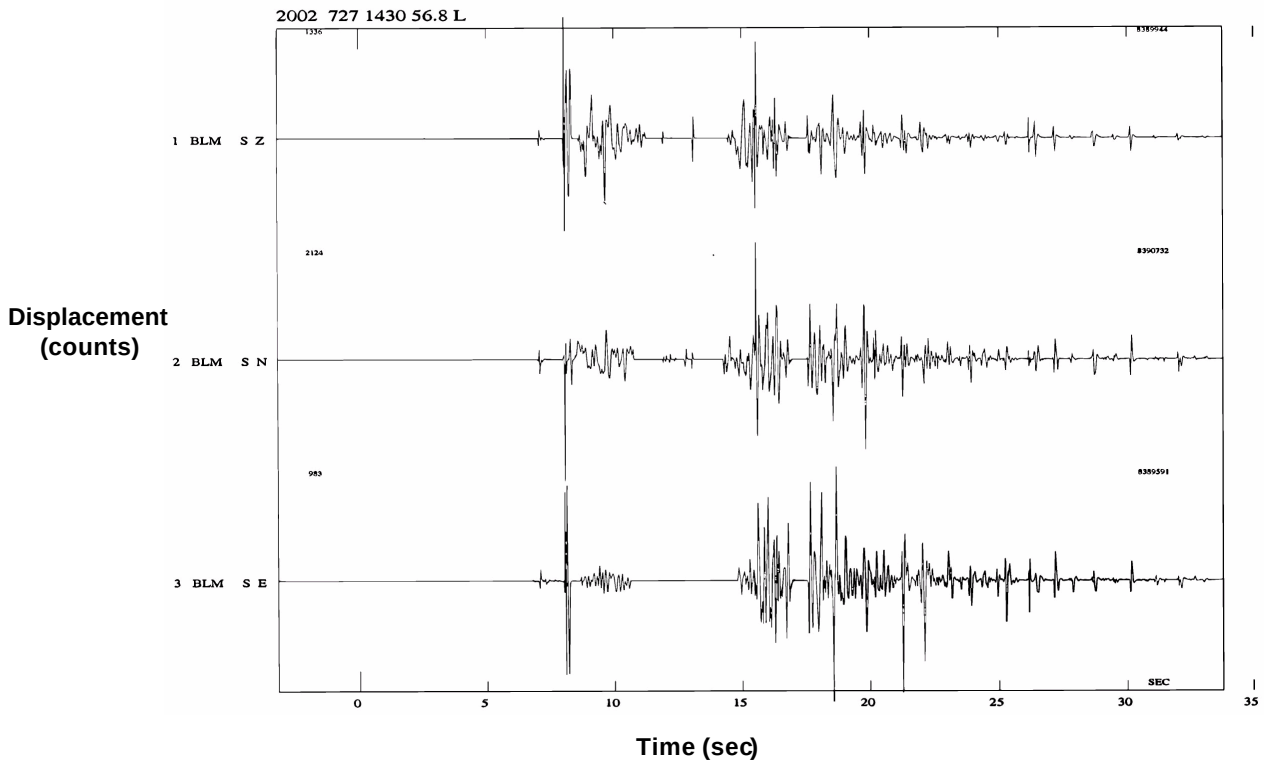


**Figure 4.11:** The seismic trace at 5 m from UP16 with the pump switched on but not discharging water. The components of the geophone are shown on the vertical axis and time on the horizontal axis. The minimum and maximum counts for each event recorded by the geophone components are also shown.

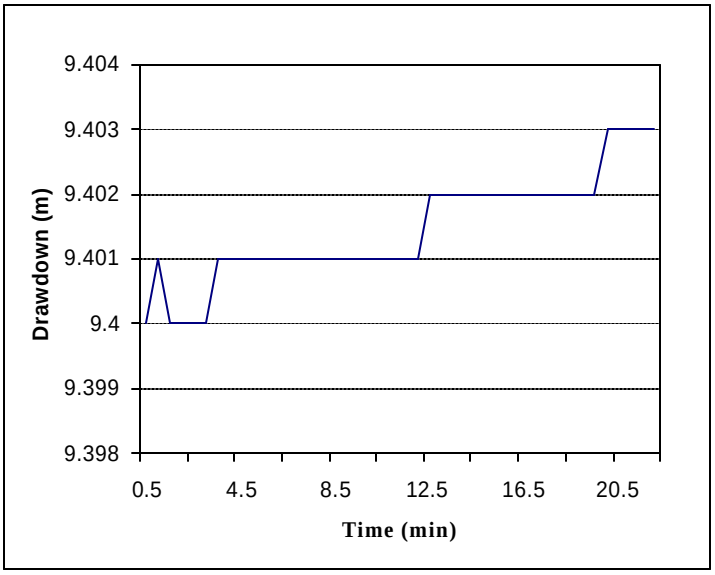


**Figure 4.12:** Drawdown observed in UP 16 with the pump on but not discharging water

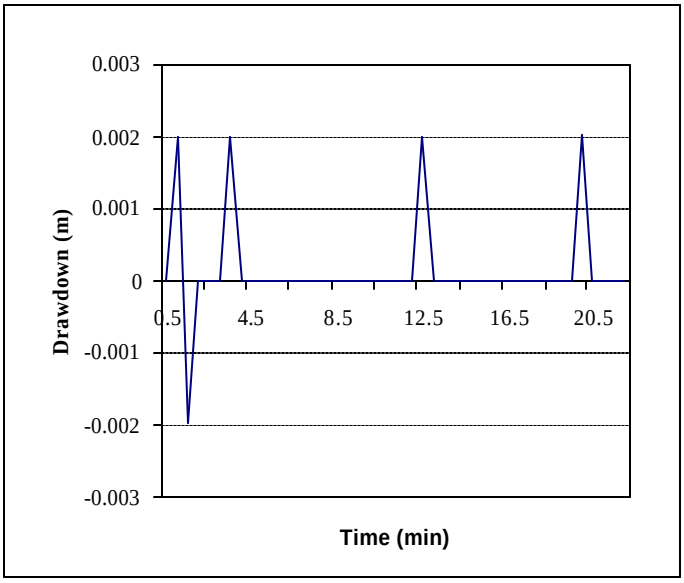


**Figure 4.13:** The first derivative of the data in Figure 4.12.

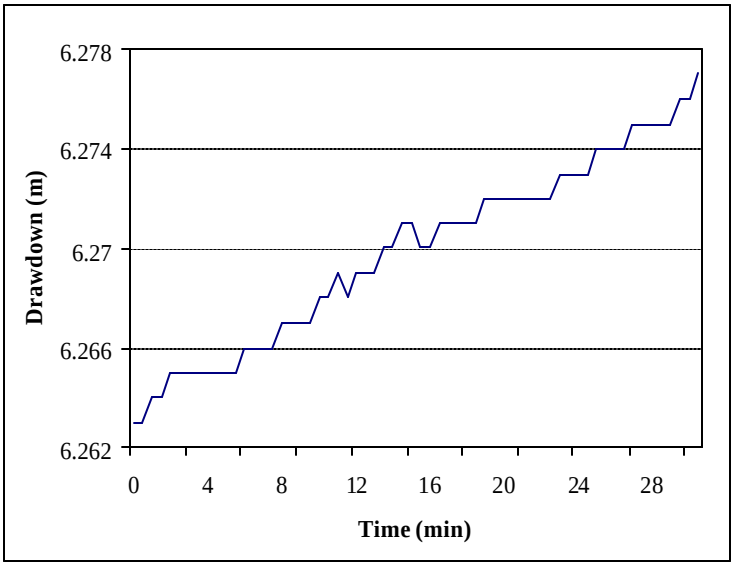


**Figure 4.14:** Drawdown observed in UO28 as UP 16 is switched on but not discharging water

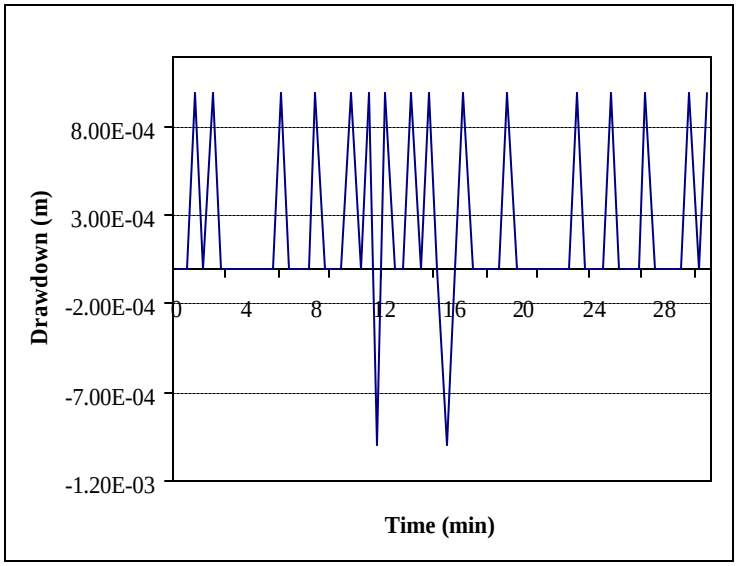


**Figure 4.15:** The first derivative of the curve in Figure 4.14

#### 4.3.3.3 Experiment 2

In the second experiment the impact of discharge rate on ground motion is investigated. The seismological motion of the ground at a fixed station was monitored as the discharge rate was varied. The details of the practical execution are shown in Table 4.4. There are two facets to this approach: the first is to derive a relationship between discharge rate and ground motion and the second is to evaluate the contribution of the hydrodynamic pressure on the development of oscillations.

**Table 4.4:** The practical execution of Experiment **2**

| Station | Date | EARS TIME | | Remarks |
|---|---|---|---|---|
| | | Starting | Finishing | |
| 2 | 7-26-2002 | 9:35 | 10:25 | Started 9:26 and stopped at 10:26. Discharge rate ~ 3.688 l/s |
| | 7-26-2002 | 10:45 | 12:09 | Started recording at 10:36 am stopped 12:10 pm. Discharge rate ~1.746 l/s |
| | 7-26-2002 | 12:49 | 13:45 | Started 12:40 am and stopped at 13:46. Discharge rate 3.249 l/s ~ 3.249 l/s |
| | 7-26-2002 | 14:06 | 14:55 | Started at 13:56 and stopped at 14:56. Discharge rate 4.026l/s |
| | 7-26-2002 | 15:14 | 16:06 | Stated at 15:05 and stopped at 16:07. No discharge. of water |
| | 7-26-2002 | 16:24 | 17:15 | Started at 16:16 and stopped at 17:16. Intervention was occurred at this point due to spillages of water at the pump. |

The geophone was positioned at 2 m from the pumping borehole and the discharge rate was varied. The drawdown curves of UP16 and UO28 when pumping the former at 4.06 L/s and the respective first derivatives are given in Figures 4.17, 4.18, 4.19 and 4.20. The quantitative results for the discharge rate of 4.06 L/s are shown in Table 4.5, and the other discharge rates seemingly did not manage to trigger the geophone. This can be explained by the fact that wave trains of different phases were generated (Foti, 2000) leading to a destructive interference resulting in no or a weaker signal.

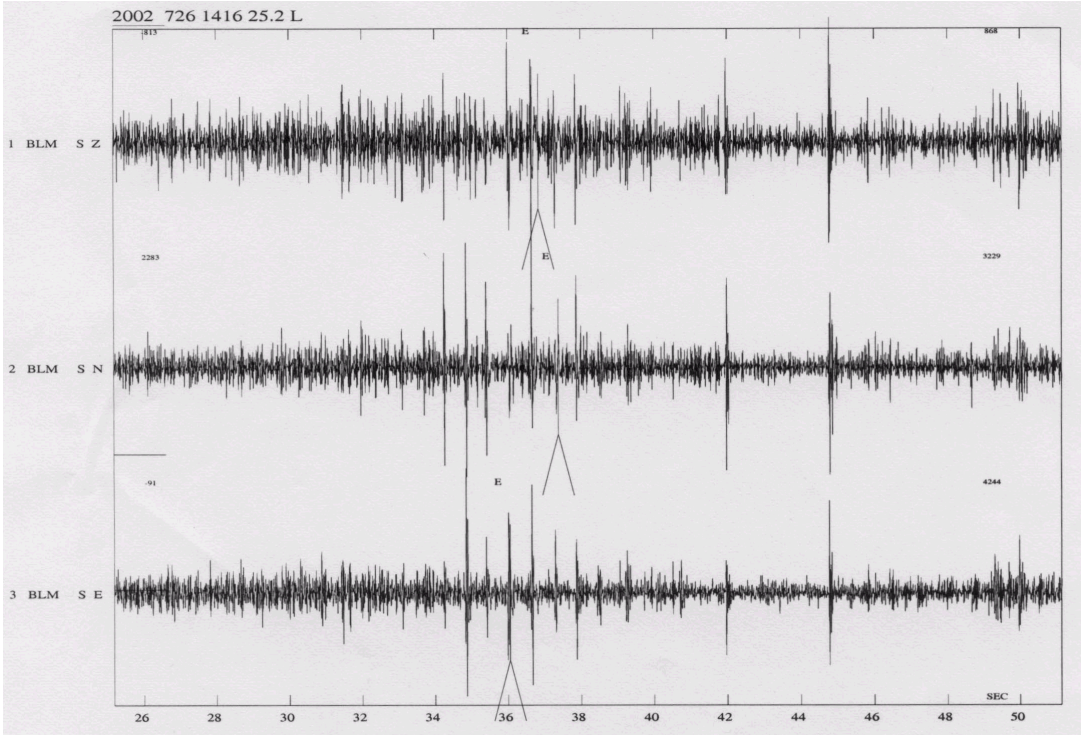


**Figure 4.16:** The seismic trace at a station 2 m from UP16 discharging water at 4.06 L/s. The components of the geophone are shown on the vertical axis and time on the horizontal axis. The minimum and maximum counts for each event recorded by the geophone components are also shown.

**Table 4.5:** The variation of ground motion with discharge rate

| Station | Discharge Rate (L/s) | Amplitude (nm) |
|---|---|---|
| 2 | 4.06 | 31.4 |

It is clear when comparing the information in Table 4.3 and Table 4.5 that when discharging water from a borehole the amplitude of the ground motion is significantly reduced. This can be attributed to the loss of hydrodynamic force to oppose the compressing effect of the pump vibrations (Figure1.6). This implies that the hydrodynamic force is smaller when the system is losing water than when not pumping.

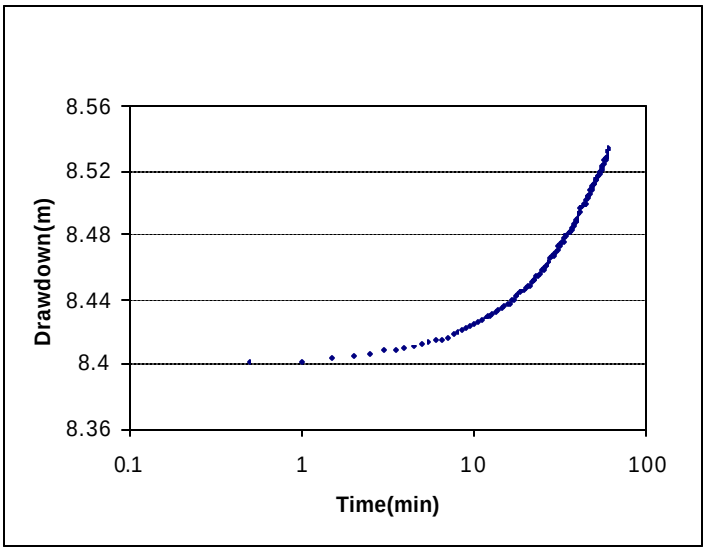


**Figure 4.17:** Drawdown curve of UP 16 when discharging at 4.06 l/s

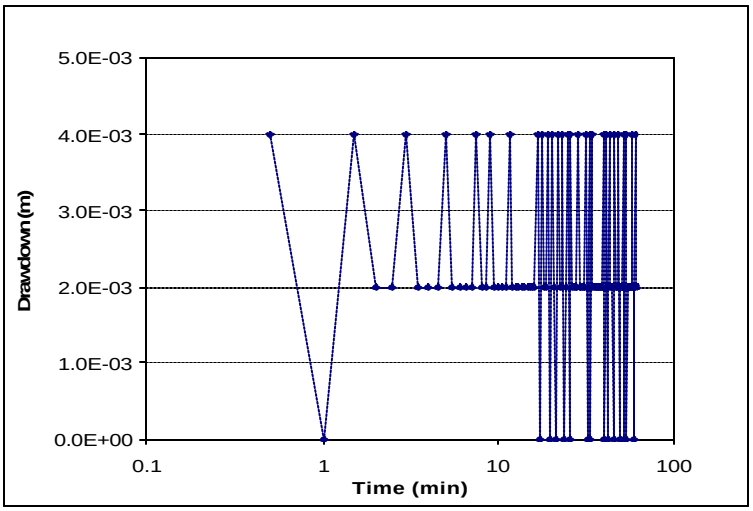


**Figure 4.18:** The first derivative of plot in Figure 4.17

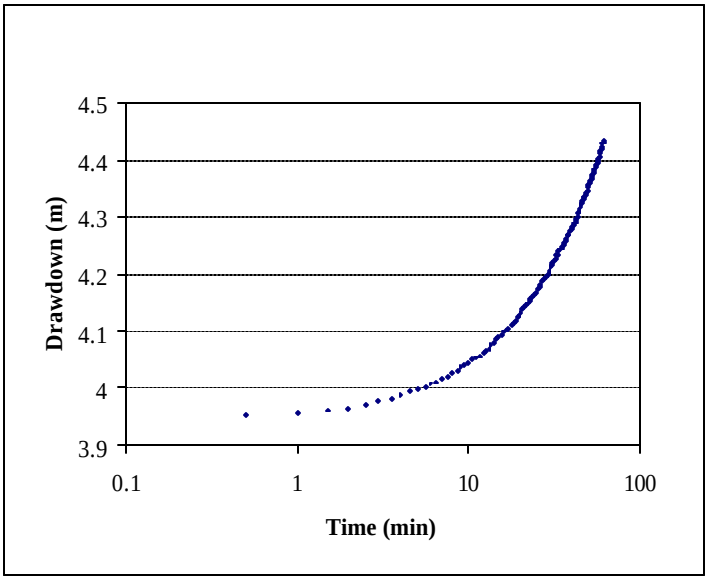


**Figure 4.19:** Drawdown curve of UO28 as UP16 discharges at 5 L/s

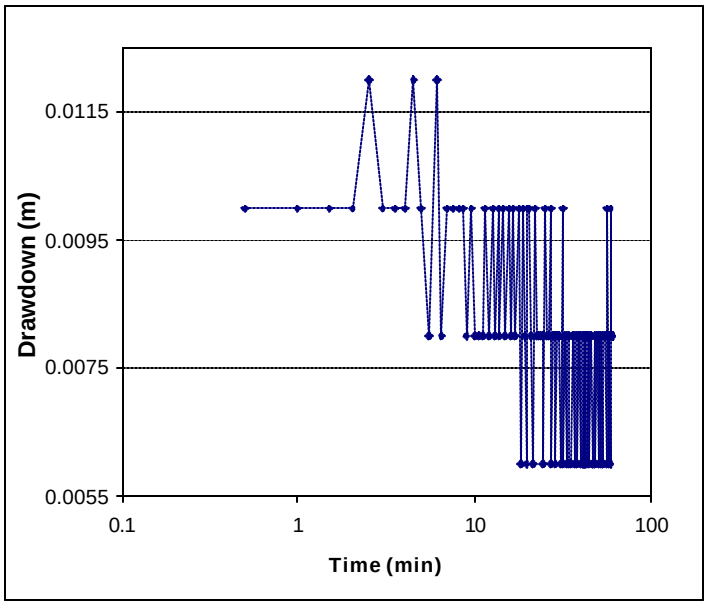


**Figure 4.20:** The first derivative of the data curve in Figure 4.19

The numerical experiments of Botha and Cloot (2002) showed that discharge rate is the main contributing factor to the failure of Karoo aquifers. The coupled effect of pump vibrations and discharge rate further complicates the entire dynamics of the system making it difficult to delineate the main causative factor.

#### 4.3.3.4 Experiment 3

In contrast to Experiment 1, the water-level fluctuations were recorded without switching on the pump. The intention was to investigate the impact of ground roll on borehole water.

The aquifer when discharging water should be viewed as being subjected to a forcing frequency resulting from the pump. Naturally the aquifer is constantly subjected to spurious forces from various sources. The natural frequencies and the forcing frequency from a pump combined (principle commonly known as frequency modulation) will have a different effect on the system than when either force is in isolation.

In the experiment, the ground roll, as the effect of natural frequencies are referred to in seismology, was monitored and so was the water level in borehole UO28 (Figure 4.21). The sources of ground roll are mainly of anthropogenic origin although natural factors such as wind may also contribute.

The water response in UO28 was monitored (Figures 4.21 and 4.22).

Unfortunately the geophone used in the monitoring of these frequencies did not record anything. This does not, however, mean that the ground is not subjected to any frequencies. The main reason may be that the frequencies were not strong enough to trigger the geophone.

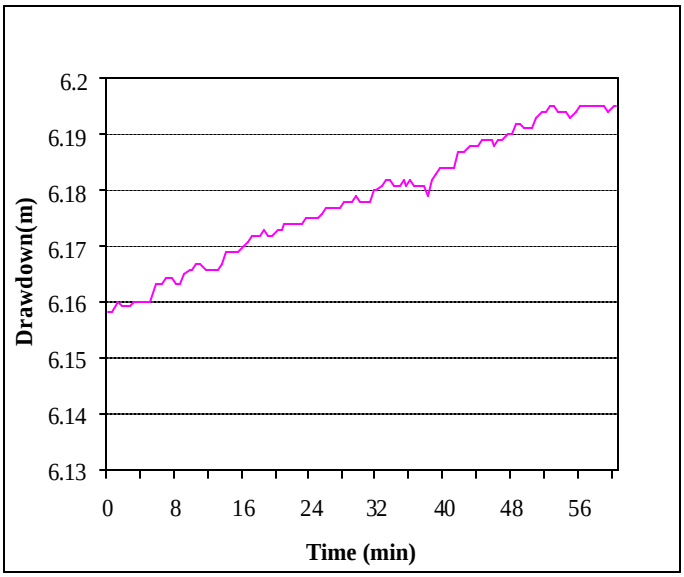


**Figure 4.21:** Water-level behaviour in UO28 when no water was pumped from the aquifer.

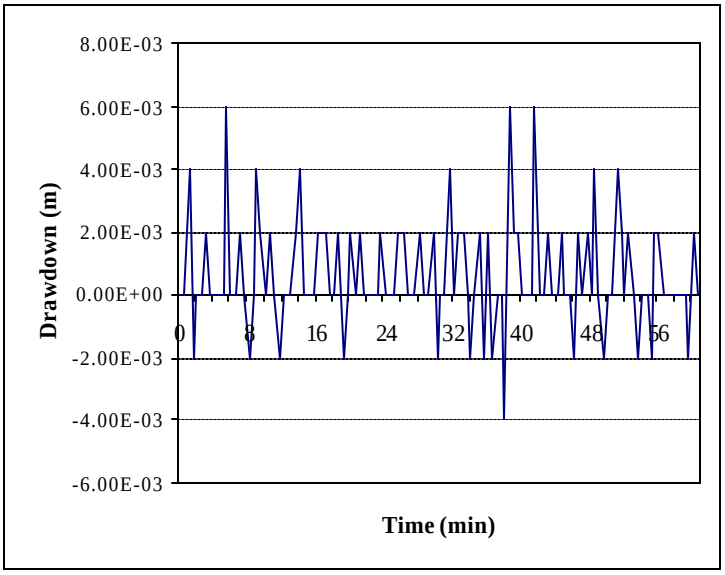


**Figure 4.22:** The first derivative of data in Figure 4.21

#### 4.3.3.5 Experiment 4

This experiment was a repetition of Experiment 1 except that water was discharged. The corresponding ground motion was captured (Figure 4.23) and a frequency spectrum of the seismic trace was analysed (Figure 4.24).

From the spectrum, it is clear that there are at least six dominant frequencies; however, only two are of interest to the study, namely, around the 5 Hz and near the 10 Hz marks. The threshold frequency needed to trigger the geophone should be 4.5 Hz (Table 4.2), and from the spectrum, Figure 4.24, that frequency does not exist, indicating the pump dominance on aquifer behaviour. This subsequently suggests that the lack of response from the geophone in Experiment 3 implies that the ground roll frequencies were below the threshold limit of 4.5 Hz. It is worth noting that the frequency of the ground roll depends on the strength of the extraneous sources and therefore is not fixed.

The quantitative ground characteristics are given in Table 4.6. The drawdown curves and the first derivatives of UP16 and UO28 are shown in Figures 4.25, 4.26, 4.27 and 4.28.

Comparing the data in Tables 4.3 and 4.6, the amplitude of ground motion is larger when the borehole is pumped at 1.025 L/s than when not pumping. In contrast, the maximum amplitude recorded when pumping at 1.025 l/s (1.807 mm) is larger than the maximum amplitude when pumping the aquifer at 4.06 L/s (31.4 nm). *This implies that there is an optimum discharge rate at which the hydrodynamic force and the force resulting from vibrations are in equilibrium.*

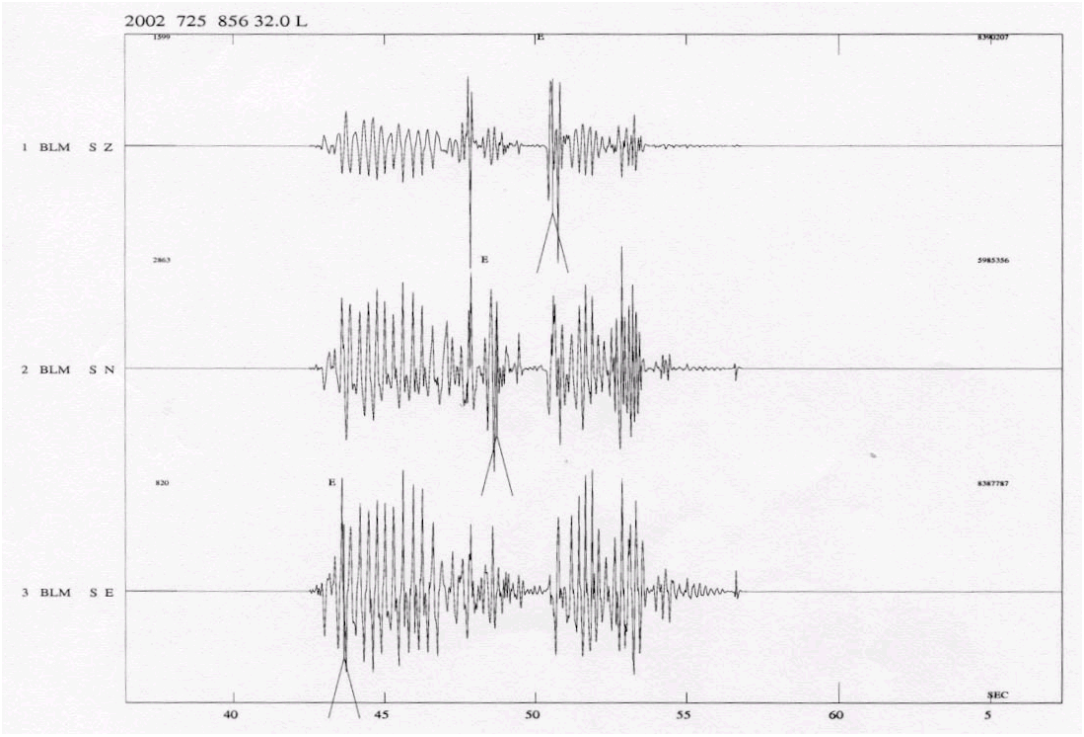


**Figure 4.23:** The seismic trace captured at 4 m from UP16 discharging at 1.025L/s. The components of the geophone are shown on the vertical axis and time on the horizontal axis. The minimum and maximum counts for each event recorded by the geophone components are also shown.

**Table 4.6:** Maximum ground amplitudes recorded at 4 metres from UP 16 discharging at 1.025 L/s

| Ground Displacement (nm) | Ground Velocity (nm $s^{-1}$) | Ground Acceleration (nm $s^{-2}$) |
|---|---|---|
| 1806972.0 | 57807748.0 | 3193180672.0 |

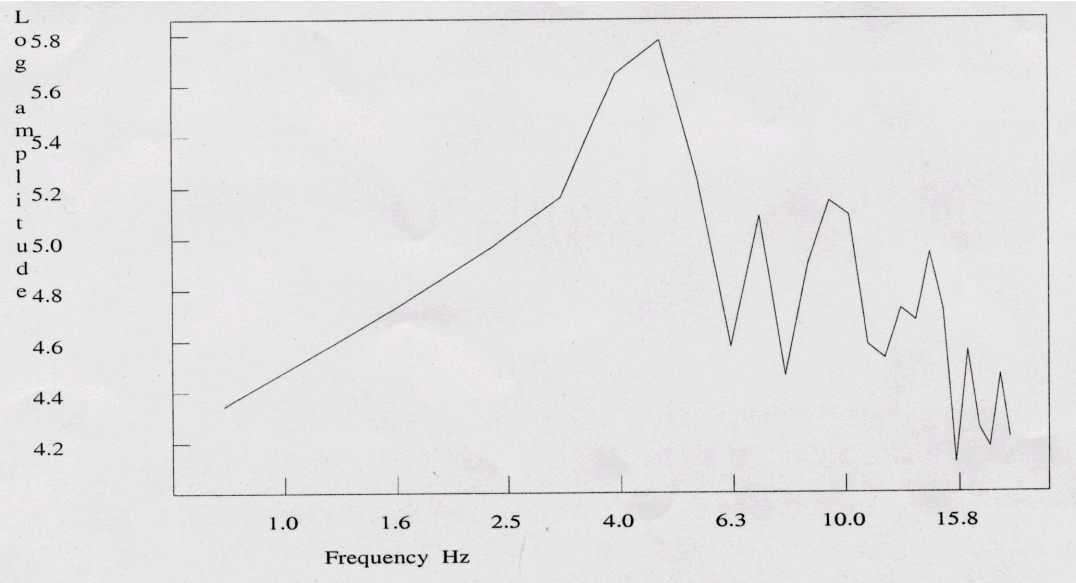


**Figure 4.24:** The frequency spectrum of the seismic trace shown in Figure 4.23.

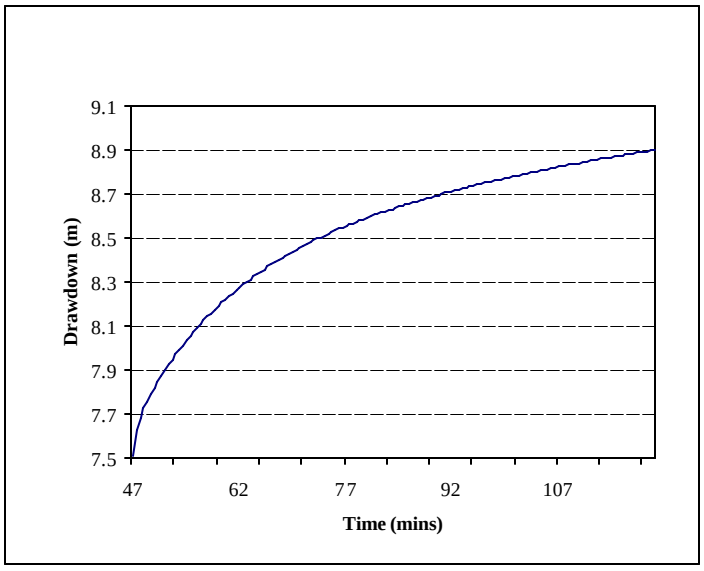


**Figure 4.25:** Drawdown curve of UP 16 when discharging at 1.025 l/s

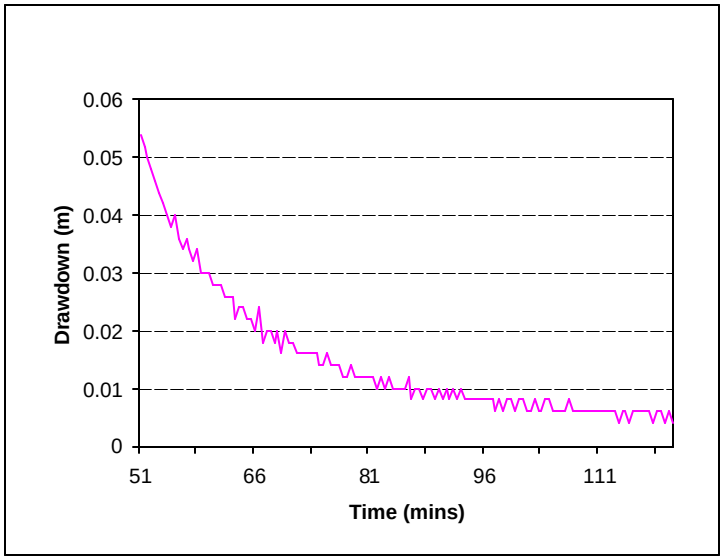


**Figure 4.26:** The first derivative of the drawdown curve in Figure 4.25

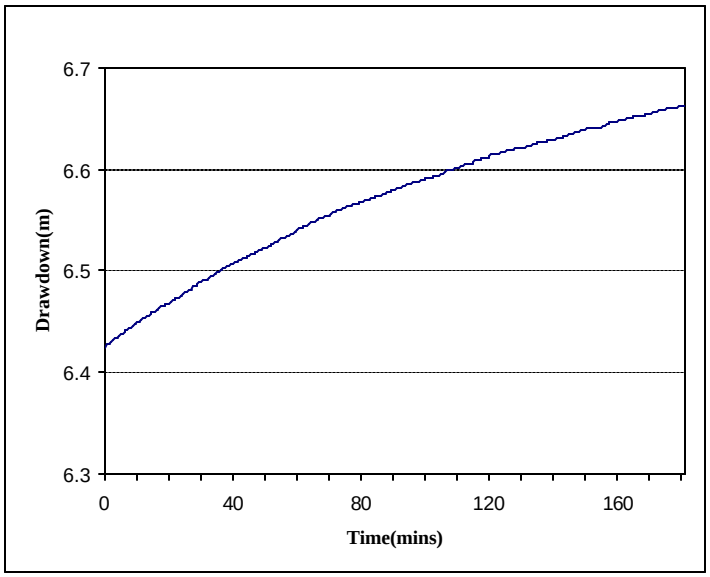


**Figure 4.27:** Drawdown curve of UO 28 as UP 16 discharges at 1.025 l/s

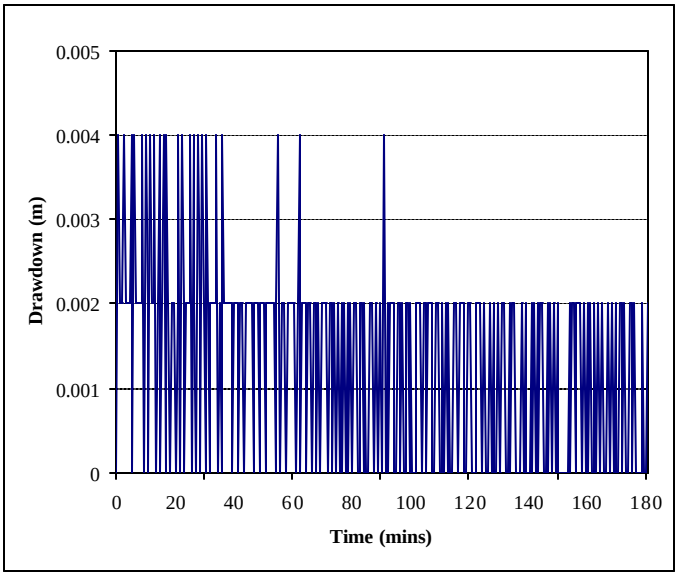


**Figure 4.28:** The first derivative of the graph in Figure 5.27

### 5.3.3.6 Experiment 5

A seismic sounding was conducted with a hammer-plate placed a metre from the sensor in the survey line between boreholes UP16 and UO28. A typical seismic signature generated by a hammer is shown in Figure 4.29 and the ground reaction is tabulated in Table 4.7.

The response of the water level was continuously recorded throughout the experiment. The borehole water response in UO28 is shown in Figure 4.30 and its derivative in Figure 4.31.

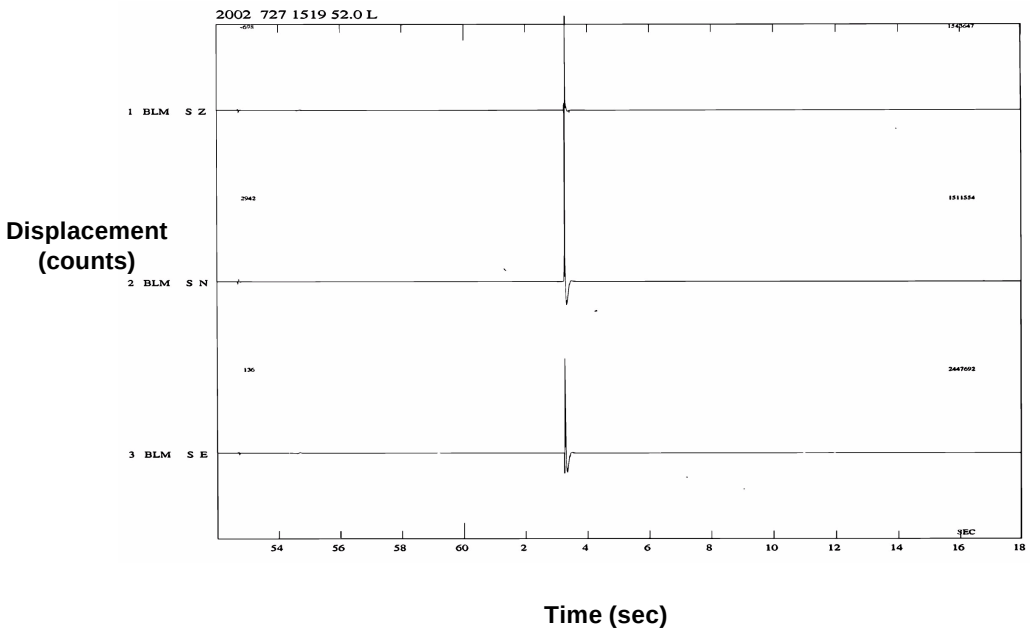


**Figure 4.29:** The seismic trace generated by hammering the ground. The components of the geophone are shown on the vertical axis and time on the horizontal axis. The minimum and maximum counts for each event recorded by the geophone components are also shown.

**Table 4.7:** The response of the ground to a shock wave shown in Figure 4.29

| Ground Displacement (nm) | Velocity ($nm\ s^{-1}$) | Acceleration ($m\ s^{-2}$) |
|---|---|---|
| 517 658.1 | $2.546 \times 10^{7}$ | $1.5 \times 10^{-1}$ |

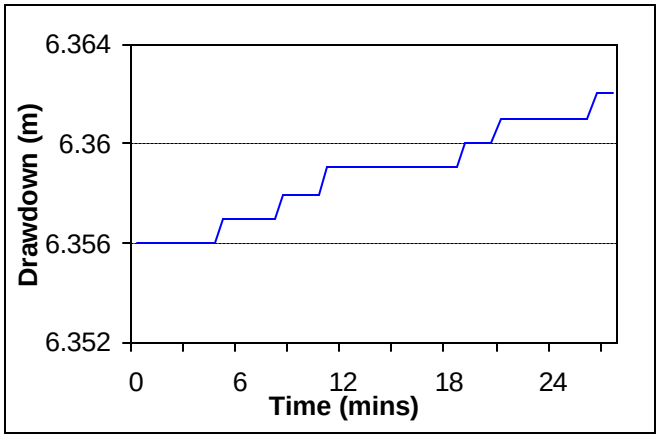


**Figure 4.30:** The water response in UO28 as an external force is applied with a hammer and the sensor positioned at one metre away.

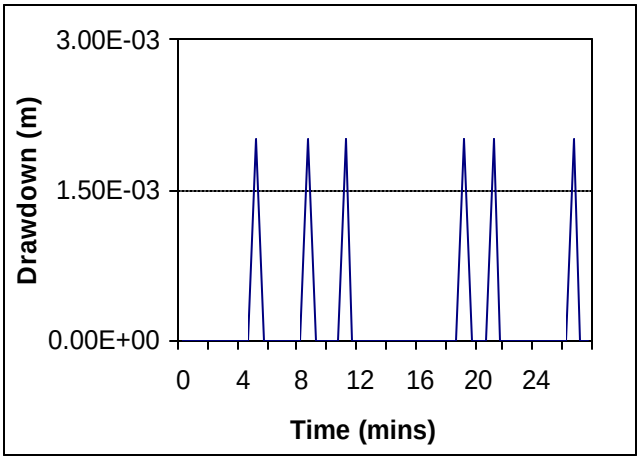


**Figure 4.31:** The first derivative of data in Figure 4.30

By comparing Figures 4.21 and 4.30, it is clear from the observations that the borehole water reacted to the external energy. The ground was struck at 2-minute intervals. The step signature of Figure 4.30 may be due a to summation effect of the

seismic energy as the water was flushed from the borehole. It should be noted that UP16 was not pumping.

#### 4.3.3.7 Experiment 6

Experiment 5 was repeated except that both the source and the sensor were in the same position. The water-level responses are shown in Figures 4.32 and 4.33. In terms of seismology the data captured has no significant meaning but the corresponding water fluctuations do have some significance.

As in Experiment 5 the borehole water response displayed a step function. Again this indicates that the hammer effect was reaching the borehole water level.

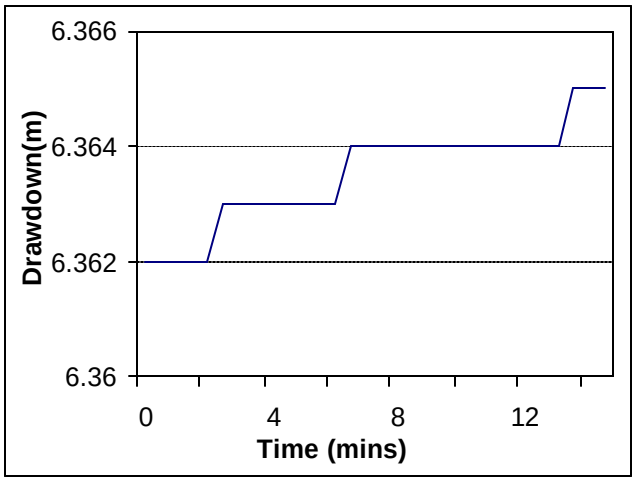


**Figure 4.32:** The water response in UO 28 as an external force is applied with a hammer and the sensor positioned at the same station

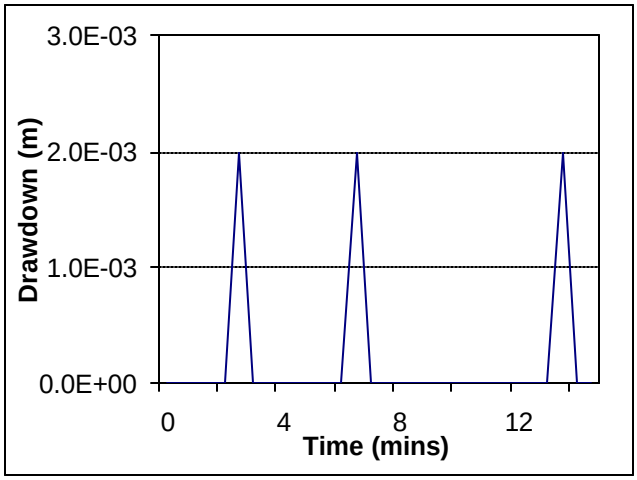


**Figure 4.33:** The first derivative of UO28 data in Figure 4.32

#### 4.3.3.8 Experiment 7

The source and sensor were placed at borehole UO28 with the pump in UP16 switched off. The arrangement enhanced the impact of sound wave and pressure from a Rayleigh wave on the water level. The borehole water responded in the same way as in Experiment 5 and 6 but the step effect was more defined, probably because the hammering was done at the borehole. Ground hammering was done every minute.

The arrangement enhanced the impact of sound waves and pressure from a Rayleigh wave on water level. The seismic wave in this case could have propagated through the matrix and along the borehole walls because of the proximity of the source to the borehole. Direct waves are usually the first arrivals in such a set-up (Telford *et al.*, 1990).

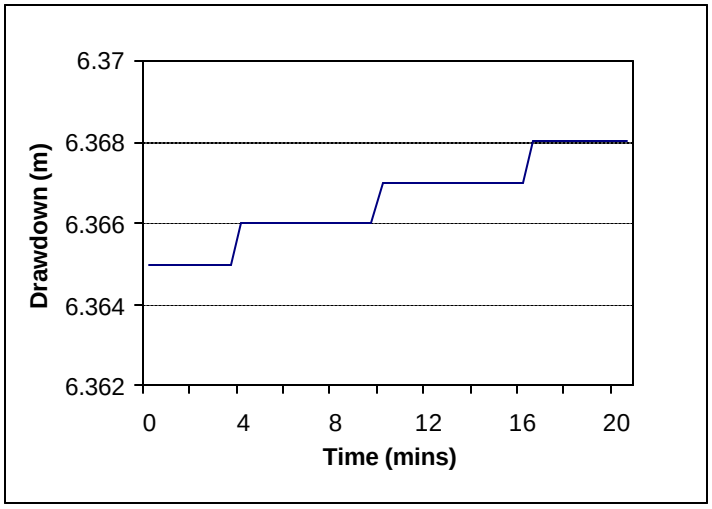


**Figure 4.34:** The water response in UO 28 as an external force is applied with a hammer and the sensor is positioned at UO28.

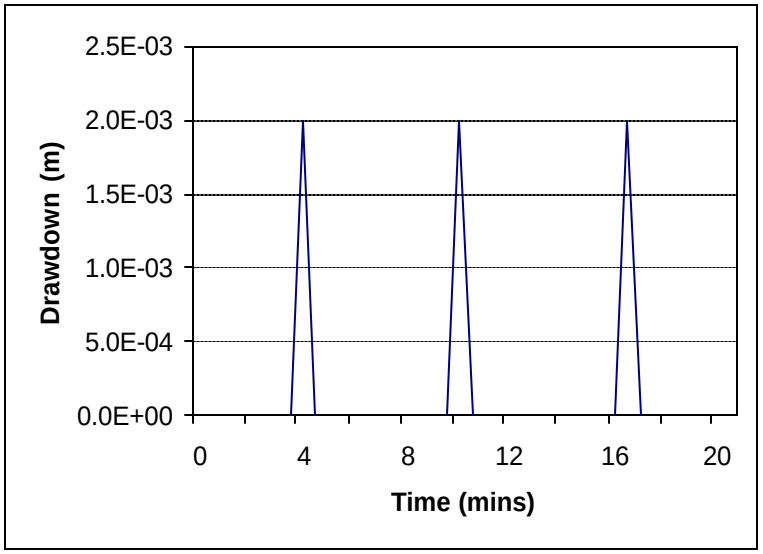


**Figure 4.35:** The first derivative of the data curve in Figure 4.34

#### 4.3.3.9 Experiment 8

In this experiment the borehole discharged at maximum discharge rate and was allowed to recover. The drawdown curve during pumping is shown in Figure 4.36 and the corresponding derivative in Figure 4.37. Throughout the experiment ground

motion was captured at 0.5 m from UP16. The seismic graphs drawn up at the following times in the morning, 6:22, 6:24 and 6:39, are shown in Figures 4.38, 4.39 and 4.40 respectively. The quantitative results are to be found in Table 4.8.

**Table 4.8:** The ground response as the water level drops

| Time | Ground Displacement (nm) | Velocity (nm $s^{-1}$) | Acceleration (nm $s^{-2}$) |
|---|---|---|---|
| 6:22 | 30.8 | 6007.1 | 1318235.5 |
| 6:24 | 86.6 | 5801.0 | 972978.4 |
| 6:39 | 101.1 | 14834.8 | 2807780.0 |

The results clearly show that as the water level decreases the ground motion increases. According to Figure1.6, as the borehole discharges, the hydrodynamic force decreases causing an imbalance in forces leading to the dominance of the driving force resulting from pump vibrations. It should be noted that a submersible pump loses discharge rate gradually as the water level decreases and thus as observed the smaller the discharge rate the larger the ground motion.

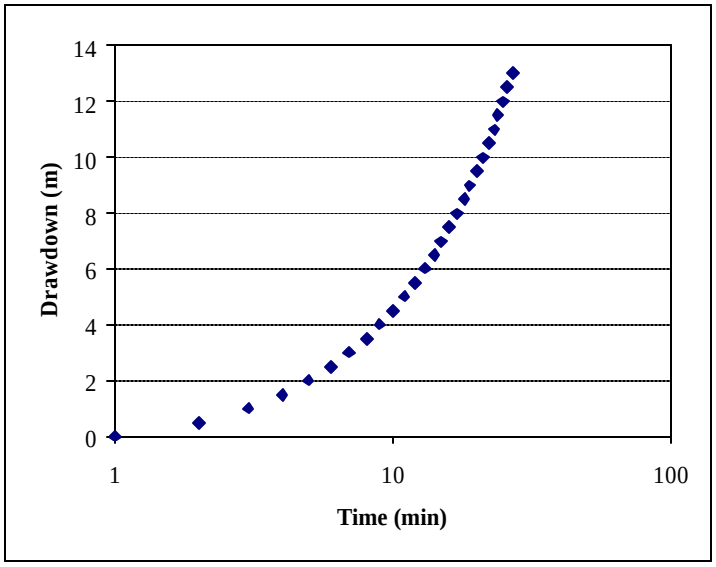


**Figure 4.36:** The water response in UO 28 as UP16 is discharge at its maximum rate of over 5 L/s.

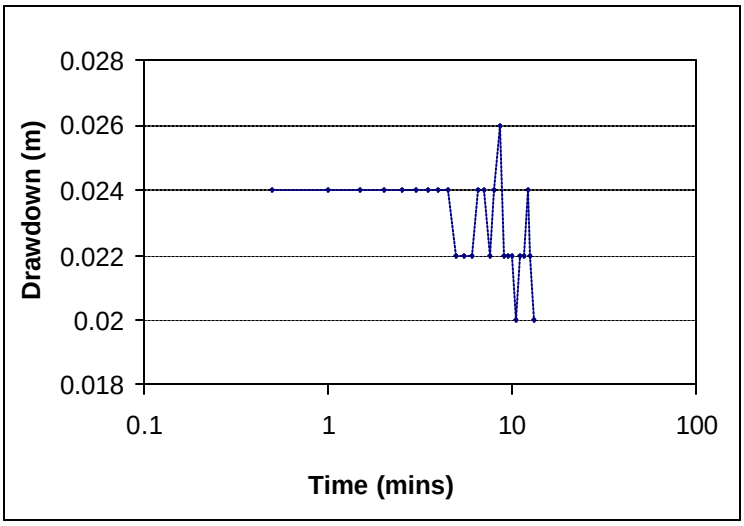


**Figure 4.37:** The first derivative of drawdown curve in Figure 4.36.

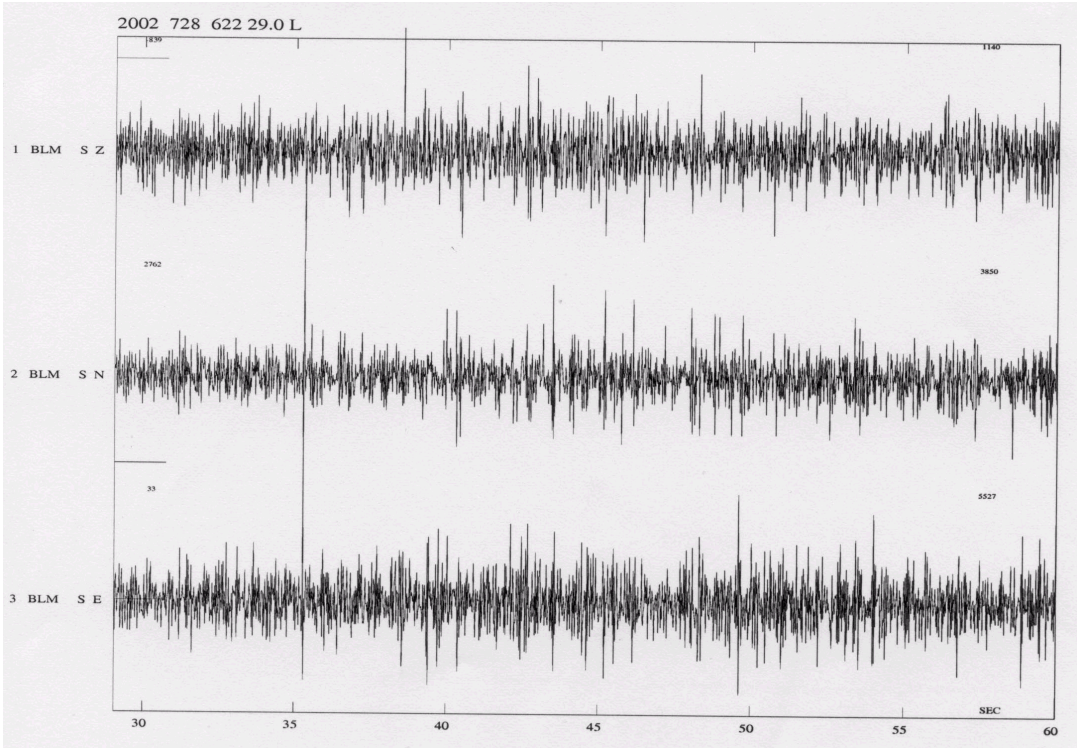


**Figure 4.38:** The seismic trace at 0.5 m from UP16 at time 06:22 as the borehole discharges at 5L/s. The components of the geophone are shown on the vertical axis and time on the horizontal axis. The minimum and maximum counts for each event recorded by the geophone components are also shown.

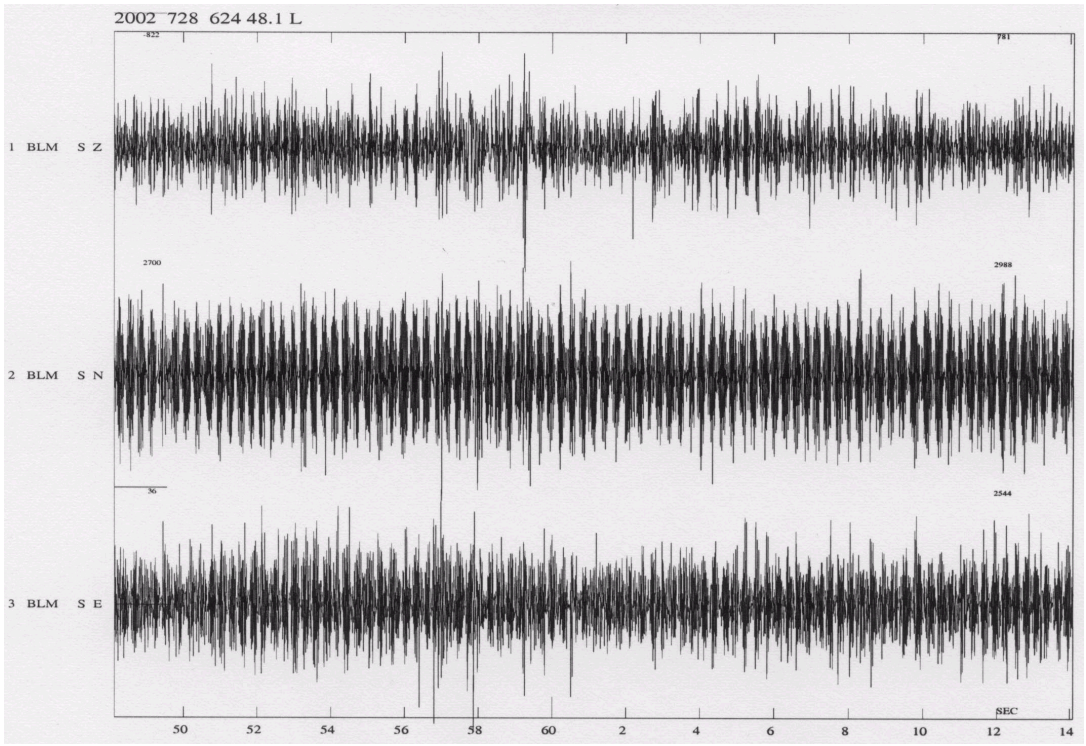


**Figure 4.39:** The seismic trace at 0.5 m from UP16 at time 06:24 as the borehole discharges at 5 L/s. The components of the geophone are shown on the vertical axis and time on the horizontal axis. The minimum and maximum counts for each event recorded by the geophone components are also shown.

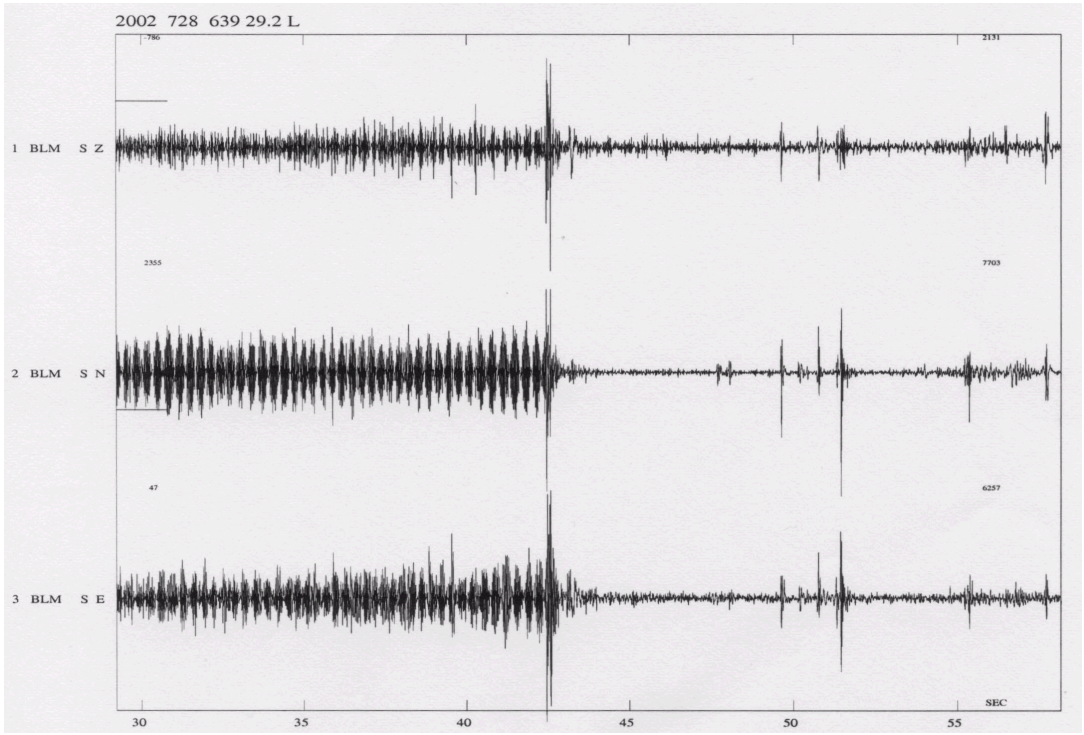


**Figure 4.40:** The seismic trace at 0.5 m from UP16 at time 06:39 as the borehole discharges at 5 L/s. The components of the geophone are shown on the vertical axis and time on the horizontal axis. The minimum and maximum counts for each event recorded by the geophone components are also shown.

## 4.4 NUMERICAL RESULTS

### 4.4.1 General

Pivotal to the simulations conducted in this section is the field data. The data include the water levels, frequencies and amplitudes of ground motion. The characteristics of ground motion are deduced from the seismic traces and the water responses are recorded by the pressure transducers.

In the one-dimensional model, the aquifer parameters such as aquifer stiffness, frequency and amplitudes of ground motion are the inputs, with the corresponding

output being the borehole water response. The water responses are compared with the observed field data for accuracy.

In order to maintain consistency with the work of Botha and Cloot (2002), the approach applied to the problem is similar to theirs, particularly the defining of the spatial extent of the problem. Some of the aquifer parameters such as aquifer stiffness are directly adopted from their work. The deviations of the model results should be as a result of the inclusion of pump seismicity in the problem.

### 4.4.2 Finite element implementation

The finite element implementation of the model followed essentially the same procedure as that followed by Botha and Cloot (2002). The aquifer of interest is 520 m in the radial direction and 50 m thick. The bedding fracture situated at a depth of 21 m is the main concern since it has a tremendous effect on the convergence and accuracy of the numerical solution.

For the two-dimensional model, a grid of $520 \times 50$ m$^2$ was selected and divided into 28 columns and 46 rows. Six rows were spaced at vertical distances of 0.01 m, 0.2 m and 0.3 m above and below the centre plane of the aquifer (Figure 4.41). The problem domain was systematically defined by Botha and Cloot (2002) after a series of experiments aimed at checking convergence and accuracy.

The groundwater flow equations as solved by Botha and Cloot (2002) were not changed. However, the boundary conditions described in Chapter 3 were added to the system.

By redefining and careful choice of nodes, all scenarios in Chapter 3 were incorporated into the single model and solved. By assigning the pump vibrations at the aquifer section and monitoring the water response, the effect of pump seismicity and the hammer-plate scenarios are simulated.

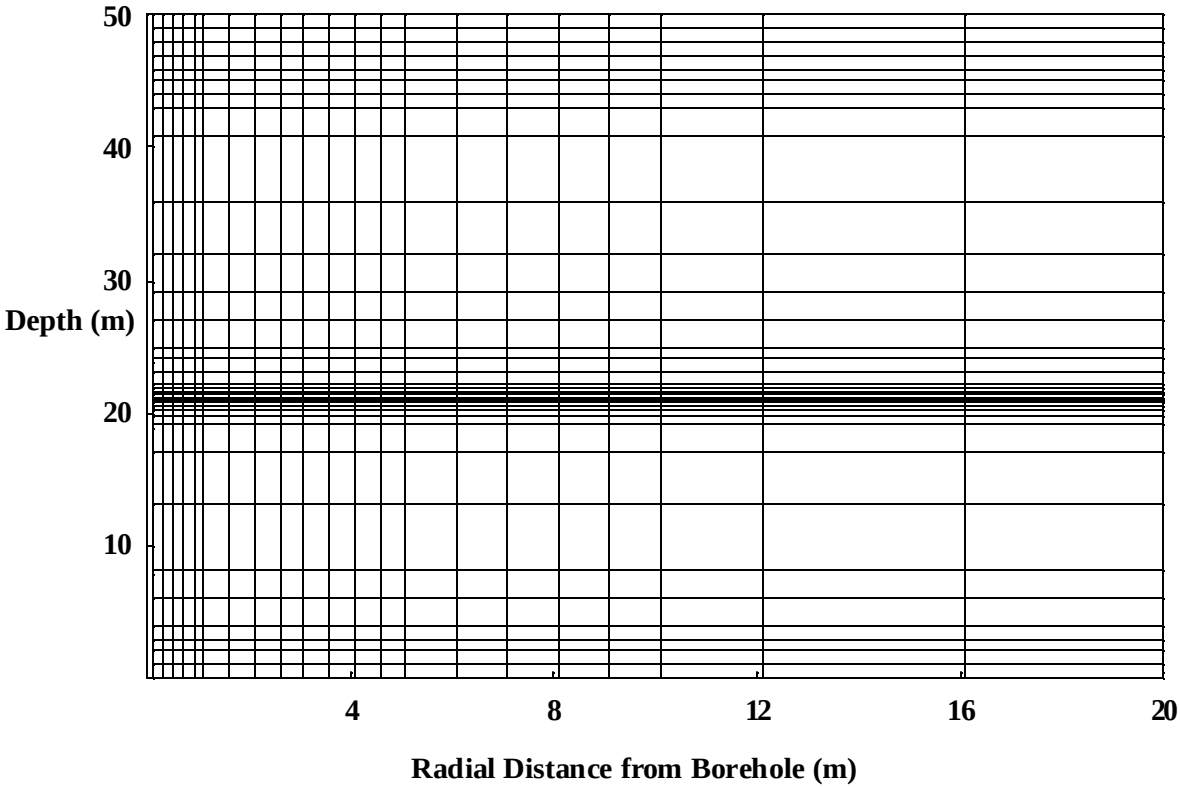


**Figure 4.41:** A section of the finite element mesh used in the simulations with the two-dimensional model

### 4.4.3 Parameters

The Young Modulus values of 7.5 E+07 Pa and 7.5E+08 Pa were assigned to the matrix and the fracture respectively. Some of the parameters used in the numerical models are shown in Table 4.9.

#### 4.4.3.1 One-dimensional model results

The one-dimensional model in Chapter 2 was developed to simulate borehole water response to ground motion resulting from pump vibrations. To calibrate the model the data in Table 4.9 was used. These data represent the intrinsic properties of the Campus Test Site aquifer and the discharge rate used to deduce the ground motion.

The amplitude of 1.53E-03 m used in the analysis (Table 4.3) was determined from a seismic trace recorded at station 4 m with the pump in borehole UP 16 switched on but not discharging water.

The resultant water response was compared with the field data. In this experiment the pump served as source of seismicity to the aquifer.

In applying the model, a single row grid with 400 columns was generated with an interspacing of 0.01 m. The discretisation distance of 0.01 m was chosen for convergence and accuracy in the solution. The numerical solutions for different stiffness are shown in Figures 4.42 and 4.43.

**Table 4.9:** Parameters used in the numerical model

| Stiffness (Pa) | Young Modulus (Pa) | Frequency (Hz) | Amplitude (m) | Porosity | Poisson |
|---|---|---|---|---|---|
| 16000 | 7.5E+07 | 10 | 1.53E-03 | 0.25 | 0.25 |
| 160000 | 7.5E+08 | 10 | 1.53E-03 | 0.25 | 0.25 |

The outcome of the simulations was not focused on the overall behaviour of drawdown but on oscillations in the data. For the purpose of the analysis, the computational results are compared to the data in Figure 1.4. Clearly there is some resemblance, although in Figure 1.5 the frequency and amplitude are not regular and consistent, indicating a more complicated phenomenon than that simulated.

There may be several other reasons for the discrepancies observed. The main reason lies with the complexity of the evolution of the seismic waves as they propagate through different geological units. As pointed out by Foti (2000) and repeated in Section 2.3.2, the Rayleigh waves develop different modes at a given frequency. The original signal would have been transformed on reaching the target feature. The model did not incorporate these different modes. Another important aspect not accounted for by the model is the effect of the sound produced by the pump. The resultant wave that triggers the proposed deformation could be a convolution of the seismic wave resulting from the mechanical vibrations and the sound wave from the pump.

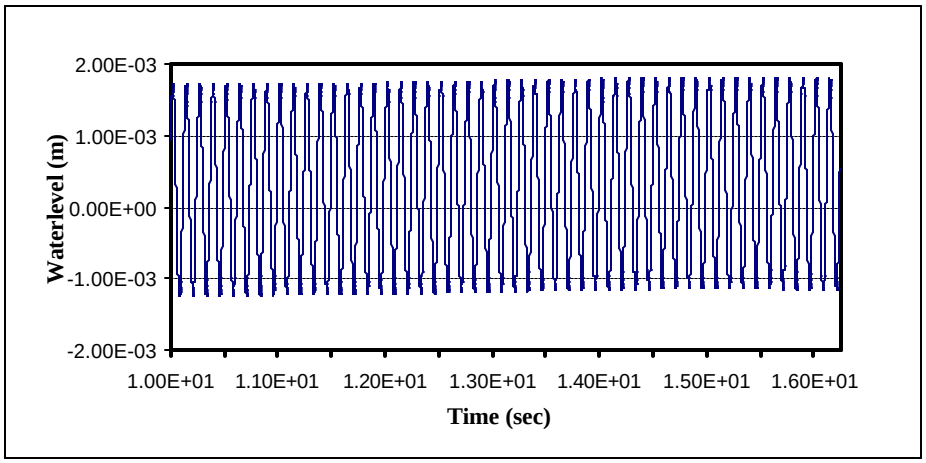


**Figure 4.42:** The one-dimensional result with stiffness of 16 000 Pa

This aspect was not incorporated in the model. As observed in Figure 4.24, there is no clear frequency of 50 Hz, which should represent the mains supplied to the pump. The absence of such a frequency shows that frequency evolves as it propagates in the media, an aspect that was not addressed by the model.

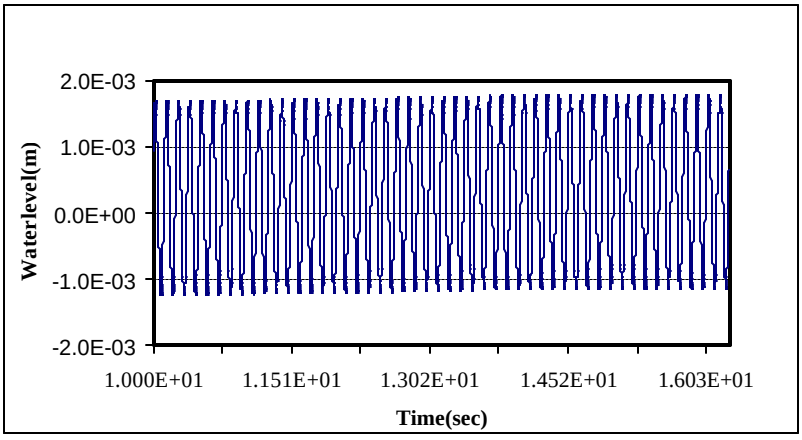


**Figure 4.43:** The one-dimensional result with stiffness of 160000 Pa

The modulation of the ground roll frequency and that of the pump results in a blended spectrum. This therefore implies that it is not only the harmonic effect of the pump vibrations that cause the proposed deformation but a convolution of waveforms of different frequencies, phases and amplitudes.

The amplitudes in Figure 4.43, however, bear a close resemblance to those measured in the field. This confirms that the fracture stiffness used is within the correct range.

#### 4.4.3.2 Two-dimensional model results

##### 4.4.3.2.1. General

The system of equations outlined in Chapter 3 is solved numerically by addressing the scenarios involved, that is, the effect of the *pump cups* (impellers), the impact of pump vibrations and the effect of ground hammering. These scenarios were incorporated into the model by switching the boundary and initial conditions of the model given in Chapter 3.

##### 4.4.3.2.2 Impeller scenario

The effect of pump impellers on the oscillations observed in the drawdown curves emanates from the fact that angular velocity has to be involved for the water to be discharged to the surface. The process is not smooth and continuous. The continuous flashing in and out of water in a borehole into the surrounding geological formation initiates fracture constriction and dilatation.

In simulating the scenario, the data in Table 4.5 and Table 4.9 were used. The discharge of 4.06 L/s was taken from Table 4.5 and aquifer properties from Table 4.9. The simulated ground motion is shown Figure 4.44. The graphical results depicted in Figure 4.44 show that as the borehole discharges water, the ground displacement gradually rises to a maximum and then gradually falls away. This trend is confirmed by the data in Table 4.8. According to Figure1.6, the hydrodynamic forces increase momentarily as a result of the influx of water but as pumping continues the water level falls below the fracture position leading to an approximate exponential decay of ground motion. This behaviour is analogous to an inflated balloon that loses its rigidity as it gradually deflates. Pumping the borehole is like inflating a balloon, as it draws water into a region where pump seismicity is dominant but, as it continues with time, water loss creates disequilibrium with the driving force leading to a decrease in ground amplitudes. It is important to note that the graph is broadest around the 30 nm

which is close to 31.4 nm, the maximum amplitude measured in the field when pumping at a discharge rate of 4.06 L/s (Table 4.5).

It is the continuous manifestation of such a phenomenon that is suspected of causing the fracture failure in the Karoo aquifers (Rasmussen, 1998).

However, the failure of the signal (Figure 4.44) to resemble the seismograph in Figure 4.16 is due to the fact that in the field several spurious seismic sources are present that distort the primary signal (Figure 4.24). In addition, by virtue of multi-stratified geology, vibrations can undergo multiple reflections before reaching a target feature and the resultant signal becomes a distortion of the primary signal.

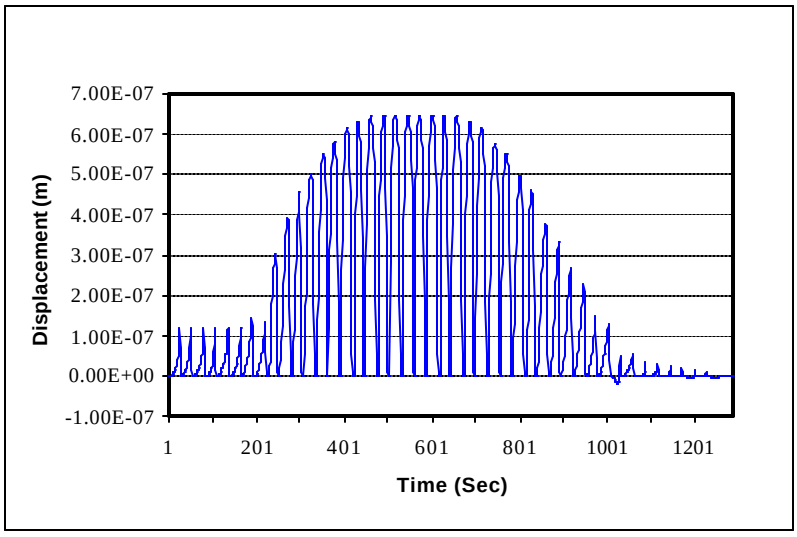


**Figure 4.44:** Ground motion with time as a borehole is pumped at 4.06 L/s.

#### 4.4.3.2.3 Hammer scenario

The simulations were aimed at reproducing the results of Experiments 5, 6 and 7. The data in Table 4.7 were used as initial conditions in the simulation. The simulated data is shown in Figures 4.45 and 4.46. There is a close similarity between the experimental results and those simulated for the first few minutes. Both curves show intrinsic step function behaviour and the difference between the two is the periodicity. After prolonged hammering the deviations start to occur. This may be due to the cumulative effect that results in the combined force pushing the water level up followed by a period of low energy. In the field it is suspected that a composite wave of Rayleigh waves and sound waves is generated that propagates directly to the water level leading to the formation of water waves. This aspect of the system was not taken into account by the model. In a multi-stratified aquifer different wave modes can

result (Foti, 2000) leading to the generation of several wave trains creating water waves of different frequencies and phases in a borehole. These waves can constructively or destructively superimpose resulting in either amplification or cancellation in the resultant water wave.

#### 4.4.3.2.4 Pump excitation without discharging

The pump excitation scenario without discharging was done so as to qualitatively assess the impact of discharging on seismo-deformations. The simulated results are shown in Figures 4.47 and 4.48. The results do not differ from the field observations in Figure 4.14 and 4.15; nor do they differ from the hammer scenario. In fact, the pump is like a hammer dropped at a higher frequency, that is, according to the proposed hypothesis; it is the vertical component of the pump vibration that has a significant impact on the water level.

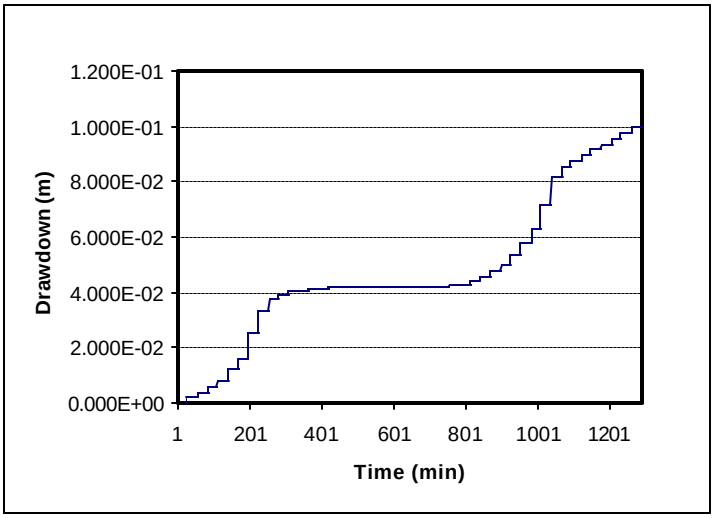


**Figure 4.45:** The simulated water response to ground hammering at 4 m from a borehole

The vibrations measured at ground level were used as initial conditions in the simulations and a frequency of 5 Hz for the response of the fracture situated at 21 m was used on the basis of the data deduced from the frequency spectrum (Figure 4.24).

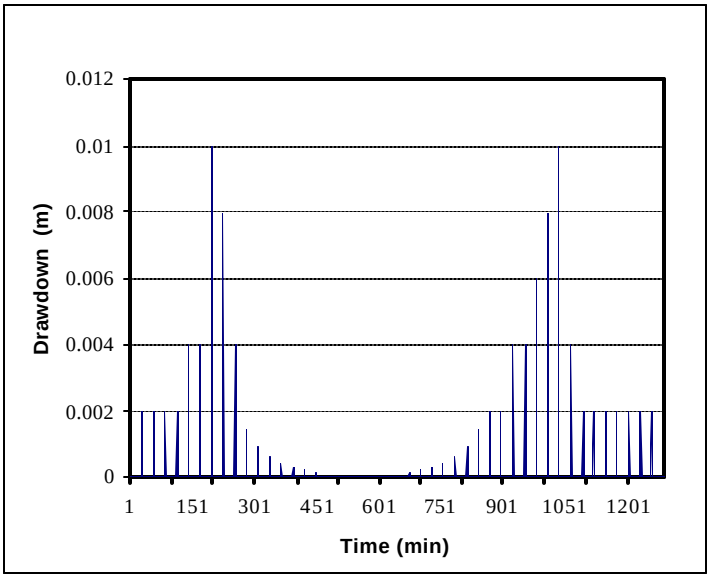


**Figure 4.46:** The first derivative of the data depicted in Figure 4.45

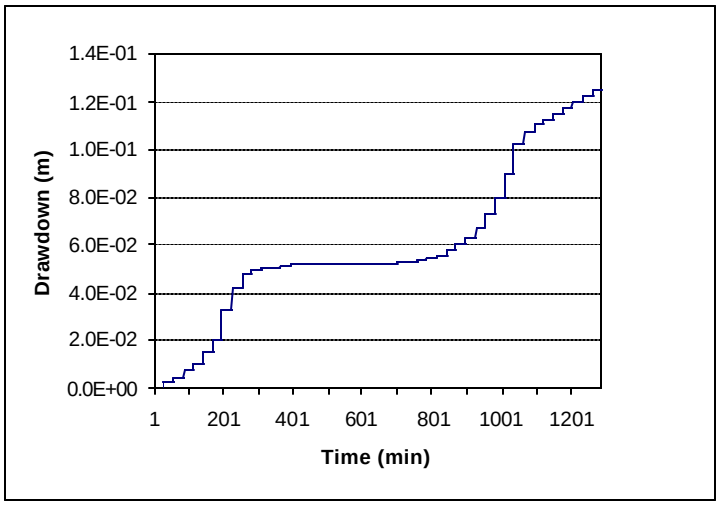


**Figure 4.47:** The water-level response resulting from a vibrating pump that is not discharging water.

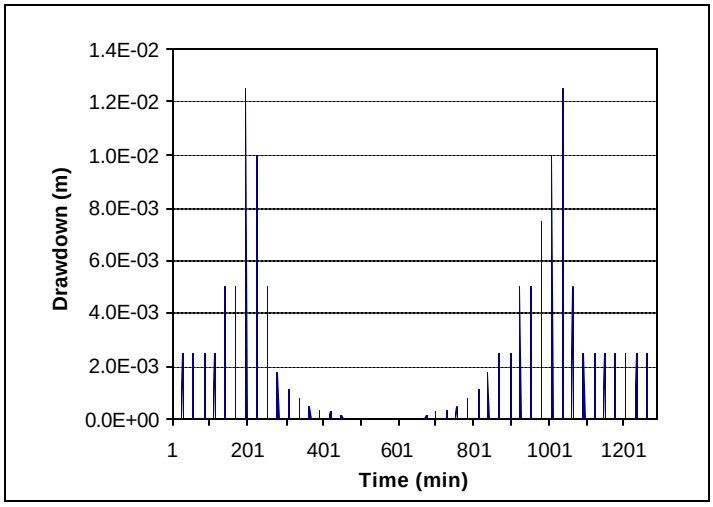


**Figure 4.48:** The first derivative of data in Figure 4.47

#### 4.4.3.2.3 A discharging and vibrating pump

This scenario is a close approximation of the field observation. The oscillations are observed in the field when the pump is discharging. The data in Table 4.5 were used as initial values in the simulation. The discharge rate of 4.06 l/s was assigned to the model and the constant ground motion amplitude was assigned over the entire aquifer length.

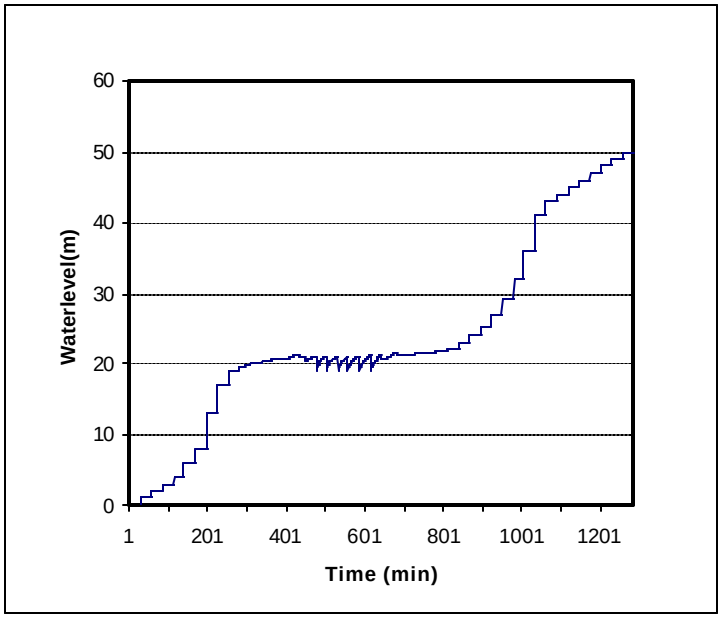


**Figure 4.49:** The drawdown curve for a borehole pumped at 4.06 L/s with pump causing ground amplitude of 31.4 nm

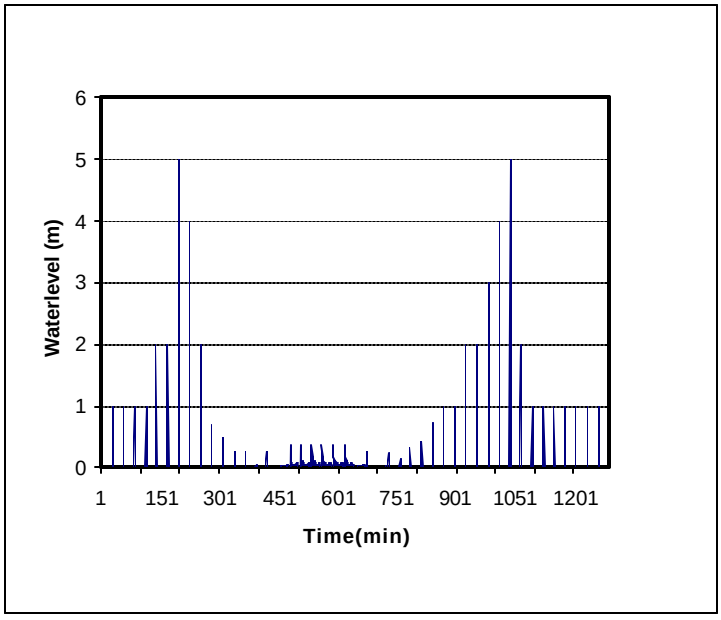


**Figure 4.50:** The first derivative of data in Figure 4.49

The oscillations in this case appeared around the 600$^{th}$ minute. It is a clear indication that for oscillations to be conspicuous in groundwater certain criteria have to be satisfied. The water level and discharge rate are two of them. The occurrence of oscillations can be related to increased volumes of water implying a larger hydrodynamic force necessary to counter the driving force. This phenomenon is exhibited at the plateau of the graph, which is associated with water at fracture position and is typical of field pumping test data captured from a horizontal fracture - controlled borehole in the Karoo aquifers. It is also analogous to a system in resonance. When a system is in resonance, the frequency of the driving force, the pump vibrations and the discharge rate in this case are in phase with the natural frequency of an aquifer. Experiment 3 showed that the natural frequency at the Campus Test Site at the time of the experiment was below 4.5 Hz, which was the cut-off frequency of the equipment used. When disturbed several frequencies are excited in response. The frequency spectrum in Figure 4.24 confirms the multi-frequencies that can be generated in a disturbed aquifer.

When a system is driven to resonance the amplitude increases (Figure 4.44 may be a typical example of frequency modulation) and in most cases it breaks. In an aquifer the presence of several frequencies can convolve with the resonating system thereby foiling destruction. The damping effect of the matrix also plays the same role. Whenever the system builds up a history of deformation (Botha and Cloot, 2002), and on exceeding a certain threshold of tolerance, the system breaks as a result of fatigue.

It is this phenomenon that is believed to cause the collapse of bedding fractures in Karoo aquifers.

### 4.4.4 Ground motion simulation

In this section ground motion is simulated when the pump is switched on and not allowed to discharge water to the surface. This should not be confused with the simulations in Section 4.4.3.2.4 where the water-level response was simulated and not the ground motion.

The field data for ground motion resulting from pump seismicity is shown in Figures 4.9, 4.10 and 4.11 for distances of 4 m, 4.5m and 5 m respectively and the overall characteristics of ground amplitude decay with distance from the vibrating pump is shown in Figure 4.8. The data were captured when the pump was on but was not allowed to discharge water.

For the purpose of the investigations, the components of the trace in Figure 4.9 are analysed in detail and compared to the numerical results. The dominant field frequency from this trace was used in the numerical simulations.

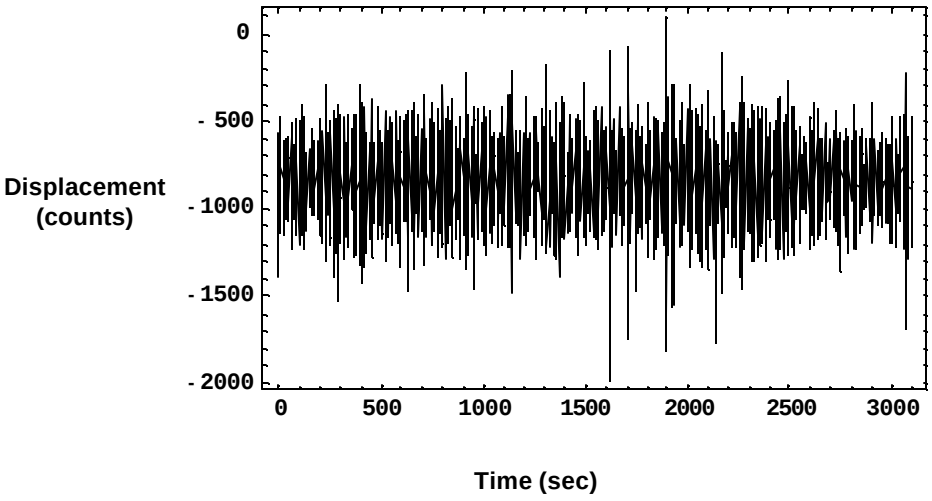


**Figure 4.51:** The S-E component of the seismic trace in Figure 4.9.

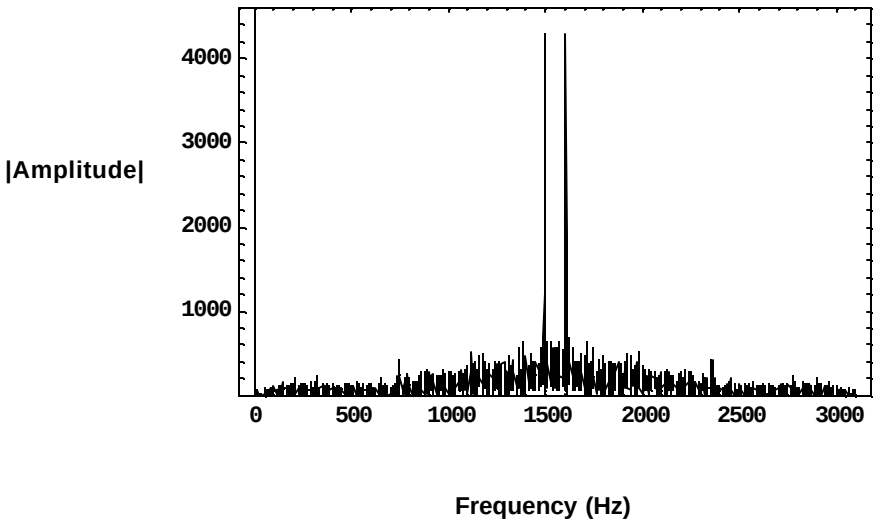


**Figure 4.52:** The Fourier transform of the trace in Figure 4.51

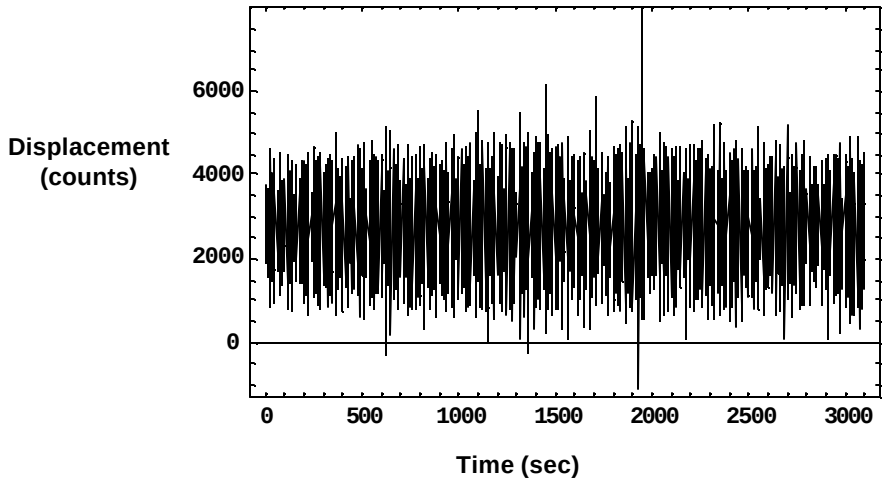


**Figure 4.53:** The S-N trace component of the seismic trace in Figure 4.9

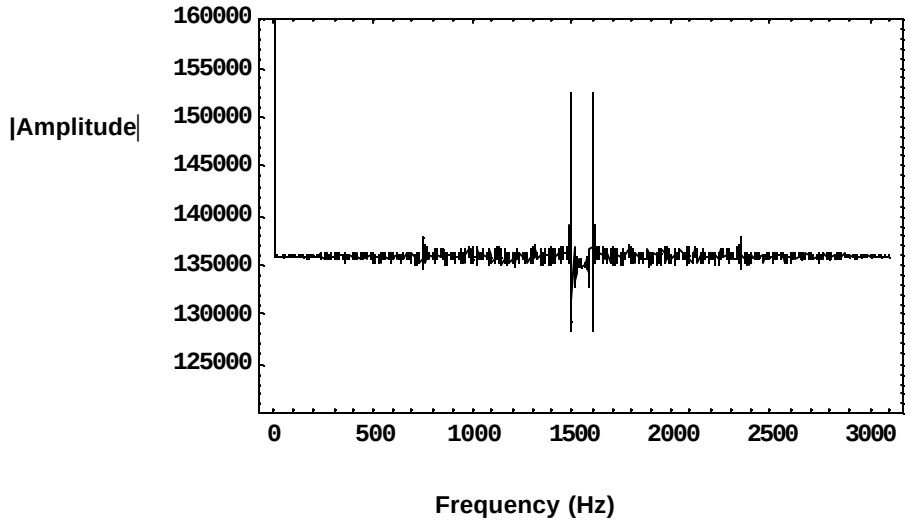


**Figure 4.54:** The Fourier transform of tracæ in Figure 4.53

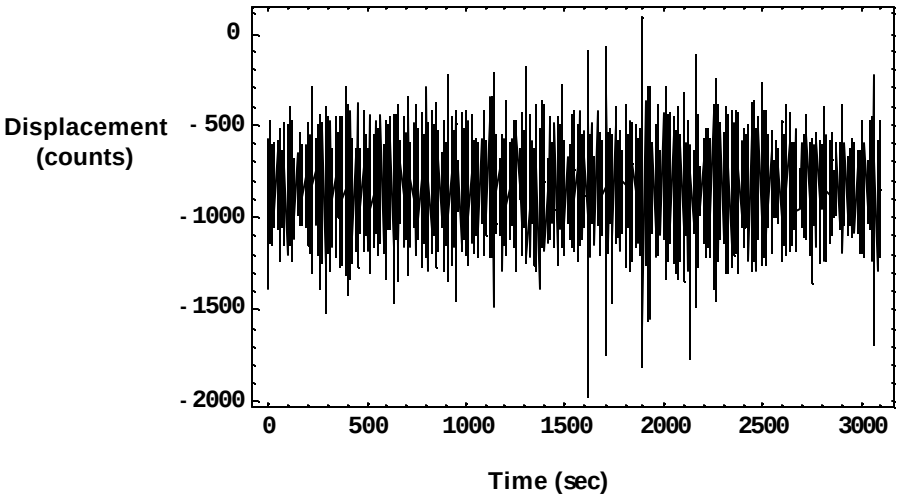


**Figure 4.55:** The S-Z component of the trace in Figure 4.9

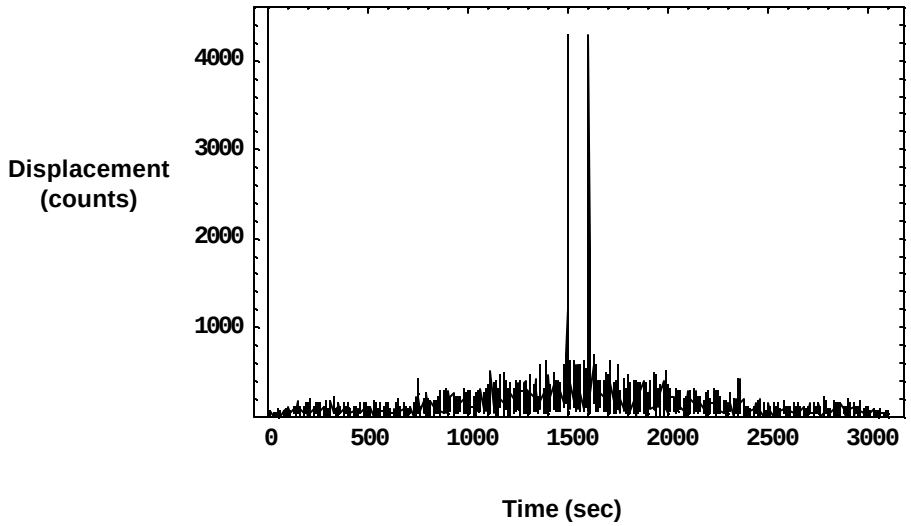


**Figure 4.56:** The Fourier transform of the trace in Figure 4.55

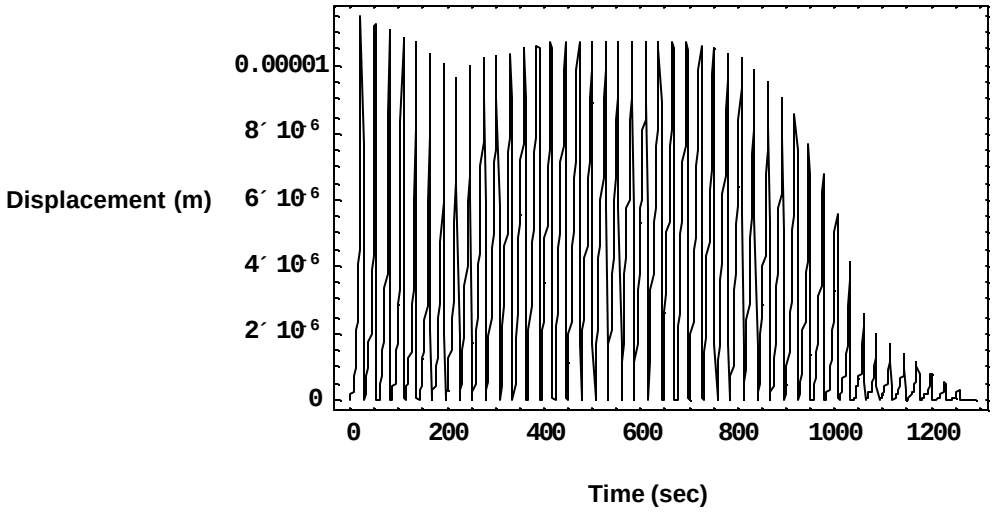


**Figure 4.57:** The numerical results of ground motion simulation obtained from the two-dimensional model for an operating pump that is not discharging water to the surface.

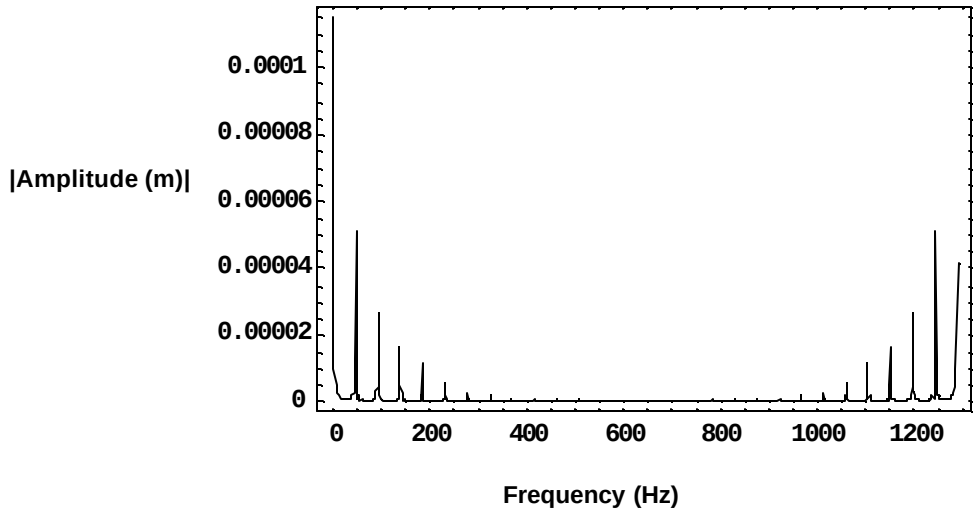


**Figure 4.58:** The Fourier transform of the simulated ground motion results shown in Figure 4.57.

The numerical results in Figure 4.57 and the field data of the trace components in Figures 4.51, 4.53 and 4.55 have similar amplitude characteristics. The effect of other frequencies present in the field, which are absent in the simulations, is the main source of difference between the two signals. The fluctuation of ground motion shown in the field data may also be caused by the operational characteristics of the pump, which is not always smooth and continuous. It may also be due to the interference of seismic waves of either different (especially where the amplitudes are low) or same phase angles (in cases where the amplitudes are high).

The Fourier transforms (Figures 4.54, 4.56 and 4.58) show the presence of a dominant frequency in all cases indicating the modulation aspect of the systems. In the field, the vibrations of the pump are modulated with the ground roll, which is always present in the system due to spurious and extraneous sources. The Fourier transforms of the simulated ground motion signal also shows the same principle to a lesser extent, but because of the complexity of the ground roll, the aspect of the dominant frequency was not clearly defined.

## 4.5 DISCUSSIONS

It should be noted that the water levels captured when using a hammer as a source of seismic wave showed positive spikes in each case, that is, in Experiments 5, 6 and 7.

The periodicity also varied with distance from the borehole of investigation. This applies to readings captured in Experiments 5 and 6 where the seismic source was shifted to and from borehole UO28. For Experiment 7, which was fixed at UO28, a constant periodicity can be observed.

It is also essential to note that the groundwater level is constantly dynamic (Figure 4.21) as a result of ground roll. However, the application of an external force (in the form of pump seismicity or a hammer in this case) enhances the behaviour. This can be seen by lack of periodicity in the first derivatives (Figure 4.22) of the water levels captured when not pumping the UP16. It can also be argued that the fluctuating readings recorded (Figure 4.21) are due to the electronics of the equipment and the counter argument is the fact that the upward trend water level shown in Figure 4.21 should fluctuate around a mean level if it was the electronics that were causing the behaviour of the water level. However, because the borehole water is subjected to aperiodic frequency the manner in which it surges in and out of the rock matrix is aperiodic and thus results in a gradual decrease in the water level.

The ground displacement amplitudes recorded when discharging are smaller than when not discharging. According to the deformation hypothesis, the hydrostatic pressure diminishes as water is lost from an aquifer and hence the corresponding amplitude gradually becomes smaller. It can equally be argued that with the Rayleigh wave different modes exist (Foti, 2000), leading to the destructive effects of waves and hence resulting in less ground motion. When executing Experiment 2 a number of the discharge rates were employed and some of the discharge rates in Experiment 2 failed to trigger the EARS. This could be as a result of the wave cancellation effect whereby waves of different modes are generated and interact destructively at the geophone position thus failing to register a signal.

The fact that the oscillations were not as obvious in the field data as they were in Figure 1.2 shows that the occurrence or the level of development of these oscillations depend on a number of factors. These factors should include pump position, critical discharge rate, the water level, distance from observation boreholes and the physical structure of the fracture of the boreholes involved. It should be noted that the oscillations in Figure 1.2 were observed when pumping borehole UO5 and not when pumping UP 16. It should be reiterated that the transducers used when capturing data in Figure 1.2 were of higher resolution than those used in the investigations covered in this thesis.

It can be safely said that oscillations occur in every pumping test data, but in most cases they are overwhelmed by the effect of discharging. The fact that oscillations

were observed when applying $\Delta t = 0.5$ minutes in the derivatives implies that the periodicity of these oscillations is even greater.

To simulate the physical observations numerically is a particularly difficult and complicated task. This is due to the diversity of frequencies and the complex geology involved that consists of lithologies of different mechanical properties. However, all was not lost in the simulations conducted, which were very close to the field observations. An important phenomenon highlighted is the possibility of the manifestation of resonance in the system. This principle forms the centre of the discrete existence of conspicuous oscillations in drawdown curves since it requires clear-cut conditions. The diversity of frequencies in an aquifer (Figure 4.24) and the damping effect of water (Biot, 1956) are essential in foiling the collapse of the physical integrity of an aquifer, a phenomenon common in resonating systems. In this case, a fracture will collapse on exceeding the critical tolerance threshold determined by its elastic properties (Botha and Cloot, 2002).

# CHAPTER 5

## SUMMARY AND RECOMMENDATIONS

### 5.1 GENERAL

Groundwater is the largest source of potable water in South Africa given that the country is semi-arid to arid with approximately 50 per cent of the geology constituting the Karoo Supergroup. Unique to these aquifers is the morpho-tectonic emplacement of more competent dolerite sills and dykes that cause the fracturing of Karoo sediments (Botha *et al*., 1998). Bedding fractures in particular have proved to be the major conduits of groundwater in these geological provinces with the matrix serving as reservoirs that fashion a multiple porous system. Given the vastness and the importance of groundwater in the country, Karoo aquifers have become the centre of attraction to many hydrogeologists and geo-scientists over the years who have viewed them with the common objective of understanding their mechanics and hydraulics.

Botha and Cloot (2002) are two of the researchers who embarked on similar investigations. The focus of their work was based on formulating a relationship between the mechanical properties and the hydraulic properties of aquifers. The approach stemmed from the idea that aquifers deform and was informed by the development of secondary features in borehole UO5 (Figure 1.1) at the Campus Test Site at the University of the Free State. The televiewer results obtained in 1996 revealed a brecciated zone which was absent in the previous periodic scans.

Central to the work of Botha and Cloot (2002) was the role abstraction plays in the longevity of Karoo aquifers, a subject that has been investigated through numerical modelling. The results showed that aquifers indeed deform when pumped and the life span of aquifers depends on the discharge rate. Botha and Cloot's (2002) numerical model did not focus on oscillations in pumping test data; however, the latter formed the basis of this research.

### 5.2 THE RESEARCH

The research was prompted in particular by the presence of oscillations in the pumping test data from borehole UO5. The borehole intercepts a bedding fracture at approximately 21 m below the ground surface. The diaphragmatic deformation of the fracture was a hypothesis postulated for the development of oscillations in the pumping test data, with the seismo-effect of the pump as the cause. The sound and the

pump vibrations form the basis of pump seismicity. The pump vibrations, as confirmed by field observations and supported by theory (White, 1965), propagate as Rayleigh waves away from the borehole and down the borehole. The inside of the borehole should be viewed as a free surface interfacing with solid rock (aquifer matrix), a criterion essential for the manifestation of Rayleigh waves.

To be effective in causing the deformation, the wave has to propagate along the borehole with the component orthogonal to the hydrostratigraphic unit instigating the deformation. The pressure variation on borehole water resulting from sound waves may be another source of oscillations. However, decoupling the effect of the sound and vibrations of the pump was not within the scope of this research, but since the latter could be quantified the work proceeded on the assumption that vibrations are the basis of the proposed diaphragmatic deformation hypothesis.

### 5.2.1 Observations

An aquifer should be viewed as a dual skeletal structure, with the geometry defined by the rigidity of the matrix and the hydroskeletal component offered by groundwater. This perception is not new in hydrogeology (Kruseman and Ridder, 1994). It is, however, essential to recognise the co-existence of these components.

Pumping not only removes water from the system but also introduces an internal force as a result of its vibrations, thus offsetting the system from equilibrium (Figure1.6). The smaller ground amplitudes observed when pumping are a clear testimony to the weakening of the hydrostatic component. Excessive pumping can lead to irreversible plastic deformation (Botha and Cloot, 2002). In essence, this implies that water serves as a cushion (or damping fluid) to the movement of the solid matrix (Biot, 1956), a principle utilised in electrokinetic systems (EKS). When a bedding fracture that is characterised by less porous fracture planes and high water content is deformed it results in water flowing to regions of low resistance, that is, in the horizontal direction. This causes the flashing in and out of water in a borehole, which generates oscillations in the ultimate drawdown curve. Fracture planes gradually lose porosity owing to the precipitation of secondary minerals such as calcite and iron oxides. The latter is common in the Karoo aquifers.

The resultant oscillations are not conspicuous owing to the overwhelming effect of discharging. However, the application of post-processing techniques, such as derivatives, enhances oscillations by suppressing the effect of abstraction. Nearly all water drawdowns post processed using the derivative technique displayed the oscillatory characteristics. This indicates that it is an intrinsic characteristic of the system.

Another important outcome is the exponential-like decay of ground amplitudes with distance from an excited pump. In the bedding-fractured Karoo aquifers, high-yielding boreholes are drilled a few metres from the failed boreholes intersecting the same geological feature (Rasmussen, 1998). This phenomenon is better explained by postulating that there is a cut-off distance where the pump-induced seismo-deformations are strong enough to cause fractures to collapse as a result of fatigue. The latter could be speeded up by abstraction. The effect of abstraction on fracture failure is investigated in Botha and Cloot's (2002) work. The work revealed that abstraction indeed causes fracture failure; however, the simulated time frames were longer than the field observations, indicating that perhaps by incorporating pump seismicity in their models the resultant simulated time frames may be within the field observations.

It should be noted that for the pump-induced seismo-deformations to be effective, the seismic wave generated should propagate along the borehole. In this research it was found that a Rayleigh wave is generated by the pump and, according to the proposed hypothesis, this is the component orthogonal to a hydrostratigraphic unit that instigates the diaphragmatic deformation. Coupled to vibrations are the effects of pressure variations on the water level resulting from the humming noise of a pump that can also cause oscillations. Experiment 7 may be a good example of the impact of sound on water level.

### 5.2.2 Contribution to hydrogeology

Pump seismicity in groundwater was never considered essential in aquifer management provided that a proper discharge rate was assigned. The co-existence of vibrations and discharge rate make it difficult to manage aquifers effectively. Considering one aspect and ignoring the other can have severe repercussions on the behaviour of the system in the long run. Aquifers should now be considered in terms of their mechanical properties in conjunction with their hydraulic properties. These sentiments are shared by Burbey (2001); and Botha and Cloot (2002).

In addition, the seismological properties of an aquifer should be integrated into aquifer management given the fact that pump-induced seismo-deformations can lead to the structural failure of an aquifer. This phenomenon is experienced quite often in the Karoo where high-yielding boreholes are drilled within a few metres from a failed borehole. As a great deal of attention is given to discharge rate, the seismic characteristics of a pump should also be considered when selecting or installing a pump. Precautions should be taken to reduce the direct transmission of pump seismic waves into an aquifer mainly via the borehole casing.

It is unequivocally clear that pump-induced seismo-deformations exist and their effect on aquifers can be far-reaching in the long run.

## 5.3 RECOMMENDATIONS AND FUTURE WORK

Since pump seismicity plays a significant role in the overall performance of an aquifer, it is high time attention is focused on improving the mechanical performance of pumps so as to minimise the seismic impact on aquifers. Instead of focusing on discharge rate only, attention should also be directed at selecting a pump with the right mechanical properties, such as low frequency and low noise. Modifications such as adding shock absorbers and frequency toning gadgets should also be considered.

The pressure transducers used in this research were of a lower resolution compared with the initial equipment used in capturing the data presented in Figure 1.2. Low resolution has a tendency to mask the effect and hence the inconspicuousness of the oscillations in the raw data captured in this research. Future work should involve equipment with high resolution. The use of hydrophones, which are more sensitive than transducers, to capture the seismic response of borehole water should be investigated.

The emphasis of the work covered was more hydrogeological than seismological. Future work should try to model the seismological evolution of the pump vibrations as they propagate to a hydrostratigraphic unit of interest. This approach would improve the numerical models employed in the thesis tremendously. It would also enable the quantification of deformation with high level of precision, as the amount of energy reaching a hydrostratigraphic unit of interest and its mechanical properties would be known.

## REFERENCES


Aki, K. and Richards, P.G. (1980) Q*uantitative seismology theory and methods.* Vol. I.W.H. Freeman and Company , San Francisco.

Bangoy, L.M, Bidaux, P., Drogue, C., Plégat, R. and Pistre, S. (1992) *A new method of characterizing fissured media by pumping tests with observation wells.* Journal of Hydrology, 138, 77-88.

Bangoy, L.M. and Drogue, C. (1994) *Analysis of intermittent pumping tests in fissured fractal aquifers: theory and applications.* Journal of Hydrology. 158, 47-59.

Barker, J.A. (1988) *A generalised radial flow model for hydraulic tests in fractured rock*. Water Resources Research, 24, 796-804.

Bear, J. (1972) *Dynamics of fluids in porous media*. New York: Elsevier.

Bear, J. (1979) *Hydraulics of groundwater*: *water resources and environmental engineering.* New York: McGraw-Hill.

Biot, M.A. (1941) *General theory of three-dimensional consolidation.* Journal of Applied Physics, 12, 155-164.

Biot, M.A. (1952) *Propagation of elastic waves in cylindrical bore containing a fluid*. Journal of Applied Physics, 23, (2), 997-1005.

Biot, M.A. (1956) *Theory of propagation of elastic waves in a fluid-saturated porous solid.* I. Low-frequency range. Journal of Applied Physic*s*, 28, (2), 168-178.

Botha, J.F. (1996) *Groundwater theory.* Unpublished lecture notes, Institute for Groundwater Studies. University of the Free State, Bloemfontein.

Botha, J.F. and Cloo, A.H. (2002) *Karoo aquifers: deformations, hydraulic and mechanical properties.* Draft report to the Water Research Commission on the project: "Flow and transport characteristics of groundwater in Karoo formations". Pretoria: Water Research Commission.

Botha, J.F. and Pinder, G.F. (1983) *Fundamental concepts in the numerical solution of differential equations.* John Wiley & Sons, New York.

Botha, J.F., Verwey, J.P., van der Voort, I, Vivier,J.J.P., Buys, J., Colliston,W.P. and Loock, J.C. (1998) *Karoo aquifers: their geology, geometry and physical properties*. WRC Report No. 487/1/98. Water Research Commission., P.O. Box 824, Pretoria 0001.

Burbey, T.J. (2001) *Storage coefficient revisited: is purely vertical strain a good assumption.* Ground Water. Vol. 39(3), 458-464.

Cakmak, A.S., Botha, J.F. and Gray, W.G. (1987) *Computational and applied for engineering mathematics analysis.* Springer-Verlag, New York.

Chevallier, L., Goedhart, M. & Woodford, A.C. (2001) *The influences of dolerite sill and ring complexes on the occurrence of groundwater in Karoo fractured aquifers: A morpho-tectonic approach.* WRC Report No. 937/1/01. Pretoria: Water Research Commission.

Chavellier, L. and Woodford A.C. (1999) *Morpho-tectonics and mechanism of emplacement of the dolerite rings and sills of the western Karoo, South Africa.* South African Journal of Geology, vol. 102, No 1, 43-54.

Chiang, W-H. and Riemann, K. (2001) *Guidelines for aquifer parameter estimation with computer models*. WRC Report No. K5/114. Water Research Commission, P.O. Box 824, Pretoria 0001. South Africa.

Childs, E.C and Collis-George, N. (1950) *The permeability of porous media*. Proceedings of the Royal Society, Series A. 201, 392-405.

D'Arnaud Gerkens, J.C. (1989) *Foundation of exploration geophysics*. Elsevier. Tokyo.

De Marsily, G. (1986) *Quantitative hydrogeology.* Academic Press, Inc., New York.

Driscoll, F.G. (1989) *Groundwater and wells*. Johnson Filtration Systems Inc., St. Paul, Minnesota 55112.

Dullien, F.A.L. (1979) *Porous media fluid transport and pore structure.* Academic Press, New York.

Foti, S. (2000) *Multistation method for geotechnical characterization using surface waves*. Unpublished PhD thesis. Politecnico di Torino. Università degli studi di Genova.

Havskov, J. and Ottemöller, L. (2001) *SEISAN: The earthquake analysis software for Windows, Solaris and Linux. Version 7.2*. Institute of Solid Earth Physics, University of Bergen, Allégen 41, 5007 Bergen, Norway.

Helweg, O.J. (1994) *A general solution to the step-drawdown test*. Ground Water, 32, No.3, 363-366.

Hughes, W.F. and Brighton, J.A. (1967) *Theory and dynamics of fluid dynamics*. Schaum's Outline Series. McGraw-Hill Book Company, New York.

Jaeger, J.C. (1969) *Elasticity, fracture and flow: with engineering and geological applications.* Methuen. & Co Ltd, London

Kearey, P. and Brooks, M. (1995) *An introduction to geophysical exploration.* 2nd Edition. Blackwell Science.

Kent, L.E. and The South African Committee for Stratigraphy (SACS), (1980) *Stratigraphy of South Africa: Part 1: Lithostratigraphy of the Republic of South Africa.* South West Africa/Nambia and the Republics of Bophuthatswana, Transkei and Venda. Handbook 8. Geological Survey, South Africa.

Kruseman, G.P. and De Ridder, N.A. (1994) *Analysis and Evaluation of Pumping Test Data*.(2nd Edition. Publication 47.International Institute for Land Reclamation and Improvement, P.O.Box 45, 6700 Wageningen, The Netherlands.

Lombaard, B.V., (1952) *Karoo dolerites and lavas*. Transvaal Geological Society, S.Afr., 55, 175-198.

Rasmussen, J. (1998) *Noupoort groundwater investigation.* T + P Report No. 980149. Toens and Partners cc. 9 Lester Road, Wynberg, 7800. Cape Town.

Scheidegger, A.E. (1974) *The physics of flow through porous media*. (3rd Edition) University of Toronto Press. Toronto.

Scheidegger, A.E. (1953) *Theoretical models of porous matter.* Producer's Monthly**,** 17 (10), 17-23.

Telford, W.M., Geldart, L.P. and Sheriff, R.E. (1990) *Applied Geophysics.* 2nd Edition. Cambridge University Press.

Theis, C.V. (1935) *The relation between the lowering of the piezometric surface and the rate and duration of discharge of a well using groundwater storage*. Transactions of the American Geophysical Union. 16, 519-524.

Truswell, J.F. (1970) *Historical Geology of South Africa.* Purnell, Cape Town.

Wang, H. F and Anderson, M.P. (1982) *Introduction to groundwater modeling, finite difference and finite element methods.* W.H. Freeman and Company, San Francisco

Warsi, Z. U.A. (1993) *Fluid dynamics theoretical and computational approaches*. CRC Press. Boca Raton.

White, J.E. (1965) *Seismic waves; radiation, transmission and attenuation*. McGraw-Hill Book Company. New York.

## A B S T R A C T

The research unequivocally showed that pump-induced seismo-deformations exist, especially in boreholes equipped with electric and diesel pumps. Central to seismo-deformations are the mechano- and the geo-acoustic effects on both the borehole water and the aquifer. These aspects of the pump instigate the proposed diaphragmatic deformation hypothesis. In an aquifer the pump vibrations manifest as Rayleigh waves. By virtue of the driving source, the waves are harmonic (White, 1965). To be effective in engineering the proposed diaphragmatic deformation on a hydrostratigraphic unit situated several metres below the ground surface, the waves propagate along the borehole. The component of the Rayleigh wave orthogonal to the unit instigates the deformation and thus oscillations are generated in drawdown curves. Oscillations are a common feature in pumping test data and the masking effect of abstraction makes them inconspicuous. However, the derivative technique when applied to the signal enhances the phenomenon. The technique suppresses the abstraction effect in the data leaving the time-dependent oscillations. The spikes obtained in some of the derivatives of the pumping test data may suggest a one-sided deformation, probably the upper lip to a hydrostratigraphic unit. Coupled with the effects of Rayleigh waves is the pressure variation on the water level caused by the sound. The humming sound of a pump in operation is capable of subjecting borehole water to constant pressure variations thus leading to inherent oscillations in the pumping test data. The conspicuousness of oscillations in the raw pumping test data (Figure 1.2) can be attributed to the high resolution of the equipment used and interferences of different wave forms existing in the system.

For a borehole that is continuously in operation, the impact of seismo-deformations on the physical integrity of an aquifer can be detrimental. In hard-rock fractured Karoo aquifers, the induced seismo-deformations can be of astronomical severity. The fact that successful boreholes are drilled in the Karoo within a short distance of a failed or “dried up” borehole is a clear evidence of structural failure. Bedding fractures in particular are very susceptible (Rasmussen, 1998). The radial extent of failure depends on the strength of the vibrations which are habitually intense close to the borehole and decay exponentially-like with distance. The ultimate failure of hydrostratigraphic units after prolonged pumping, which is common in the Karoo, may be due to the evolution history of deformation that accumulates as residual strains and stresses (Botha and Cloot, 2002).

The research also revealed that ground displacements are smaller when discharging than when not. According to the hypothesis, this is due to the decreasing hydrostatic pressure essential in opposing the normal stress from a pump. It is in this view that groundwater should be considered as a hydroskelatal component of an aquifer and the rationale of lowering the discharge rate should not only be seen as a process to prevent dewatering but as a mechanism for preserving the dynamic equilibrium between the normal stress emanating from a pump and the hydrostatic force offered by water. Offsetting the equilibrium can lead to irreversible plastic deformation and aquifer subsidence (Botha and Cloot, 2002).

The failure of numerical models to simulate the oscillations completely indicates that the wave that triggers the proposed diaphragmatic deformation of a fracture is more complicated than the simple harmonic waveform caused by pump vibrations. The wave should be a convolution of the vibrations, sound and the natural ground roll. Besides, the pump vibrations on reaching a geological feature of interest in a multi-stratigraphic geologic terrain would have undergone multiple reflections and transmissions with the ultimate waveform being a distortion of the primary signal.

The research conducted showed that pump-induced seismo-deformations should have the same status as the discharge rate in aquifer management. It is clear that the introduction of measures aimed at reducing the transmission of seismic waves to an aquifer should be a priority in order to deter the pump-induced seismo-deformations. This includes preventing the pump and the borehole casing from coming into direct contact; incorporating gadgets to tone down the frequency of the mains; and installing shock absorbers between the pump and the ground. The selection of pumps should be based on the seismological properties of the aquifer that is to be used and its hydrogeological properties.